NASA TN D-1946

TECHNICAL NOTE

D-1946

FULL-SCALE WIND-TUNNEL INVESTIGATION OF A FLEXIBLE-WING MANNED TEST VEHICLE

By Joseph L. Johnson, Jr., and James L. Hassell, Jr.

Langley Research Center
Langley Station, Hampton, Va.

NATIONAL AERONAUTICS AND SPACE ADMINISTRATION
WASHINGTON

August 1963

NATIONAL AERONAUTICS AND SPACE ADMINISTRATION

TECHNICAL NOTE D-1946

FULL-SCALE WIND-TUNNEL INVESTIGATION OF A FLEXIBLE-WING MANNED TEST VEHICLE

By Joseph L. Johnson, Jr., and James L. Hassell, Jr.

SUMMARY

An investigation has been conducted in the Langley full-scale tunnel to determine the performance and static stability and control characteristics of a flexible-wing manned test vehicle. This airplane is a simplified research machine, which consists basically of a cargo platform attached to a parawing by means of an overhead truss arrangement. In addition to the basic control tests, a few tests were made to evaluate several alternate control systems which involved deflections of the aft portion of the parawing keel and wing tips.

The tunnel tests showed that the maximum lift coefficient of the airplane occurred at a keel angle of attack of 42° and was 1.24 with power off and 1.33 with power on. The maximum lift-drag ratio was about 5.5. With stick fixed, the airplane had about neutral static longitudinal stability at keel angles of attack below 20°, a moderate degree of stability from 20° to 35°, and longitudinal instability, or pitch-up, from 35° to 42°. At a keel angle of attack of 42° the airplane again became stable. With the stick free, the longitudinal stability was generally worse with the airplane being unstable at the lower angles of attack, about neutrally stable in the intermediate range, and unstable at the higher angles of attack. The airplane, in general, was directionally stable and had positive effective dihedral throughout the angle-of-attack range investigated. The lateral control provided by banking the wing did not appear to be satisfactory because of inadequate rolling moments and excessively high stick forces. Analysis of the tunnel data indicated that the rudder was generally a better roll-control device with power on (inasmuch as the rudder is in the slipstream of the pusher propeller) than the wing-bank control system provided on the airplane. The rudder was not very effective with power off. The hinged wing-tip control device tested on the airplane (which had been developed earlier at the Langley Research Center in small-scale model tests) appeared promising in that it provided higher rolling effectiveness and lower estimated stick forces than those of the wing-bank control system provided on the airplane.

INTRODUCTION

For the past few years, the National Aeronautics and Space Administration has been conducting a general investigation to provide some basic information on

configurations employing the parawing concept. (For example, see refs. 1 to 3.) This early work eventually led to the design and construction of a flexible-wing airplane configuration, which was proposed as a test vehicle to demonstrate flight characteristics of the parawing concept as well as to provide a prototype for the development of a manned combat utility vehicle. This airplane is a simplified research machine which consists basically of a cargo platform attached to a parawing by means of an overhead truss arrangement. The vehicle is powered by a pusher propeller located at the aft end of the platform and has a cockpit located at the front. Control is obtained by banking or pitching the wing with respect to the cargo platform. A rudder operating in the propeller slipstream provides directional control. A model generally similar in design to the vehicle of this investigation was flight tested in the Langley full-scale tunnel, and the results of this investigation are reported in reference 4. A preliminary flight evaluation of the full-scale configuration of the present investigation is given in reference 5. As part of the overall research effort on the parawing concept, a force-test investigation has been conducted in the Langley full-scale tunnel on the full-scale vehicle to determine static stability and control and performance parameters for correlation with the earlier flight tests as well as to extend the present research program to include wind-tunnel data on large-scale parawings.

The present investigation consisted of static tests to determine the basic aerodynamic and longitudinal and lateral stability and control characteristics of the airplane over an angle-of-attack range of the keel from about 14° to 44° with power off and on. These tests were conducted at several different values of dynamic pressure to evaluate the effects of aerodynamic loading on the characteristics of the wing up to simulated steady level flight (1 g) conditions. Included in the investigation were tests of the airplane with the rudder off and on and with the wing off. In addition, tests were made to study the effects of boltrope and batten modifications to the parawing trailing edge. A few tests were also made to evaluate several alternate means of providing control. Comparisons of the wind-tunnel data with flight-test data obtained on the airplane (ref. 5) have been made where possible.

SYMBOLS

All forces, moments, and velocities are presented with respect to the stability-axis system originating at the reference center-of-gravity position shown in figure 1. All measurements are reduced to coefficient form and are based on the dimensional characteristics of the flat plan geometry of the wing (45° leading-edge sweep).

S	wing area, sq ft
b	wing span, ft
c_k	keel length, ft
V	free-stream velocity, fps

q	free-stream dynamic pressure, lb/sq ft
α_k	angle of attack of keel, deg
α_p	angle of attack of platform, deg
i_w	angle of incidence of parawing keel with respect to platform, $\alpha_k - \alpha_p$, deg
β	angle of sideslip, $-\psi$, deg
ψ	angle of yaw, deg
ϕ	angle of roll, positive right wing tip down, deg
W	weight, lb
L	lift, lb
D	drag, lb
L/D	lift-drag ratio
W/S	wing loading, lb/sq ft
F_Y	side force, lb
T	thrust, lb
M_h	hinge moment (positive when M_h tends to deflect keel or wing-tip trailing edge downward in the XZ-plane or wing-tip trailing edge outward in the XY-plane), ft-lb
M_Y	pitching moment, ft-lb
M_X	rolling moment, ft-lb
M_Z	yawing moment, ft-lb
C_L	lift coefficient, L/qS
C_D	drag coefficient, D/qS
T_c	thrust coefficient, $\left[C_D \text{ (power on)} - C_D \text{ (power off, propeller stopped)}\right]_{\alpha_p=0^\circ}$
C_h	hinge-moment coefficient, M_h/qSb for roll, M_h/qSc_k for pitch

C_Y lateral-force coefficient, F_Y/qS

C_m pitching-moment coefficient, M_Y/qSc_k

$C_{m,o}$ pitching-moment coefficient at zero lift

C_n yawing-moment coefficient, M_Z/qSb

C_l rolling-moment coefficient, M_X/qSb

$\frac{\partial C_m}{\partial C_L}$ slope of pitching-moment curve with lift coefficient

$C_{Y_\beta} = \frac{\partial C_Y}{\partial \beta}$, per deg

$C_{n_\beta} = \frac{\partial C_n}{\partial \beta}$, per deg

$C_{l_\beta} = \frac{\partial C_l}{\partial \beta}$, per deg

g acceleration due to gravity, 32 ft/sec^2

p rolling velocity, radians/sec

$C_{l_p} = \frac{\partial C_l}{\partial \frac{pb}{2V}}$, per radian

δ_r rudder deflection, deg

δ_t wing-tip deflection, deg

x,z horizontal and vertical distances from airplane center of gravity to wing pivot, respectively, ft

AIRPLANE AND APPARATUS

A three-view drawing of the airplane and photographs of the airplane mounted for force testing in the Langley full-scale tunnel are presented in figures 1 and 2, respectively. Characteristics of the airplane are presented in table I. The parawing used on the vehicle consisted of a dural box-beam keel and two airfoil-shaped leading edges hinged together at the apex of the wing. A fixed leading-edge sweep angle of 50° was maintained by a spreader bar which was attached to the parawing leading edges and to the keel at approximately the

35-percent keel station. The fabric used to form the membrane of the parawing was made of 7-ounce-per-square-yard dacron impregnated with weather-resistant polyester. The warp of the cloth was parallel to the keel. The trailing edge of the parawing was scalloped and had battens and a boltrope (3/32-inch aircraft cable) installed. The boltrope had a 1-inch asymmetric setting to provide lateral trim. These modifications to the trailing edge were made in the preliminary flight evaluation program (see ref. 5) and were considered as part of the basic airplane configuration.

The wing could be pitched or rolled about the pivot point through a system of bellcranks, cables, and push-pull rods. An electric actuator mounted on the parawing keel was used to position the wing forward or rearward with respect to the pivot point in order to provide a means of trimming the machine longitudinally.

Power for the vehicle was supplied by a 180-horsepower engine and a fixed pitch propeller. A rudder was mounted to the platform structure and to the wing keel directly behind the pusher propeller to provide directional control.

The airplane was mounted for force testing by attaching the tunnel support struts rigidly to the front and rear of the platform. (See fig. 2.) The wing was remotely pitched or rolled with respect to the platform through aircraft actuators which were installed in the longitudinal and lateral control systems of the airplane. The wing deflection angles were measured at the wing pivot point. The gearing ratio of control column, or wheel deflection to wing deflection, was 8.5 in pitch and 7.9 in roll.

Several alternate control systems, which required some modifications to the basic structure, were tested on the airplane. These installations are illustrated in figure 3 and shown in photographs of actual test setups in figure 4. One modification consisted of removing the fabric from the rear portion of the keel and reattaching the fabric to a rectangular lightweight framework which was hinged to the keel so that it could be deflected up and down for pitching control. Another modification consisted of removing the fabric from one wing tip and reattaching the fabric to a control arm which was hinged and allowed to move inward and outward for roll control (designated wing-tip control A). A third modification involved the installation of a hinged longitudinal member near the wing tip which could be deflected in a vertical plane to change the basic wing contour at the trailing edge to provide control (designated wing-tip control B). In control system B, the fabric remained attached to the wing leading edge, and as the hinged longitudinal member was deflected downward, the wing fabric was permitted to seek its own position under this member. (In other words, the fabric was not attached to the hinged member and therefore did not transmit any lateral hinge moments.) In all of these modifications, provision was made for the installation of strain gages to allow for the determination of hinge-moment and stick-force characteristics.

TESTS

The investigation was conducted in the Langley full-scale tunnel. A complete description of the tunnel and test apparatus is given in reference 6. The static

longitudinal and lateral stability and control characteristics of the airplane were determined from force measurements obtained from the tunnel scale-balance system for a range of angles of attack of the keel from about 14° to 44° for several values of wing incidence, dynamic pressure, and power settings.

The power-off tests were made with the propeller stopped, and no tests were made with the propeller removed. Since the drag of the stopped propeller was probably very small, it was assumed that the thrust coefficient T_c was zero for the power-off tests. The power-on tests were made by holding the propeller rotational speed constant over the angle-of-attack range investigated. Several power-on runs were made in this manner to cover a range of trim conditions. In both the power-off and power-on cases, tests were made at wing-incidence angles of $22\frac{1}{2}^\circ$, 25°, and $28\frac{1}{2}^\circ$, which correspond approximately to the wing-incidence range investigated in the flight tests of reference 5. The 25° incidence was considered the basic condition, however, and most of the tests were made at this condition. Most of the tests were conducted at a dynamic pressure of 3.07 pounds per square foot. Included in the investigation, however, were tests at several different values of dynamic pressure to evaluate the effects of aerodynamic loading on the aerodynamic characteristics of the configuration up to simulated steady level flight (1 g) conditions.

The lateral stability tests were made at sideslip angles of 5° and -5°, and the lateral control tests were made at wing roll angles of 5° and -5° and at rudder deflection angles ranging from -20° to 20°.

Included in the investigation were tests of the airplane with the rudder off and on and with the wing off. In addition, a few tests were made to obtain some information concerning the effect of trailing-edge boltrope tension and changes in batten geometry (length and arrangement) on the stability and control characteristics of the airplane. A number of tests were also made to evaluate several proposed alternate control systems which included a hinged-keel (trailing edge) control system for pitch control and two hinged-wing-tip control systems for lateral control.

The range of dynamic pressures used in the investigation varied from about 1.60 to 5.60 pounds per square foot, which corresponds to an airspeed range from about 37 to 69 feet per second at standard sea-level conditions and to a Reynolds number range from about 6.6×10^6 to 12.4×10^6 based on the parawing keel length of 28 feet.

CORRECTIONS

The force and moment data presented have been corrected for airstream-misalinement, jet-boundary, and blockage effects. Because of the large size of the airplane with respect to the tunnel test section, it was necessary to mount the airplane fairly close to the ground board (ratio of height of wing pivot above the ground board to wing span is 0.50) in order to allow high angles of attack.

In order to properly represent flight out of ground effect, these data should be corrected to account for the effects of ground proximity on lift, drag, and pitching moment. Although there are no methods available for making accurate corrections for the ground effect in this case, a general indication of the magnitude of the effect can be obtained from previous investigations with delta-wing models in and out of the presence of the ground. (See ref. 7.) Based on this available information, ground-effect corrections have been made to the basic data in a number of cases and are presented for reference purposes.

RESULTS AND DISCUSSION

Before the force-test results are discussed, it appears desirable to first point out some of the more pronounced wing irregularities noted in the investigation since this information may be useful in interpreting the force-test results. Visual observations and camera records were made to obtain some indication of the changes in the wing fabric and support members as the tunnel test conditions were varied. Representative photographs obtained during some of the tests are presented in figure 5.

It was observed in the wind-tunnel tests of the basic configuration that at keel angles of attack below about 20° the aft portion of the wing (and in particular the inboard section) fluttered badly. It appeared that traveling waves moved rearward along the wing with amplitudes that increased as the angle of attack was reduced. In addition, high-frequency trailing-edge flutter was very pronounced at keel angles of attack below about 20°. As the angle of attack was increased above 20°, the trailing-edge flutter and wave motion of the fabric became less apparent and appeared to stop completely near an angle of attack of about 27°, but near this angle of attack, a large depression formed in the aft section of the wing, just ahead of the battens, and became more pronounced with increasing angle of attack. It appeared that the wing trailing edge had considerably more downward deflection at $\alpha_k = 27°$ than at the lower angles of attack probably because the boltrope restricted the trailing edge while the fabric forward of the trailing edge stretched as a result of the increased loading at the higher angles of attack.

The wing contour changes noted in the wind-tunnel tests are generally similar to those observed in the preliminary flight evaluation tests reported in reference 5. It is believed therefore that the force-test results are applicable for use in interpreting the flight-test results. It should be pointed out, however, that the application of these results to other parawing arrangements having different wing characteristics (such as material, direction of fabric weave and seams, and leading- and trailing-edge shapes) may be definitely limited.

It should be pointed out that in the tunnel tests and at times in the flight tests there were large fluctuations in both the pitch and roll control forces. A sample of data from the control-force measurements made in the tunnel tests is shown in figure 6. Fluctuations in stick force of as much as ±20 pounds were obtained, and there was also a shift in the general level of the readings from one time to another. The data represented by the solid line in figure 6(a) were

obtained at the beginning of a test run at a keel angle of attack of 22°, whereas the data for the dashed line were obtained several minutes later under presumably identical test conditions after runs had been made at higher angles of attack. The fluctuations in the data and the shift in level of readings from one time to another are believed to be related to such factors as trailing-edge flutter, flexibility, and fabric stretch.

Longitudinal Stability and Control

Aerodynamic data for basic configuration.- The basic longitudinal data for the airplane configuration are presented in figures 7 and 8 for the power-off and power-on conditions for wing incidences of 22.5°, 25°, and 28.5°. The data of figure 7 are plotted against the angle of attack of the wing keel whereas the data for figure 8 are plotted against angle of attack of the platform. The data of these figures were obtained with the dynamic pressure held constant during the test run. In order to represent a 1g flight condition (lift equal to aircraft weight), these data require certain corrections which can be made by using the data of figure 9.

Figure 9 presents lift, drag, and pitching-moment data for the power-off condition at $i_w = 25°$ obtained in test runs at different values of constant dynamic pressure, ranging from 1.60 to 5.60 pounds per square foot which corresponds to airspeeds of about 22 to 41 knots. The data of figure 9 show a consistently greater negative pitching moment with increasing dynamic pressure. The dashed curve intersecting the pitching-moment curves of figure 9 represents the pitching moments for a 1g flight condition. This curve was obtained from the basic relationship $C_L = \frac{W/S}{q}$ $\left(\text{or } qC_L = W/S\right)$ by using a value of W/S of 3.32 lb/sq ft for the airplane. The dashed curve intersects each of the other curves at the lift coefficient where the product of C_L and the measured q is equal to the airplane wing loading. The curve representing the 1g flight condition has a flatter slope (and therefore, less static longitudinal stability) than the curves obtained at the higher values of constant dynamic pressure, particularly in the low and moderate lift-coefficient range. A 1g curve for lift and drag data was not presented since the effect of dynamic pressure was generally small and inconsistent in these cases.

For ease of comparison, the pitching-moment curve for 1g flight and the curve obtained at the constant dynamic pressure of 3.07 lb/sq ft used in most of the tunnel tests are replotted in figure 10. Since the effects of dynamic pressure were determined only for the power-off condition at $i_w = 25°$, the pitching-moment data for other test conditions were corrected to 1g conditions by using the increments between the two pitching-moment curves of figure 10. The data corrected in this manner for the various wing-incidence and power conditions of figures 7 and 8 are presented in figure 11.

The lift curves of figure 11 appear to be normal with a lift-curve slope slightly greater than 0.05 per degree with power on and slightly less than 0.05 with power off. The maximum lift coefficient is obtained at a keel angle of attack of about 42° and is 1.24 with power off and 1.33 with power on. Although

data are presented for a combination of platform angle of attack and wing-incidence angle corresponding to angles of attack of the keel as low as 14°, the wing trailing-edge flutter which occurred at keel angles of attack below about 20° probably makes it undesirable to operate the aircraft at angles below this value. Figure 12 shows fairly good agreement between lift coefficients measured in flight and in the tunnel tests. The lift curve in figure 12 for the tunnel tests is an average of the power-on lift curves of figure 11.

Figure 11 shows that the maximum L/D of the airplane is about 5.5 and is obtained at a keel angle of attack of about 27° or 28°. An estimate of the L/D for the wing alone of about 7 was made from the data of figure 11 together with the data for the platform alone shown in figure 8(b). It should be pointed out that the L/D of the wing alone cannot be determined directly by subtracting the data of the platform alone from the data for the complete configuration because of some favorable interference effect of the platform on the wing. This effect became apparent in tests (see ref. 4) of a small-scale configuration similar to the vehicle of the present investigation in which data were obtained for the wing alone, platform alone, and wing-platform combination.

The pitching-moment data of figure 11 show neutral static longitudinal stability at keel angles of attack below about 20°, a moderate degree of stability from about 20° to 35°, and longitudinal instability, or pitch-up, from about 35° to 42°. At 42° the data of figure 11(c) indicate a stabilizing break in the pitching-moment curve. The pitch-up noted for this configuration at high angles of attack is unusual for parawing configurations based on tests of small-scale models which showed stable, pitch-down moments at the stall. One possible explanation for the pitch-up of the full-scale vehicle might be the particular changes in the trailing-edge contour, which appeared to be more severe than previously noted in other parawing studies.

Presented in figure 13 are longitudinal data for three wing pivot positions which cover the wing forward and aft pivot limits available on the airplane for longitudinal trim. The incremental changes in pitching moment indicated by the data closely approximate the changes that would be expected from consideration of the center-of-gravity shifts corresponding to these wing position changes. For example, a 4-inch shift in wing pivot (which corresponds to about a 1-percent change in center-of-gravity position) produced about a 1-percent change in static margin. Incremental changes in the lift and drag with changes in the wing pivot location are probably indicative of variations in the interference effects between the wing and fuselage.

As pointed out previously, the airplane probably experienced ground effect on lift, drag, and pitching moment in the tunnel tests. Although there are no methods available for making accurate corrections to the data for this ground effect, a general indication of the magnitude of the effect can be obtained from previous investigations with delta-wing models in and out of the presence of the ground. (For example, see ref. 7.) The results of these studies would indicate that the airplane in the full-scale tunnel tests experienced slightly higher values of lift-curve slope and L/D, and slightly more negative values of C_m than it would experience out of ground effect. It appears that any corrections for the effect of the ground on lift-curve slope and L/D would be very small.

The effect of the ground on C_m, however, may be more significant since it may involve corrections as large as $\Delta C_m = 0.01C_L$ or $0.02C_L$, and such corrections could greatly affect the longitudinal trim characteristics of the airplane as will be discussed subsequently.

Hinge-moment data for basic configuration.- The hinge-moment coefficients of the wing in pitch measured about the pivot $(0.50c_k)$ as determined in test runs at constant dynamic pressure are presented in figure 14. Figure 15 presents hinge-moment data for the power-off condition at $i_w = 25^\circ$ measured at various dynamic pressures. As in figure 9, a dashed curve has been superimposed on the other curves of figure 15 to represent the 1g flight condition. The incremental hinge moments between the condition of 1g and that of $q = 3.07$ in figure 15 were used to correct the basic data of figure 14 to 1g conditions, and the corrected data are presented in figure 16. Presented in figure 17 are the hinge-moment data for three wing pivot positions corrected in this same manner. Since the hinge-moment data in this case are equivalent to the pitching moment of the wing about the pivot point, the stick-free, static longitudinal stability of the airplane can be determined from the slope of these curves. Although the data show that the airplane is untrimmed for conditions which should be approximately trimmed according to the flight data, stick-free stability is indicated in the moderate lift-coefficient range and instability above and below this range.

Presented in figure 18 are the hinge-moment data for the power-on conditions of figure 16 and the stick forces corresponding to these hinge moments. The data show no consistent effect of wing incidence. It is believed that the differences in the shape of these curves can probably be attributed to normal scatter of data and that an average curve representative of the measured stick forces for all three wing incidences should be used rather than the individual curves. The large stick forces required for trim are believed to be associated with ground effect and will be discussed in more detail in the following section.

Interpretation of longitudinal data for basic configuration.- In figure 19 the static margin $\partial C_m/\partial C_L$ and stick forces determined in the tunnel tests are compared with values measured in flight. The left-hand plots show tunnel data uncorrected for ground effect whereas the right-hand plots indicate the effect of two assumed values of ground-effect correction: $\Delta C_m = 0.01C_L$ and $\Delta C_m = 0.02C_L$. Force-test data on delta wings in and out of ground effect have indicated that corrections of this order of magnitude may apply in the present case. (See ref. 7.)

Two plots at the top of figure 19 show the stick-fixed static margin of the airplane when trimmed at various airspeeds as determined from the tunnel data of figure 11 and from flight data of reference 5. The tunnel data show a slightly higher value of static margin than the flight-test data and indicate stick-fixed stability over a speed range from about 30 to 48 knots. No effect of the ground on static margin is shown because the type of ground effect assumed (ΔC_m as a function of C_L) changes longitudinal trim but does not change the static margin for trimmed conditions at a given lift coefficient or airspeed. Including the ground-effect correction lowers the trim airspeed for any given flight condition as indicated by the vertical lines in the upper right-hand plot.

In the lower plots of figure 19, an average stick-force curve taken from the tunnel data of figure 18 is compared with flight data taken from reference 5. Although the flight-test data shown indicate slightly stable stick forces, there were indications in the flight tests that the airplane in the stick-free condition may have been slightly unstable or neutrally stable. The pilot reported that the airplane had a tendency to drift off speed at various trim settings and that essentially zero stick force was required to move the stick from full-forward to full-aft position. The force-test data of figure 19 indicate a small amount of stick-free stability from about 35 to 41 knots and indicate stick-free instability above and below this speed range. The tunnel data indicate very large pull forces for conditions which should be approximately trimmed according to the flight data. The pull forces are made even greater when the mass unbalance present on the airplane (wing center of gravity ahead of pivot) is taken into account. The plot at the lower right shows the large effect that a correction of $\Delta C_m = 0.01C_L$ or $0.02C_L$ has on the stick-force characteristics. From these results it is seen that a correction of $\Delta C_m = 0.02C_L$ or greater to the tunnel data is required to provide trim in the speed range from 30 to 43 knots.

An indication of the longitudinal trim capability of the airplane with various wing incidences and fore and aft wing pivot positions is presented in figure 20. The tunnel data are shown for no ground-effect correction and for the two amounts of correction illustrated in figure 19. For the wing-incidence range and wing-position travel available, there appears to be ample capability for trimming at the higher speeds but only limited capability for trimming in the low speed range, unless the ground-effect correction turns out to be fairly large. However, if $\Delta C_m = 0.02C_L$ proves to be the proper ground-effect correction factor, the lower plot of figure 20 indicates that the airplane would have more than enough control power to trim to the stall.

Effect of boltrope and battens.- The results of tunnel tests to evaluate the effect of trailing-edge boltrope and battens on the longitudinal characteristics of the airplane are presented in figures 21(a) and 21(b). The data of figure 21(a) show that changing the boltrope geometry from the slack condition to the basic condition or to conditions of reduced boltrope length (up to 1 inch from the basic condition) produced relatively small changes in the lift, drag, and pitching-moment characteristics of the airplane. Reducing the boltrope length by 4.5 inches produced a large incremental change in the longitudinal characteristics and also a reduction in static longitudinal stability.

Presented in figure 21(b) are the results of tests to evaluate the effect of trailing-edge battens. These data indicate that the batten arrangements investigated had little effect on the lift, drag, and pitching-moment characteristics of the airplane.

In the tunnel tests, an attempt was made to eliminate or to minimize the large depression in the aft portion of the wing by doubling the length of the original battens and also by rearranging the double-length battens. These changes did not appear to improve the wing contour characteristics appreciably, and the depression simply moved forward on the wing remaining just ahead of the battens.

Effect of keel trailing-edge deflection for pitch control.- As part of a general study to explore other methods of providing control for parawing configurations, tests were conducted in which the trailing edge of the keel was hinged to deflect upward and downward for pitch control. The results of these tests (presented in figs. 22(a) and 22(b)) show that a downward deflection of 5° from neutral produced relatively large incremental changes in lift, drag, and pitching-moment characteristics but that the effectiveness decreased rapidly for higher deflections. An upward deflection from neutral produced the desired changes in longitudinal characteristics but caused excessive flutter in the fabric. Tests for this deflection were therefore limited to only high angles of attack where the trailing-edge flutter was less critical. The hinge-moment data of figure 22(b) show that incremental stick forces of about 50 pounds were required for 5° of deflection over the angle-of-attack range considered practical (above keel angles of attack of about 20°).

Although the results of figures 22(a) and 22(b) do not indicate a great deal of promise for this particular control system, it is felt that some type of trailing-edge control (such as boltrope, wing-tip, or keel device) could be made to operate efficiently for pitch control. Before such devices can be made practical, however, some means of providing positive $C_{m,o}$ is necessary to take advantage of an initial downward deflection as a neutral condition since upward deflections from the normal wing contour tend to produce excessive trailing-edge flutter. In connection with flutter problems of this type, it was observed in the tests with the present keel control system that a downward deflection of the rear part of the keel eliminated the trailing-edge flutter and furthermore eliminated the large depression in the aft portion of the wing which had existed throughout the test program. Photographs of the wing with the keel deflected in a downward position are shown in figure 4(a).

Lateral Stability and Control

Lateral stability.- The lateral stability characteristics of the airplane are presented in figures 23, 24(a), and 24(b) in terms of the lateral coefficients measured at sideslip angles of 5° and -5°. Most of the data are plotted against platform angle of attack except for those presented in figure 23 where it was more convenient to compare the effects of wing incidence by plotting the data against lift coefficient. For these tests, the airplane was in the basic configuration as defined previously in this report. The results indicate that for the power-on, rudder-on case (fig. 24(a)) the airplane had fairly good lateral trim at the lower angles of attack, that is, the rolling and yawing moments are approximately symmetrical at sideslip angles of 5° and -5°. It should be pointed out that this condition incorporates the 1-inch asymmetric boltrope setting for good lateral trim in powered flight. It is apparent from the remainder of the data (figs. 23 and 24) that for all of the power-off conditions and for the power-on condition with the rudder off, the airplane is out of trim in yaw to the left. These out-of-trim characteristics are apparently directly attributable to the asymmetric boltrope setting, which was necessary for lateral trim in the power-on, rudder-on condition. It appears, therefore, that the asymmetrical boltrope setting was necessary in the basic condition to offset a lateral trim change caused by some induced effect of power on the rudder.

The basic lateral stability data are summarized in figures 25 and 26 as the variation with angle of attack of the static lateral stability derivatives C_{Y_β} (the side-force parameter), C_{n_β} (the directional-stability parameter), and C_{l_β} (the effective-dihedral parameter). For a wing-incidence angle of 25° (fig. 25), the airplane was directionally stable throughout the angle-of-attack range tested except for the rudder-off conditions at the highest angles of attack. Power is shown to increase the directional stability when the rudder is installed, but there is little effect of power on the stability with the rudder off and little effect of the rudder on stability with power off. The values of the effective-dihedral parameter are rather large and generally increase with increasing angle of attack. Wing incidence has essentially no effect on the values of the derivatives for keel angles of attack up to about 35°. (See fig. 26.) The inconsistencies at higher angles of attack are probably related to stall effects and interference effects between the wing and platform.

Wing-bank control.- The variation of the lateral coefficients produced by banking the wing 5° and -5° is presented in figures 27 and 28. All of the wing-bank control tests were made with the rudder installed but undeflected. These data show the same general effects of power on lateral trim noted previously in the variation of the lateral coefficients at sideslip angles of 5° and -5°. The trim changes due to power are larger for the 28.5° wing-incidence angle than for the 25° angle, and this effect is probably related mainly to the higher value of T_c at the higher wing incidence.

The data of figures 27 and 28 are presented in figure 29 in the form of incremental lateral-force and lateral-moment coefficients due to banking the wing 5°. In general, the data indicate low rolling effectiveness and favorable yawing moments at the lower lift coefficients. The roll effectiveness decreases and becomes negative and the yawing moments become adverse at the higher lift coefficients. With power on ($i_w = 25°$, fig. 29(b)), the rolling effectiveness is somewhat improved, and the yawing moments are more favorable than with power off. There appear to be no consistent effects of wing incidence on the magnitude of the control moments, but positive roll control is indicated to higher values of lift coefficient for the wing-incidence angle of 25°. (See fig. 29(a).)

The reason for the low rolling effectiveness of the wing-bank control system is explained in figure 30, which shows for both the power-on and power-off conditions how the forces and moments from two different sources combine to produce the resultant control moments. The bottom plots of figure 30 show a comparison of the measured rolling moments (solid curves, taken from fig. 29(b)) with the moments calculated from the data of previously presented figures (short-dash curves). The short-dash curve in each case is the sum of the two long-dash curves, which represent the independent and opposite contributions of C_L and C_{l_β}. The upper long-dash curve $\left(C_L \sin \phi \frac{z}{b}\right)$ represents the rolling moment produced about the center of gravity by banking the wing lift vector over 5° with the wing pivot at a height z/b above the center of gravity. When the wing banks about an axis parallel to the wing keel as in the present case, an angle of sideslip of the wing is produced $\left(\sin \beta = \sin \alpha_k \sin \phi\right)$ and this sideslip is adverse, that is, a nose left sideslip with a right wing bank. This adverse sideslip angle introduces an

adverse rolling moment through the effective-dihedral parameter C_{l_β} as indicated by the lower long-dash curves. Inasmuch as this adverse rolling moment is almost as large as the favorable rolling moment produced by banking the lift vector, the resultant rolling effectiveness is very small.

The middle plots of figure 30 show a comparison of the measured and calculated yawing moments produced by banking the wing. In this case C_L produces adverse yawing-moment increments and β acts through C_{n_β} to produce favorable yawing moments. The wing lift vector produces an adverse yawing moment when it is tilted because it acts behind the center of gravity (that is, x/b is negative). The favorable yawing moment produced by β results from the fact that the wing is directionally stable (positive C_{n_β}) and therefore produces a positive yawing moment when the wing is banked to the right because of the accompanying adverse sideslip angle. A relatively small favorable yawing moment is produced by the displaced drag vector of the wing, and its contribution has been combined with the contribution of C_{n_β} in order to simplify this comparison. It is interesting to note that the loss of wing directional stability at the higher angles of attack accounts for the adverse yawing moments produced by banking the wing as shown in figure 29.

Presented in figure 31 are the incremental hinge-moment coefficients for a wing-bank angle of 5° as measured directly from the wheel force. In addition, hinge-moment data derived from the rolling moment about the wing pivot axis are presented for purposes of comparison. As implied in the preceding discussion, the only rolling moment produced about the wing pivot axis when the wing is banked is that moment due to C_{l_β} of the wing in combination with the adverse sideslip angle resulting from banking the wing; therefore, calculation of this rolling moment provides one means of evaluating the hinge moment due to banking the wing, and it should be equal and opposite to the hinge moment. A second means of obtaining the rolling moment about the wing pivot axis is to transfer the measured roll-control data from the center of gravity to the wing pivot axis. The agreement in the hinge-moment data obtained directly from the wheel force and those calculated from the measured rolling moments is relatively good. The stick forces shown on the right-hand side of figure 31 were computed from the average hinge moments for 1g flight conditions over the angle-of-attack range shown. The roll stick force of about 75 pounds ($i_w = 25^\circ$; $T_c = 0.135$; $\alpha_k = 25^\circ$) is in general agreement with values measured in flight tests.

The roll-control data presented in figures 27 to 29 were obtained in tunnel tests in which the platform of the airplane was mounted on the tunnel support struts and remained fixed when the wing was banked. As pointed out previously, when the wing banks about an axis parallel to the wing keel as in the present case, an adverse angle of sideslip of the wing is produced ($\sin \beta = \sin \alpha_k \sin \phi$). This test condition does not exactly represent what happens in flight when the wing is banked. Actually, when a roll control is applied in flight, the wing and platform momentarily roll and sideslip in opposite directions; the amount each moves is determined by the relative inertia and the aerodynamic moments of the two. Thus, the true flight condition following the abrupt deflection of the

wing-bank control system can be represented by a case somewhere between the two extreme cases of platform fixed at zero bank and sideslip (as in the present tunnel tests) and wing fixed at zero bank and sideslip (with the platform being deflected in bank and sideslip to provide roll control).

Figure 32 shows how the rolling-, yawing-, and hinge-moment coefficients vary between the two extreme cases. In the plots of the moments against bank angle, the wing-bank angle of 5° (and platform-bank angle of 0°) represents the test condition used in the tunnel, whereas the wing-bank angle of 0° (and platform-bank angle of -5°) represents the wing-fixed case. For the test condition illustrated ($i_w = 25^\circ$; $\alpha = 0^\circ$; and 5° right wing-bank control), there is a difference of about 2° in sideslip angle between the wing and platform, with the wing being sideslipped 2° more nose left than the platform. In the ΔC_l and ΔC_n plots, the horizontal long-dash lines represent the effect of tilting the lift vector, and the short-dash lines represent the moments produced by the wing and platform when they sideslip. The heavy solid lines are the resultant values obtained by adding the long- and short-dash lines. The tunnel-test data point is shown by the symbols at a wing-bank angle of 5°. The ΔC_h plot at the right in figure 32 was constructed in a similar manner, with the long-dash line representing the hinge moments about the pivot produced by the weight of the platform and with the short-dash lines representing the aerodynamic moments about the wing pivot produced by the wing and platform when they sideslip. The agreement appears to be satisfactory between the tunnel-test data points and the resultant curves in all three plots of figure 32.

Large effects of sideslip on all the moments are indicated in figure 32 so that the results for the wing-fixed and platform-fixed conditions appear to be quite different. For example, if the tunnel tests had been run with the wing fixed at zero bank and sideslip, the results would have shown much higher rolling moments but would also have shown adverse yawing moments for the wing-bank control system. Actually, the overall control effectiveness should be about the same for the two cases inasmuch as the yawing moments produce sideslip of the airplane (either favorable or adverse), and this sideslip, acting through the effective-dihedral parameter C_{l_β}, produces rolling moments that tend to equalize the net rolling moment acting in the two cases. Perhaps the best indication of the net roll-control effectiveness shown in the plots of figure 32 is the rolling moment for the case where the yawing moment is zero. This condition occurs at the point where the wing is banked 3.5° right and the platform 1.5° left. This proportion of initial wing bank to platform bank also appears generally reasonable on the basis of estimated relative inertias and the aerodynamic moments of the wing and platform as indicated by the results of one-degree-of-freedom, initial-response calculations. Inasmuch as the net rolling moment (rolling moment for the case when yawing moment is zero) appears to be of the most significance in evaluating control effectiveness in the wing-bank control system, an equation has been developed in the appendix to facilitate calculation of the net rolling moment when only the most fundamental aerodynamic characteristics are known.

Hinged wing-tip controls.- In view of the inadequacies of the existing wing-bank control system (low roll-control effectiveness and high hinge moments), tests were conducted to evaluate the effectiveness of two alternate roll-control systems.

These alternate control systems were described previously as wing-tip controls A and B and are illustrated in figure 3 and shown in photographs in figure 4. In both tests the wing-bank system was rigidly locked at zero deflection.

The results of the tests made to evaluate the effectiveness of these two alternate control systems are presented in figure 33, and a comparison of these data shows much better rolling moments for control A than for control B. In fact, no consistent roll effectiveness was obtained with control B. Both systems appear to have adverse yawing moments when the control is deflected in a direction to produce positive roll control, and these adverse yawing moments generally become larger with increasing angle of attack. The results presented in this comparison are for deflection of the control devices on the left wing tip only. In order to see what could be done to minimize the adverse yaw characteristics, the data of figure 33(a) have been used to prepare figure 34 for the case of differentially operated controls on both wing tips. Data are presented only for control A inasmuch as control B was found lacking in roll effectiveness. Data are shown for several neutral settings of the hinged wing tip. It is apparent that an inward neutral setting tends to reduce the adverse yawing moments due to control deflection at the higher angles of attack such that with both tips initially set at 5° inward, the adverse yawing moments due to control deflection are essentially reduced to zero throughout the angle-of-attack range. For this case, the rolling moments with a wing-tip deflection of only 5° or -5° (ΔC_l = 0.011 to 0.015) are appreciably larger than values obtained with the wing-bank control system, and also, roll-control effectiveness is maintained at the higher angles of attack. The hinge moments are also appreciably lower than those obtained with the wing-bank system; and, for the zero-angle-of-attack condition previously cited, they would result in wheel forces about half as great as those experienced in flight tests.

Comparison of roll-control systems.- The wing-bank-control characteristics of the airplane are summarized in figure 35. Also presented in this figure for comparison are data for hinged wing-tip control system A. In addition, estimated control characteristics are presented for this wing-bank control system with negative geometric dihedral of the wing added.

In the left plot of figure 35, incremental rolling-moment coefficient ΔC_l is plotted against incremental roll hinge-moment coefficient ΔC_h. The horizontal dashed line represents the value of ΔC_l required to produce a value of $pb/2V$ of 0.09, based on the relationship $\frac{pb}{2V} = \frac{C_l}{C_{l_p}}$ and an estimated value of the damping-in-roll parameter C_{l_p} of -0.15. The value of $pb/2V$ of 0.09 is the minimum value specified in the handling-qualities requirements for a light liaison airplane. This criterion is presented here merely to establish a reference for purposes of comparison and is not intended to imply that a value of $pb/2V$ of 0.09 is a valid requirement for parawing applications. For recovery-system applications, a much smaller value may well prove to be acceptable; whereas, for utility-airplane applications (which may involve flight at very low speeds in confined areas), an even larger value than 0.09 may be required. In any event, considerably more research and flight experience will be required to establish

the proper criteria for the various applications envisioned for the parawing. Also indicated along the ΔC_h scale are the hinge-moment coefficients that correspond to stick forces of 50 to 100 pounds. The solid circle at the lower right, representing the wing-bank control system installed on the airplane (net roll control as represented by the $\Delta C_n = 0$ case), shows that banking the wing 5° requires about 70 pounds of stick force and only produces about one-third of the rolling effectiveness required by the $pb/2V = 0.09$ criterion. Calculations indicate (open symbol) that reducing C_{l_β} by using a negative geometric dihedral angle of the wing of 18° would decrease the stick force to about 45 pounds and increase the effectiveness to about one-half of the criterion value. The wing-tip control system appears to be quite effective in that a wing-tip-control deflection of approximately 7° produces a value of $pb/2V$ of 0.09 with appreciably lower stick force than that of the wing-bank system (30 to 45 pounds, depending on neutral setting of the tips).

The right-hand plot of figure 35 shows the incremental yawing moments produced by the various roll-control arrangements. The yawing moment is zero for the wing-bank control system because this condition was specifically selected from figure 32 to give the best indication of net roll effectiveness.

Although the yawing moments with the hinged wing-tip control appear to be quite small for the angle-of-attack condition represented in this figure ($\alpha_p = 0^\circ$; $i_w = 25^\circ$), adverse yawing moments of considerable magnitude would be encountered at higher angles of attack unless an initial inward neutral setting of the tips was used. An inward neutral setting of about 5° in combination with about $\pm 7^\circ$ differential deflection of the wing tips should provide roll control of sufficient magnitude to meet the $pb/2V = 0.09$ criterion with no adverse yaw throughout a keel angle-of-attack range from 20° to 35°.

Rudder control.- The rudder-effectiveness data are presented in figure 36 in the form of side-force, yawing-moment, and rolling-moment coefficients. The rudder was not very effective in producing yawing moments with power off, but the effectiveness increased by a factor of about 5 with power on ($T_c = 0.192$). The rolling moments produced by rudder deflection were negligible in both the power-off and power-on cases. If the yawing-moment coefficient produced by a rudder deflection of 20° is equated to C_{n_β} for the power-on condition, then the sideslipping capability of the airplane through rudder deflection can be estimated. From the sideslip angle produced in this manner, the rolling moment produced by the wing through the effective dihedral C_{l_β} can then be estimated. Calculations made from this relationship indicated that a rudder deflection of 20° with power on would produce an incremental rolling moment about double the net value obtained by banking the wing 5°. This increased rolling effectiveness is one of the reasons the pilot made extensive use of the rudder in flying the airplane. It should be pointed out, however, that the roll response obtained through this indirect control is subject to appreciable time lag and other dynamic effects, and therefore the control effectiveness may be considerably different for such a control system than that estimated on the basis of static derivatives alone.

SUMMARY OF RESULTS

The results of the full-scale tunnel investigation of the performance and static stability and control characteristics of a flexible-wing manned test vehicle are summarized as follows:

1. The tunnel tests showed that the maximum lift coefficient of the airplane occurred at a keel angle of attack of 42° and was 1.24 with power off and 1.33 with power on. The maximum lift-drag ratio was about 5.5.

2. With stick fixed, the airplane had about neutral static longitudinal stability at keel angles of attack below 20°, a moderate degree of stability from 20° to 35°, and longitudinal instability, or pitch-up, from 35° to 42°. At an angle of attack of the keel of 42° the airplane again became stable. With the stick free, the longitudinal stability was generally worse with the airplane being unstable at the lower angles of attack, about neutrally stable in the intermediate range, and unstable at the higher angles of attack.

3. The airplane, in general, was directionally stable and had positive effective dihedral throughout the angle-of-attack range investigated.

4. The lateral control provided by banking the wing did not appear to be satisfactory because of inadequate rolling moments and excessively high stick forces. This result is in agreement with flight-test results.

5. Analysis of the factors contributing to the low rolling effectiveness obtained by banking the wing indicated that the use of negative geometric dihedral of the wing to reduce the high values of positive effective dihedral may be a relatively simple means of improving the effectiveness of this type of roll-control system.

6. Analysis of the tunnel data indicated that the rudder was generally a better roll-control device with power on (since the rudder is in the slipstream of the pusher propeller) than the wing-bank control system. The rudder provides roll control in an indirect manner by sideslipping the airplane and making use of the large value of effective dihedral (rolling moment due to sideslip).

7. The hinged wing-tip control device tested on the airplane appeared promising in that it provided higher rolling effectiveness with lower stick forces than that of the wing-bank control system provided on the airplane.

Langley Research Center,
National Aeronautics and Space Administration,
Langley Station, Hampton, Va., June 4, 1963.

APPENDIX

DERIVATION OF AN EXPRESSION FOR CALCULATING THE NET ROLLING MOMENT PRODUCED BY THE WING-BANK OR CENTER-OF-GRAVITY-SHIFT CONTROL SYSTEM

Sketch 1 shows the relationship of the lift, drag, and resultant-force vectors of a parawing configuration in trimmed, level flight. For such a condition, the resultant-force vector must pass through the center of gravity and, therefore, from the geometry in this case it can be shown that $\frac{z/b}{x/b} = \frac{L}{D}$.

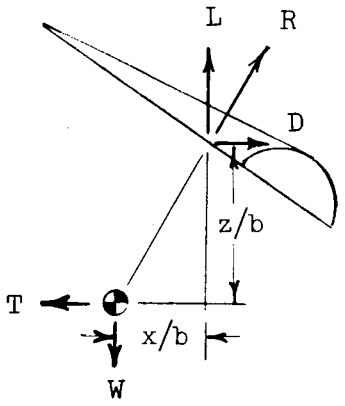

Sketch 1

When the wing is banked for roll control, the lift vector is tilted and has a lateral component $C_L \sin \phi$ as shown in sketch 2. For the condition shown, it is seen that the lateral component of the lift vector produces a rolling moment about the center of gravity through the arm z/b $\left(\text{thus, } \Delta C_l = \frac{z}{b} C_L \sin \phi\right)$. Also, since this vector component is behind the center of gravity, it produces an adverse yawing moment about the center of gravity through the arm x/b $\left(\text{thus, } \Delta C_n = \frac{x}{b} C_L \sin \phi\right)$. In order to determine the net rolling moment in this case (the rolling moment for zero yawing moment), it is necessary to take into account the equilibrium sideslip condition where:

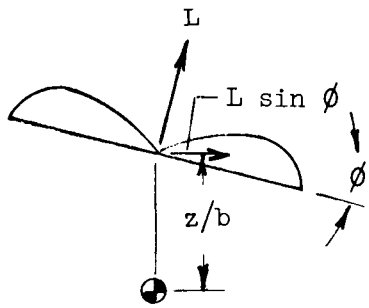

Sketch 2

$$\beta = \frac{\Delta C_n}{C_{n_\beta}} = \frac{\frac{x}{b} C_L \sin \phi}{C_{n_\beta}} \qquad \text{(A1)}$$

From this established value of β, the incremental rolling moment introduced through the effective-dihedral parameter C_{l_β} can then be determined as

$$\Delta C_l = C_{l_\beta} \beta = C_{l_\beta} \frac{\frac{x}{b} C_L \sin \phi}{C_{n_\beta}} \qquad \text{(A2)}$$

For normal conditions, the directional-stability and effective-dihedral parameters of parawings are positive $\left(+C_{n_\beta},\ -C_{l_\beta}\right)$ and, therefore, in a right wing bank the value of ΔC_l determined from equation (A2) would be adverse, or negative, and would subtract from the favorable rolling moment produced by the lift vector. The net incremental rolling moment produced in this case can therefore be written as

$$\Delta C_{l,\text{net}} = \frac{z}{b} C_L \sin \phi + \frac{C_{l_\beta}}{C_{n_\beta}} \frac{x}{b} C_L \sin \phi \tag{A3}$$

or

$$\Delta C_{l,\text{net}} = \frac{z}{b} C_L \sin \phi + \frac{C_{l_\beta}}{C_{n_\beta}} \frac{x}{b} \frac{z/b}{z/b} C_L \sin \phi \tag{A4}$$

Factoring out $\frac{z}{b} C_L \sin \phi$ and substituting L/D for $\frac{z/b}{x/b}$ gives

$$\Delta C_{l,\text{net}} = \frac{z}{b} C_L \sin \phi \left(1 + \frac{C_{l_\beta}}{C_{n_\beta}} \frac{1}{L/D}\right) \tag{A5}$$

The term $1 + \frac{C_{l_\beta}}{C_{n_\beta}} \frac{1}{L/D}$ is called the rolling-effectiveness factor and is convenient for estimating very readily the percentage of rolling effectiveness that is actually available for a configuration employing the wing-bank or center-of-gravity-shift control system. When this factor approaches 1.0 the loss of roll-control effectiveness is minimized, whereas, when this factor approaches 0 the net roll-control effectiveness also approaches 0. For configurations having high negative values of $\frac{C_{l_\beta}}{C_{n_\beta}}$ and low values of L/D, the rolling-effectiveness term becomes small and therefore the net rolling moment produced in such cases is reduced. Configuration changes which would tend to reduce the ratio $\frac{C_{l_\beta}}{C_{n_\beta}}$ and increase L/D are obviously desirable from the standpoint of net roll-control effectiveness. One of the most obvious improvements would be to reduce the derivative C_{l_β} by introducing negative geometric dihedral of the wing. (Reduction of C_{l_β} by reducing z/b would defeat the purpose because the primary roll-control term $\left(\frac{z}{b} C_L \sin \phi\right)$ would also be reduced.)

For purposes of comparison, values of $\Delta C_{l,\text{net}}$ calculated from equation (A5) are presented in figure 37. These calculations were made for the rudder-on

configuration, with power off and on, by using the measured force-test data corresponding to these conditions. The calculated data show the loss in rolling effectiveness at the higher angles of attack indicated previously by the measured data of figure 29 although, as expected, the calculations generally show higher rolling effectiveness than the measured data in the lower angle-of-attack range. Good agreement is shown between values of $\Delta C_{l,net}$ calculated from equation (A5) and those determined graphically in figure 32 for $\alpha_p = 0^\circ$ $(i_w = 25^\circ)$ since in both cases the rolling moments were calculated on the basis of zero yawing moment.

REFERENCES

1. Rogallo, Francis M., Lowry, John G., Croom, Delwin R., and Taylor, Robert T.: Preliminary Investigation of a Paraglider. NASA TN D-443, 1960.

2. Naeseth, Rodger L.: An Exploratory Study of a Parawing as a High-Lift Device for Aircraft. NASA TN D-629, 1960.

3. Hewes, Donald E.: Free-Flight Investigation of Radio-Controlled Models With Parawings. NASA TN D-927, 1961.

4. Johnson, Joseph L., Jr.: Low-Speed Wind-Tunnel Investigation to Determine the Flight Characteristics of a Model of a Parawing Utility Vehicle. NASA TN D-1255, 1962.

5. Landgraf, F., Everett, W. L., Burich, J. H.: Flexible-Wing Manned Test Vehicle. TCREC Tech. Rep. 62-25 (Ryan Rep. 61B131A), U.S. Army Transportation Res. Command (Fort Eustis, Va.), June 25, 1962.

6. DeFrance, Smith J.: The N.A.C.A. Full-Scale Wind Tunnel. NACA Rep. 459, 1933.

7. Scallion, William I.: The Effect of Ground on the Low-Speed Aerodynamic, Control, and Control Hinge-Moment Characteristics of a Delta-Wing—Fuselage Model With Trailing-Edge Controls. NACA RM L54H03, 1954.

TABLE I.- CHARACTERISTICS OF THE AIRPLANE

Airplane weight, lb	1,840
Keel and leading-edge length, ft	28
Leading-edge sweep angle (flat plan geometry), deg	45
Span (based on 45° leading-edge sweep), ft	39.6
Wing area (flat plan geometry, 45° leading-edge sweep), sq ft	555
Leading-edge sweep angle (flight condition), deg	50
Wing aspect ratio	2.82
Engine power, hp	180
Propeller diameter, ft	6
Rudder dimensions:	
Area, sq ft	13.4
Span, ft	4.75
Chord, ft	3.75
Aspect ratio	1.70

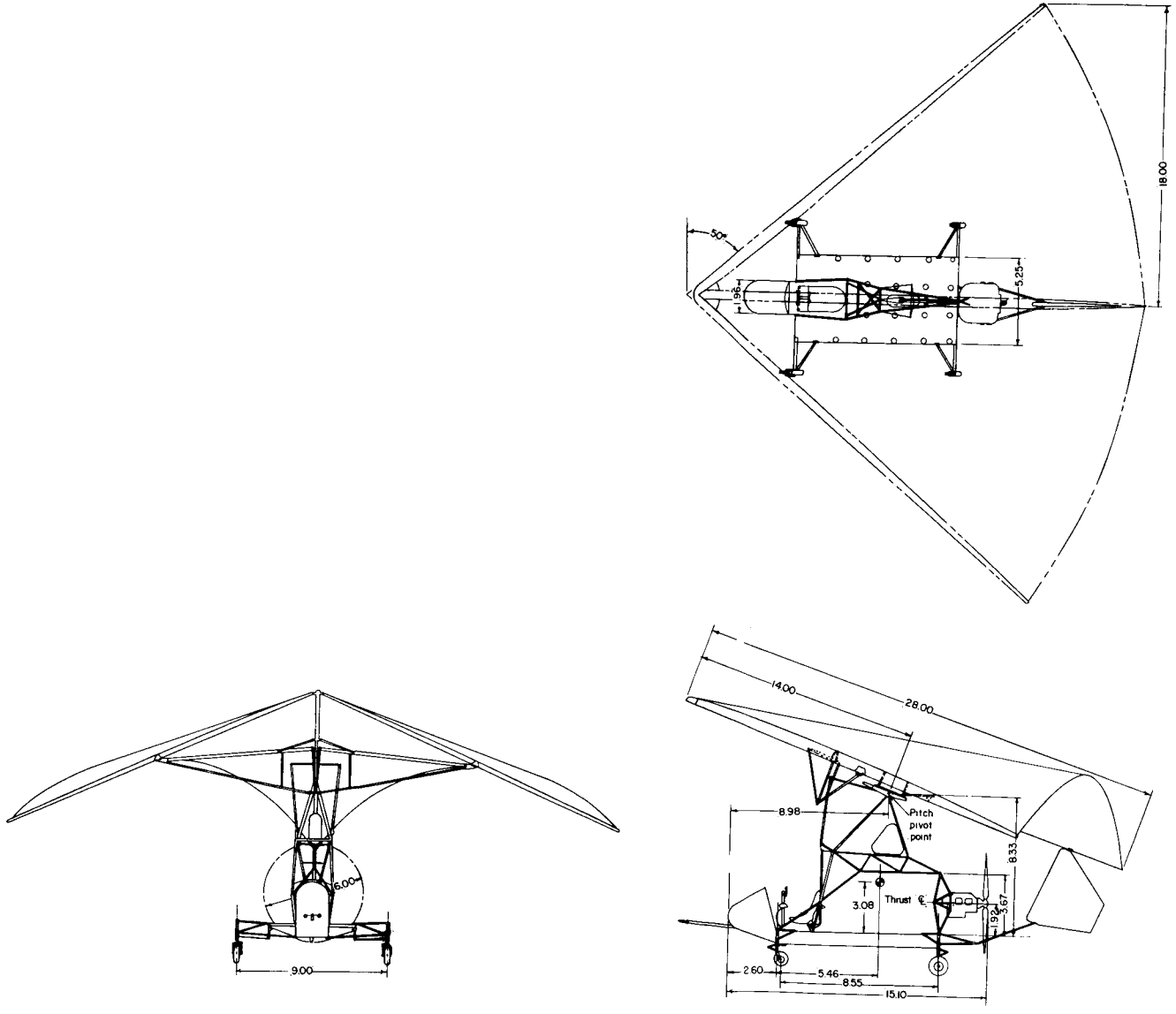

(a) Basic configuration.

Figure 1.- Three-view drawing of flexible-wing airplane used in investigation. All dimensions are in feet.

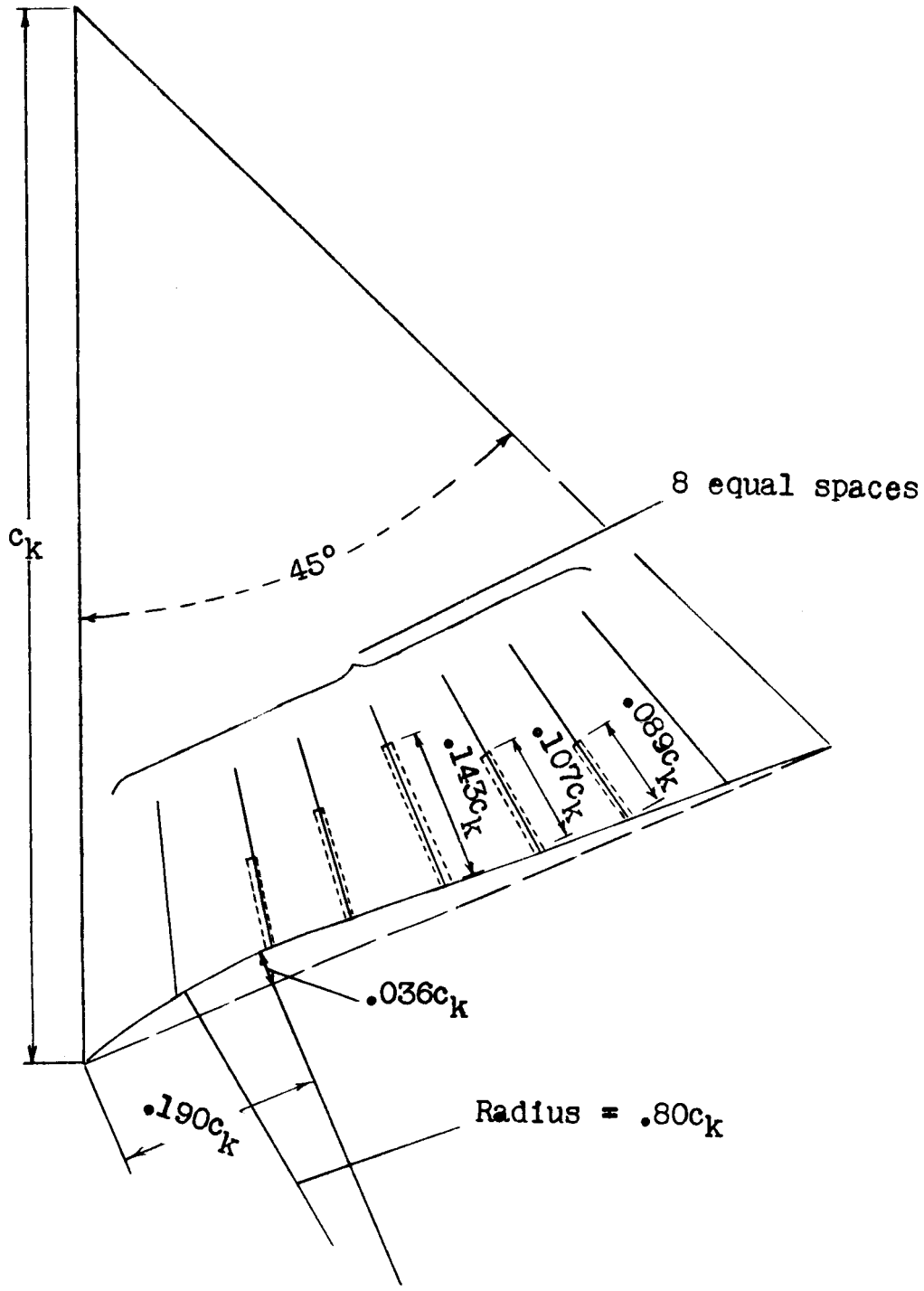

(b) Flat plan geometry of wing showing battens and trailing-edge scallop.

Figure 1.- Concluded.

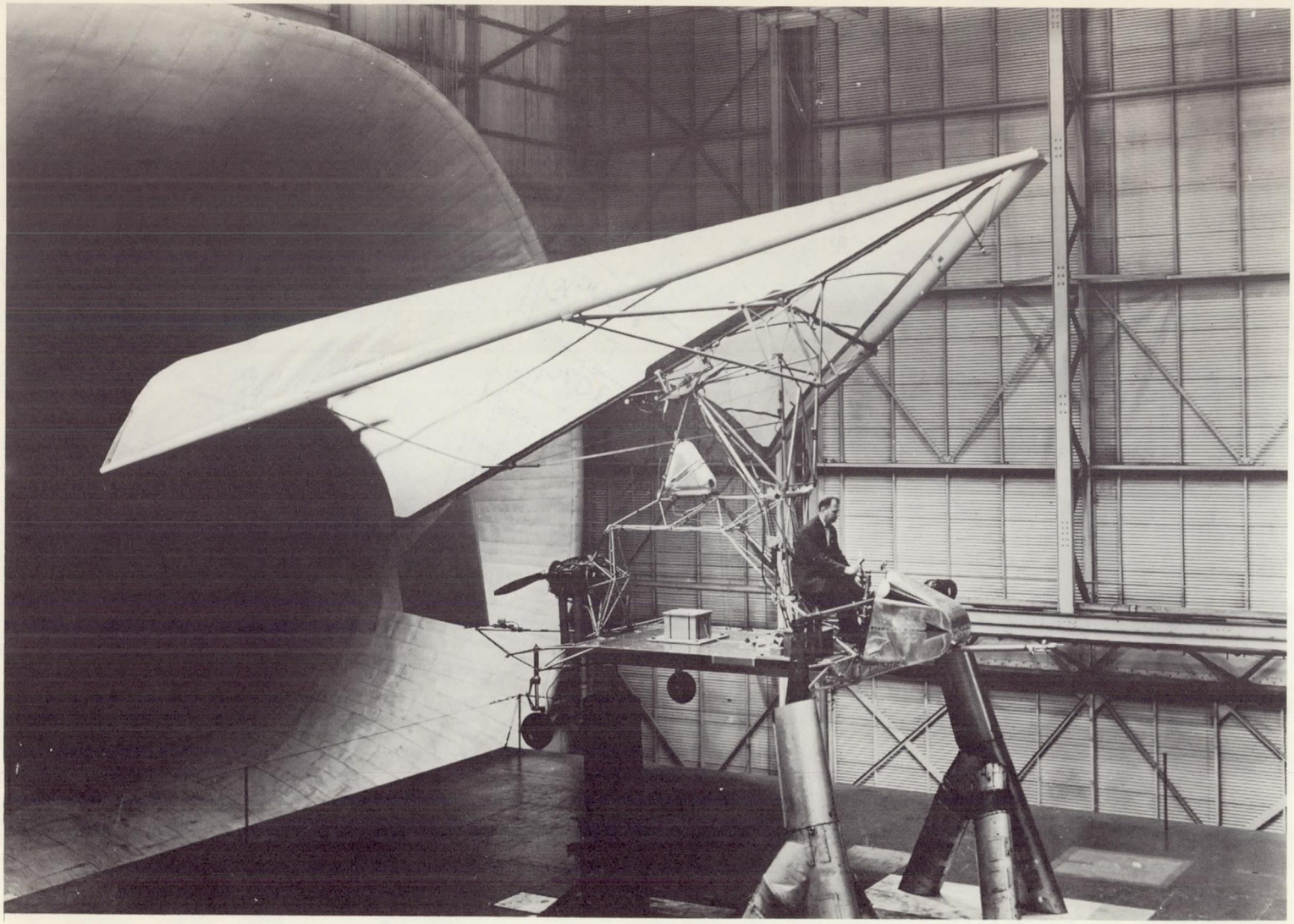

(a) Three-quarter front view showing support-system details. L-62-631

Figure 2.- Photographs of airplane mounted for force testing in Langley full-scale tunnel.

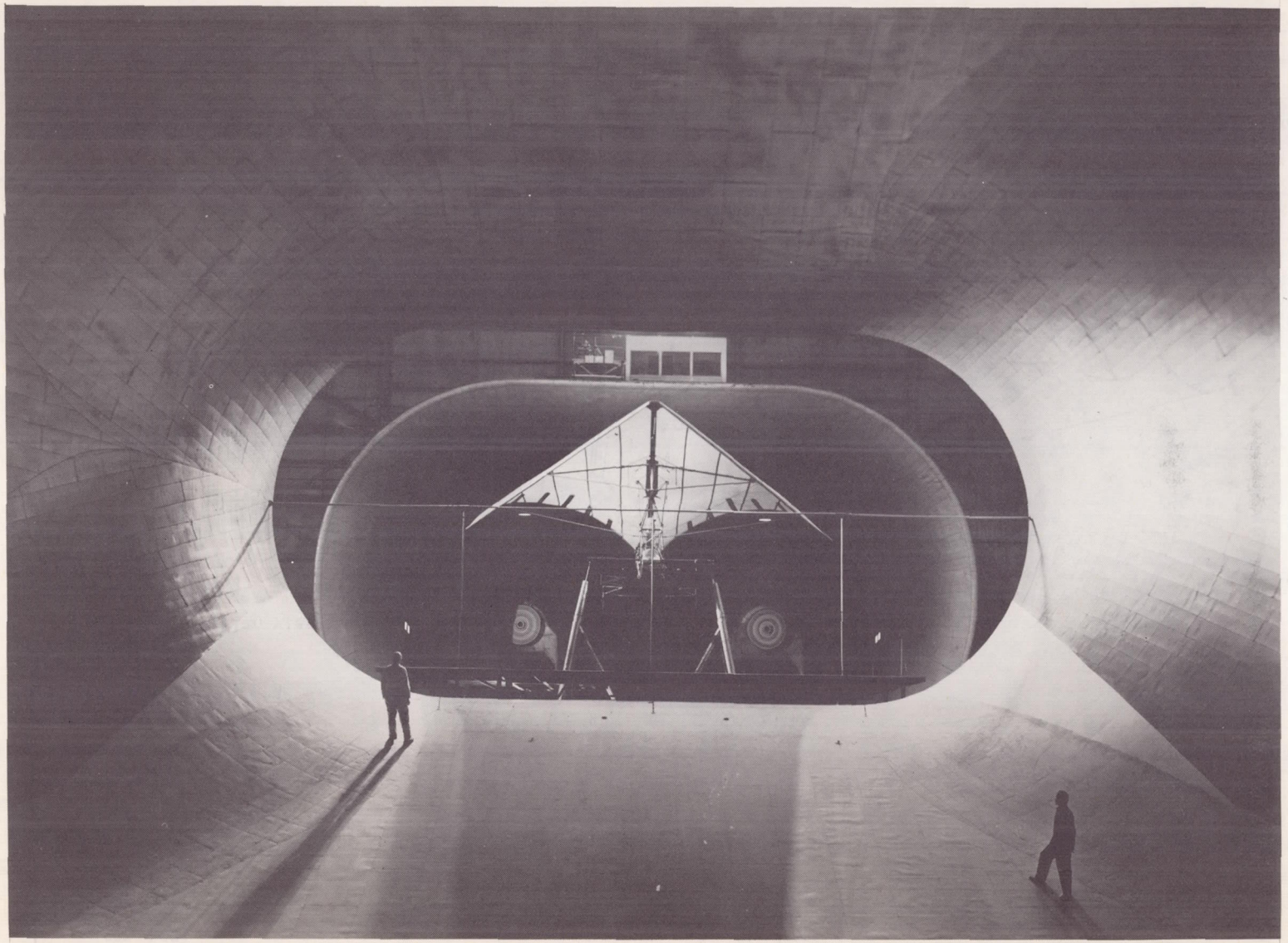

(b) Front view showing relation of airplane to test section. L-62-627

Figure 2.- Concluded.

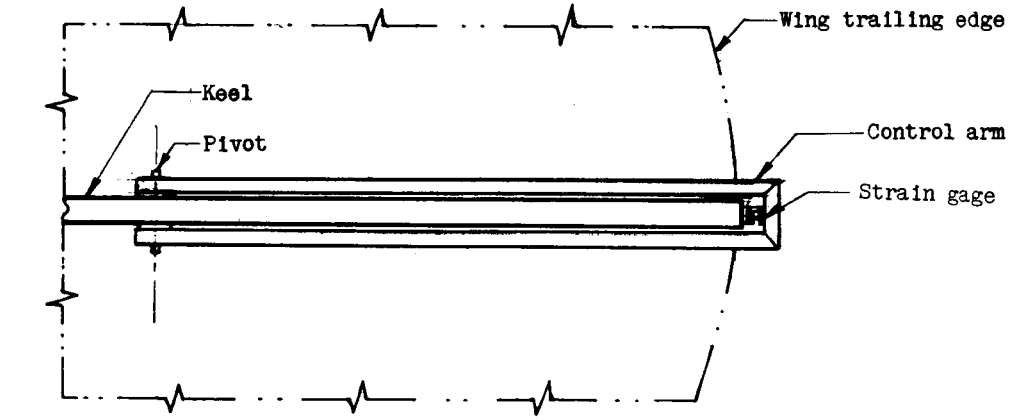

Plan view

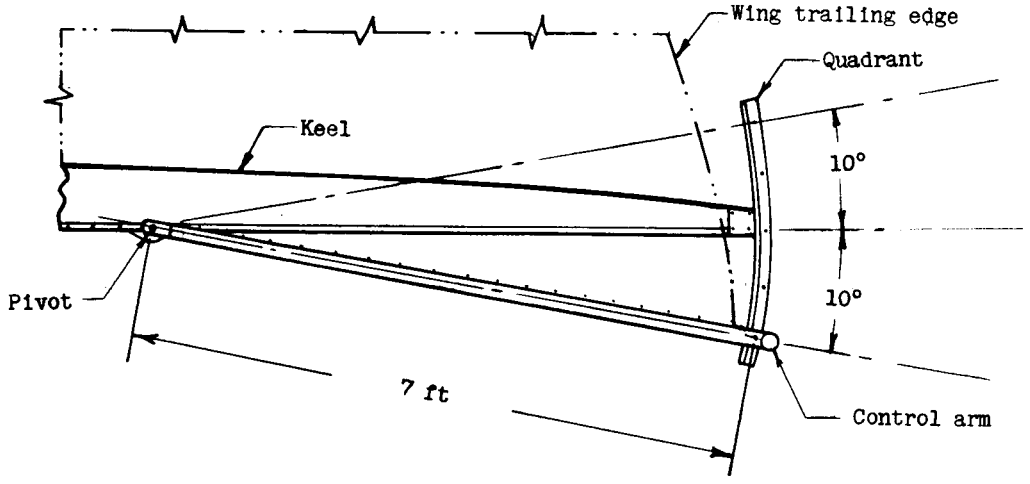

Side view

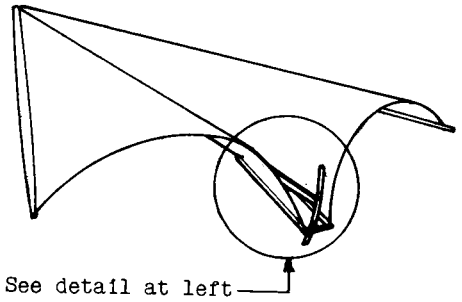

Perspective view of wing showing keel trailing-edge control in downward position

(a) Keel trailing-edge control system.

Figure 3.- Schematic drawing of alternate control systems used in investigation.

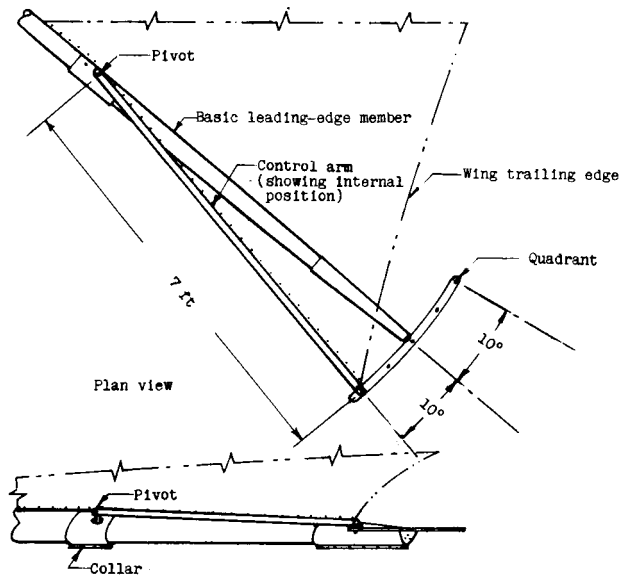

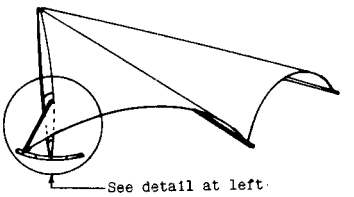

Perspective view of wing showing control in outward position

(b) Wing-tip control A.

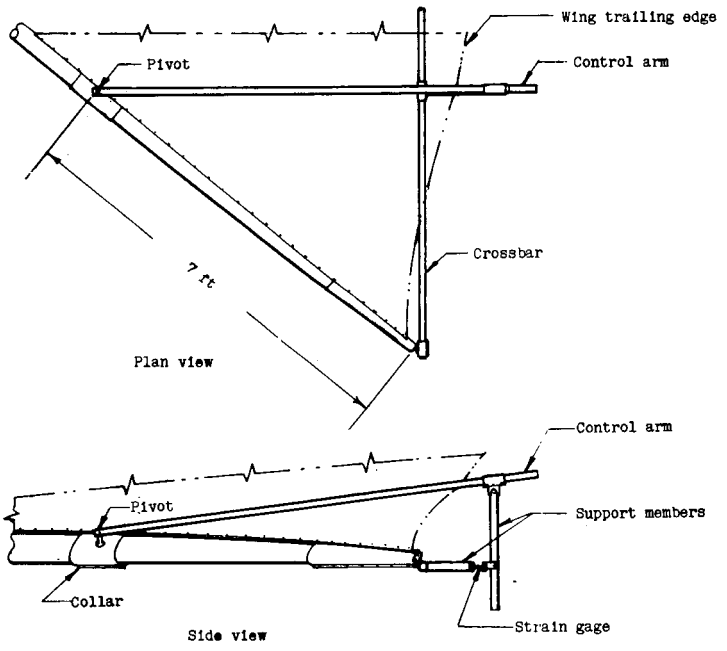

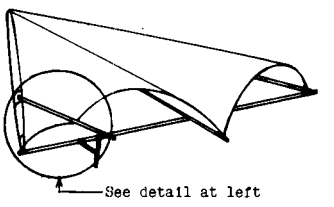

Perspective view of wing showing control in downward position

(c) Wing-tip control B.

Figure 3.- Concluded.

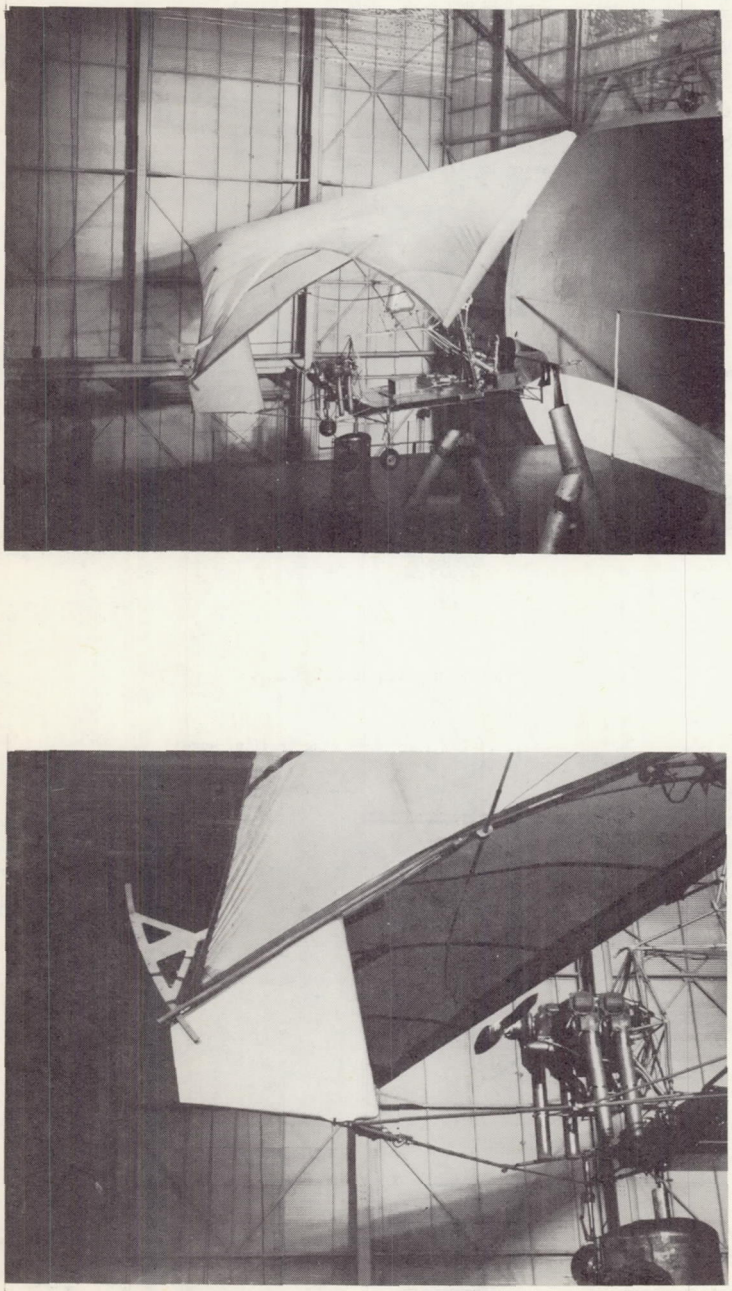

(a) Keel trailing-edge control system. L-63-3162

Figure 4.- Alternative control systems used in the investigation.

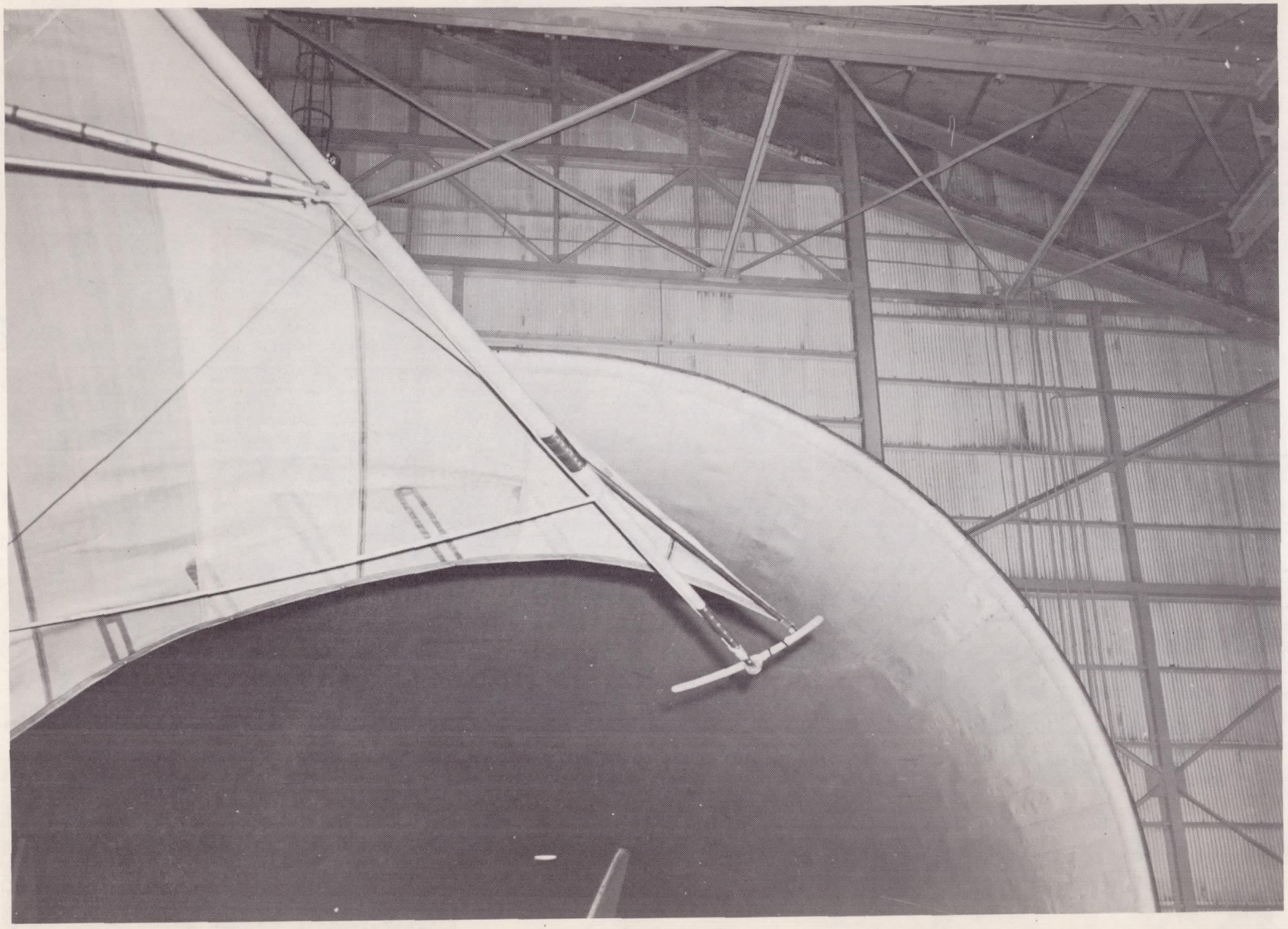

(b) Wing-tip control A. L-62-1259

Figure 4.- Continued.

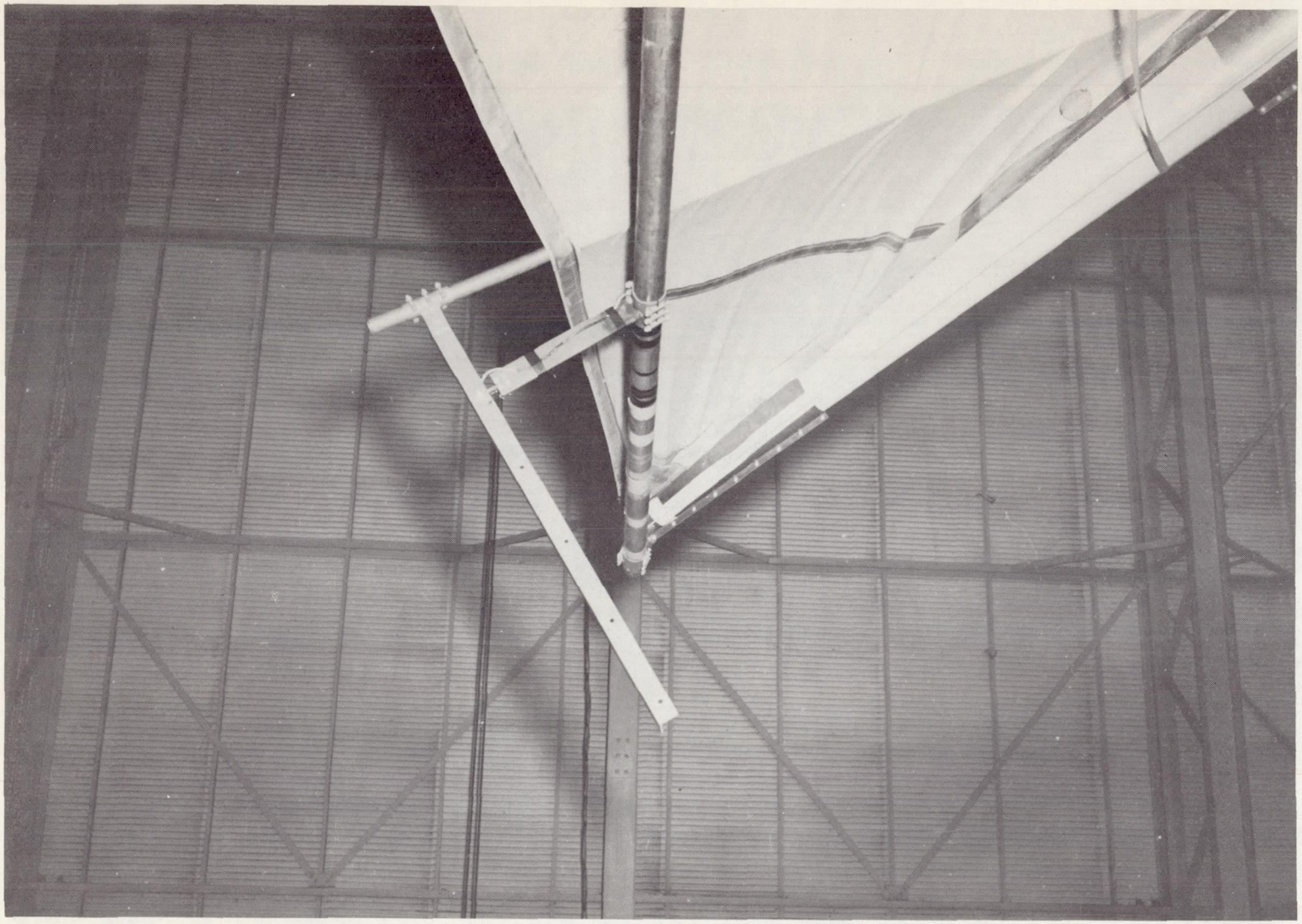

(c) Wing-tip control B. L-62-1351

Figure 4.- Concluded.

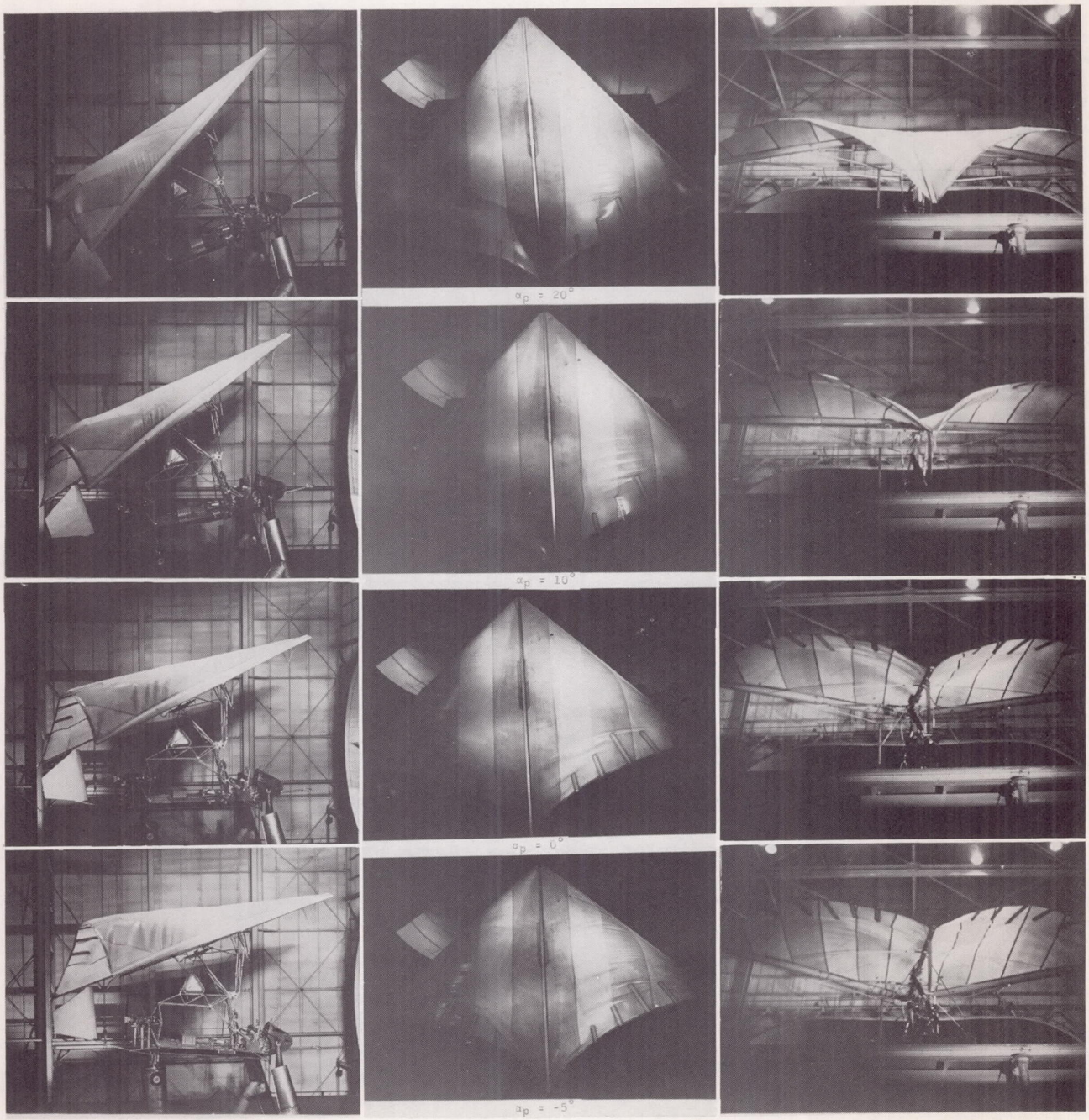

(a) Basic configuration; $\beta = 5^\circ$. L-63-3163

Figure 5.- Photograph of airplane showing wing contour irregularities. Power off; $i_w = 25^\circ$.

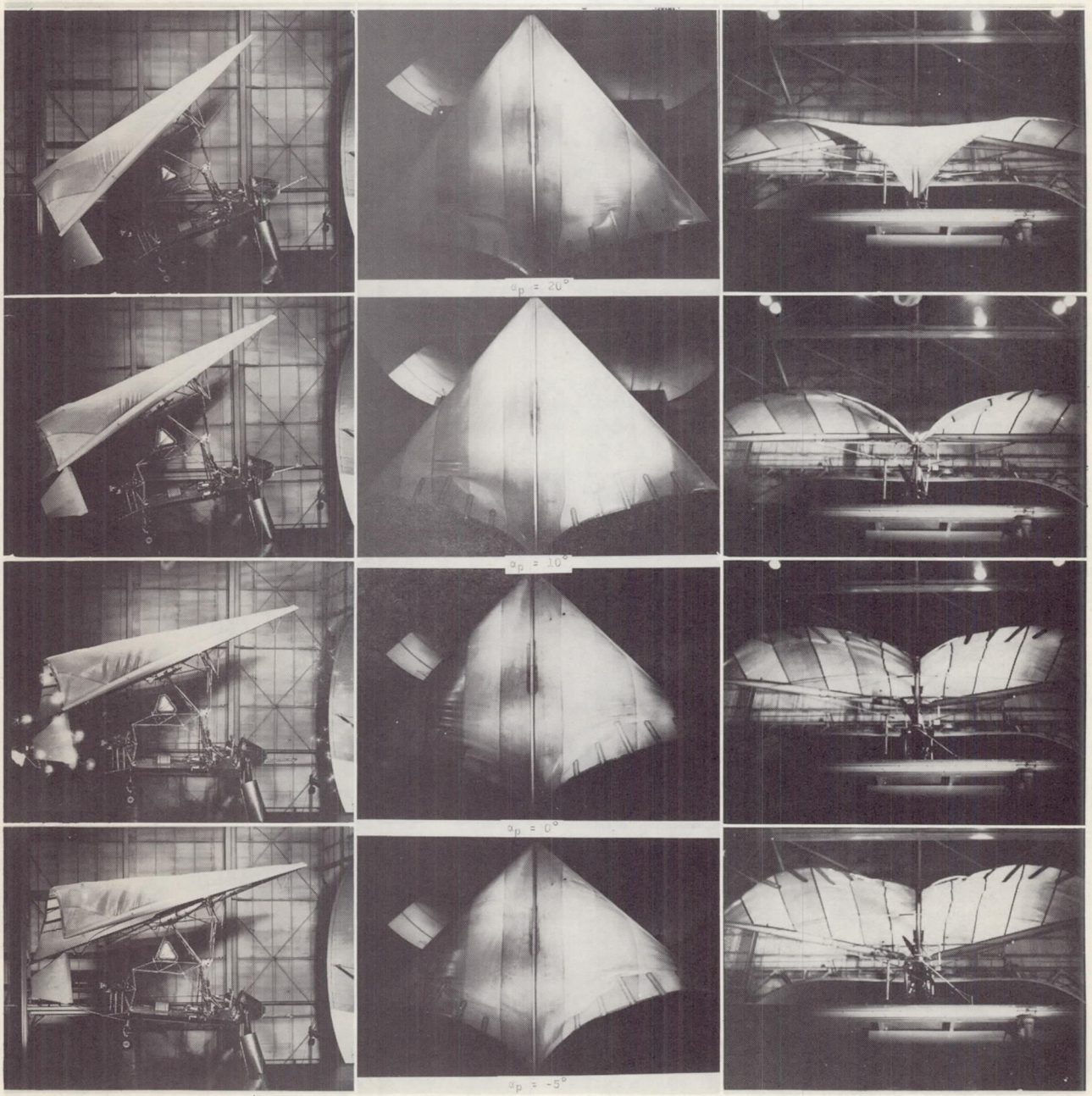

(b) Boltrope slack, battens in; $\beta = 0^{\circ}$. L-63-3164

Figure 5.- Continued.

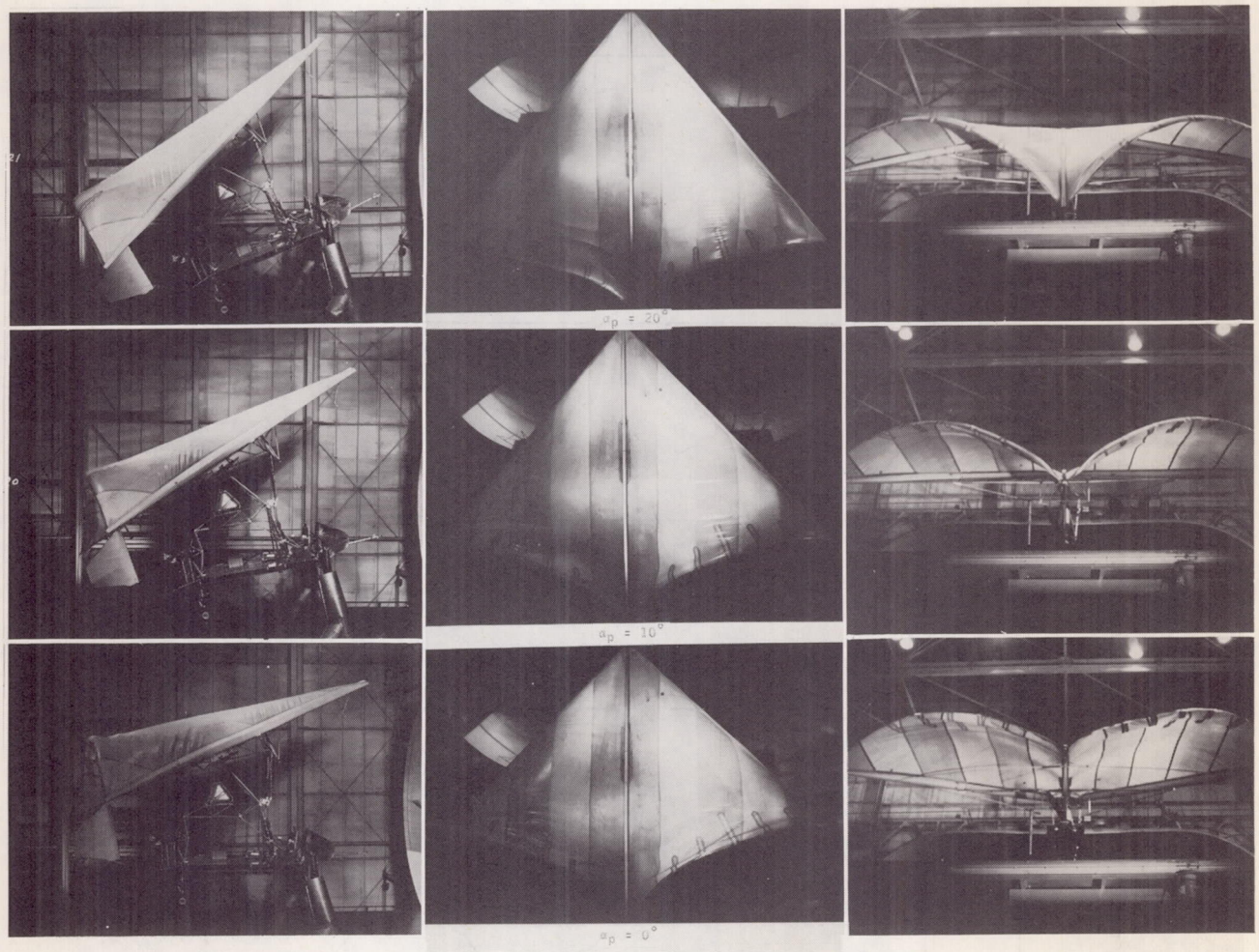

(c) Boltrope slack, battens out; $\beta = 0^{\circ}$. L-63-3165

Figure 5.- Concluded.

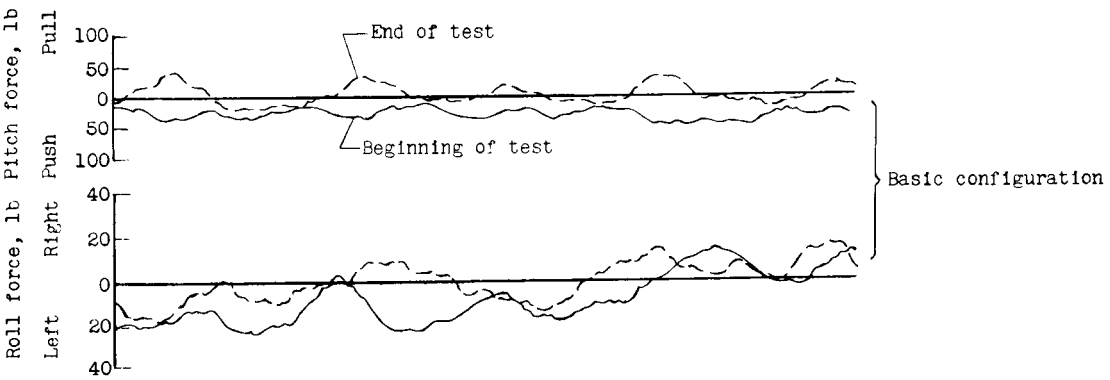

(a) $\alpha_k = 22^\circ$.

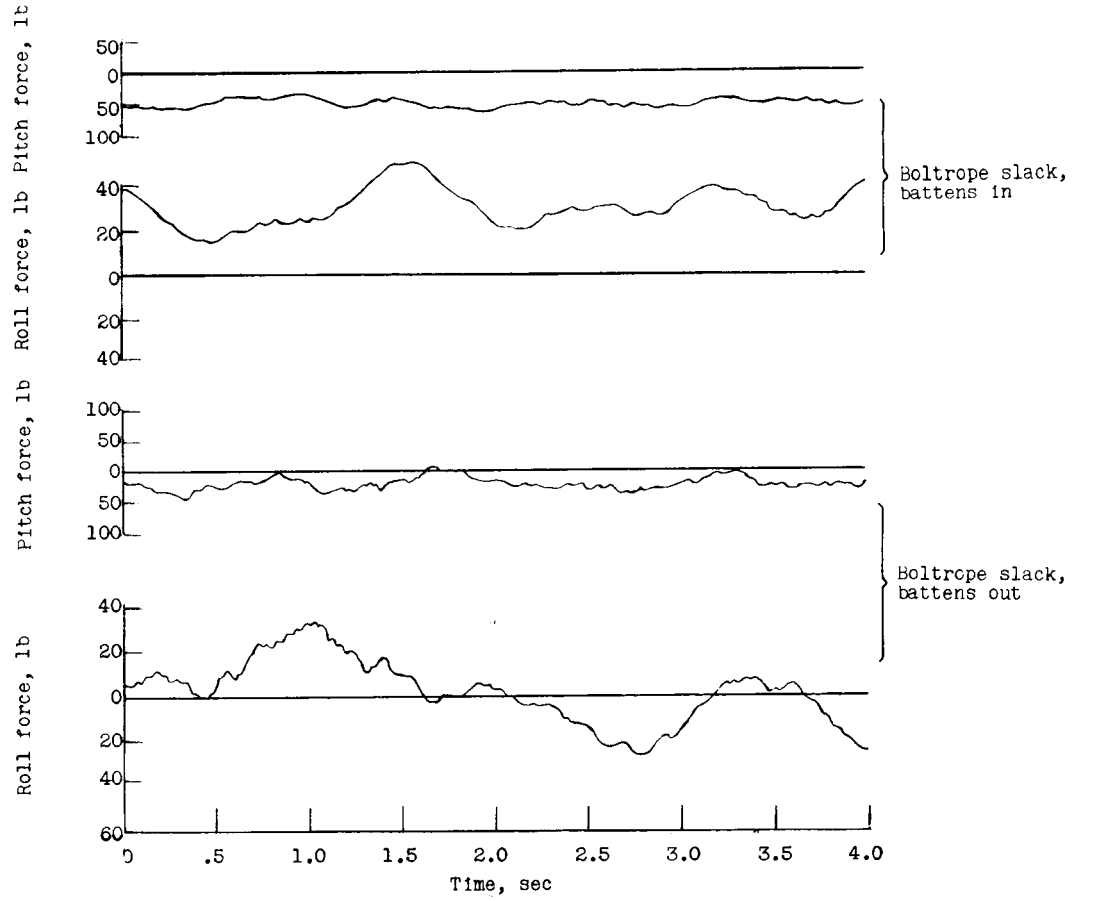

(b) $\alpha_k = 26^\circ$.

Figure 6.- Time history of control forces measured in tunnel tests. $i_w = 25^\circ$; $T_c = 0$; $q = 3.07$ lb/sq ft.

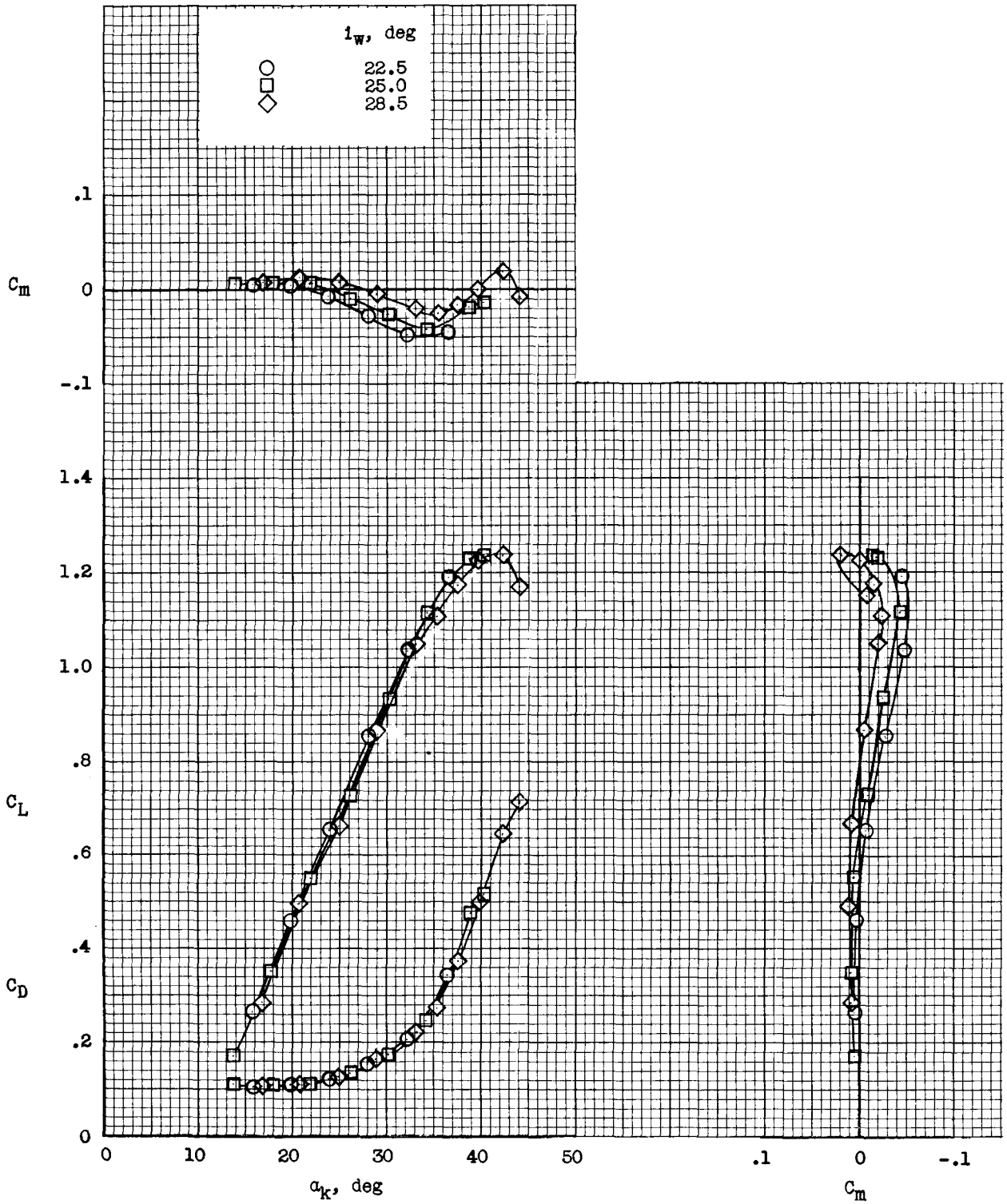

Figure 7.- Static longitudinal characteristics of airplane. T_c = 0; q = 3.07 lb/sq ft.

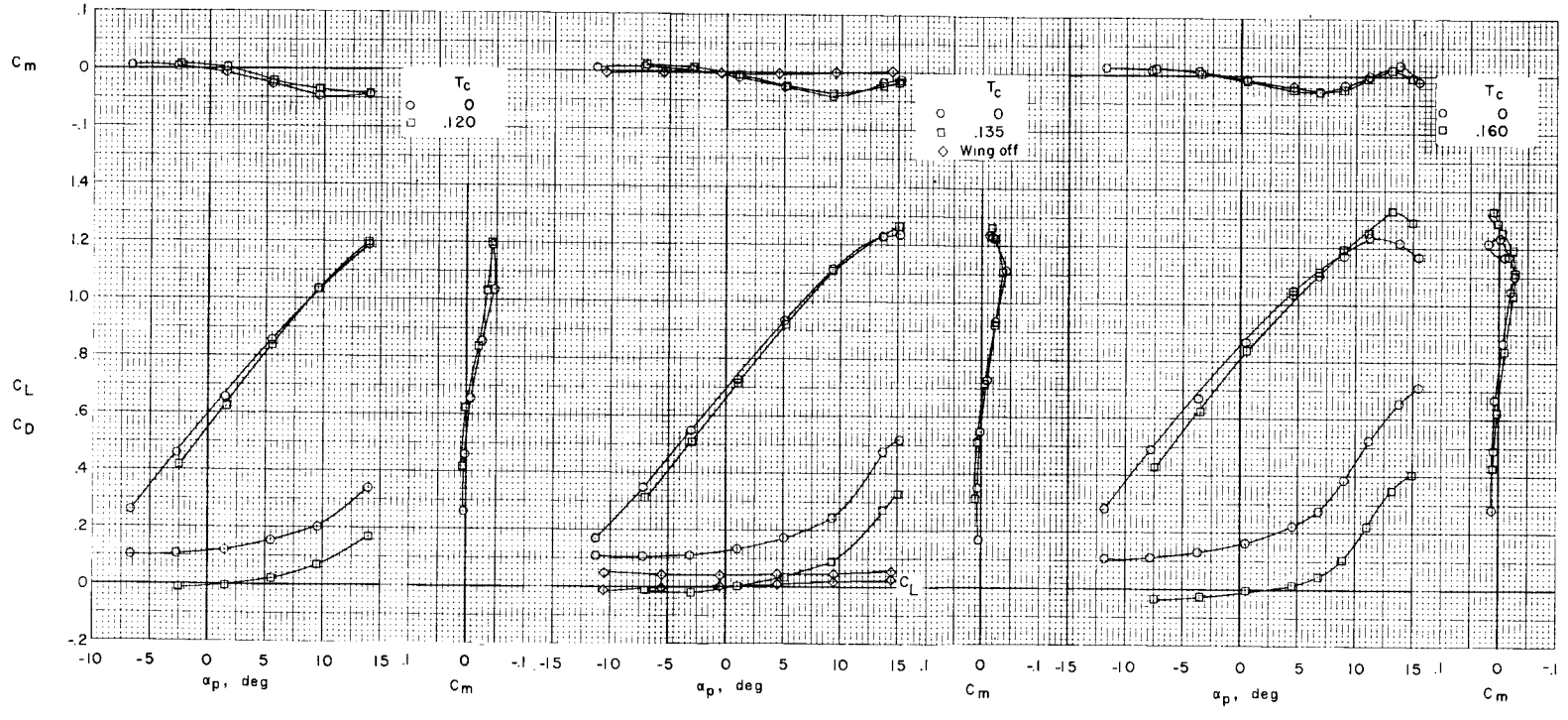

(a) $i_w = 22.5^\circ$. (b) $i_w = 25.0^\circ$. (c) $i_w = 28.5^\circ$.

Figure 8.- Static longitudinal characteristics of airplane. q = 3.07 lb/sq ft.

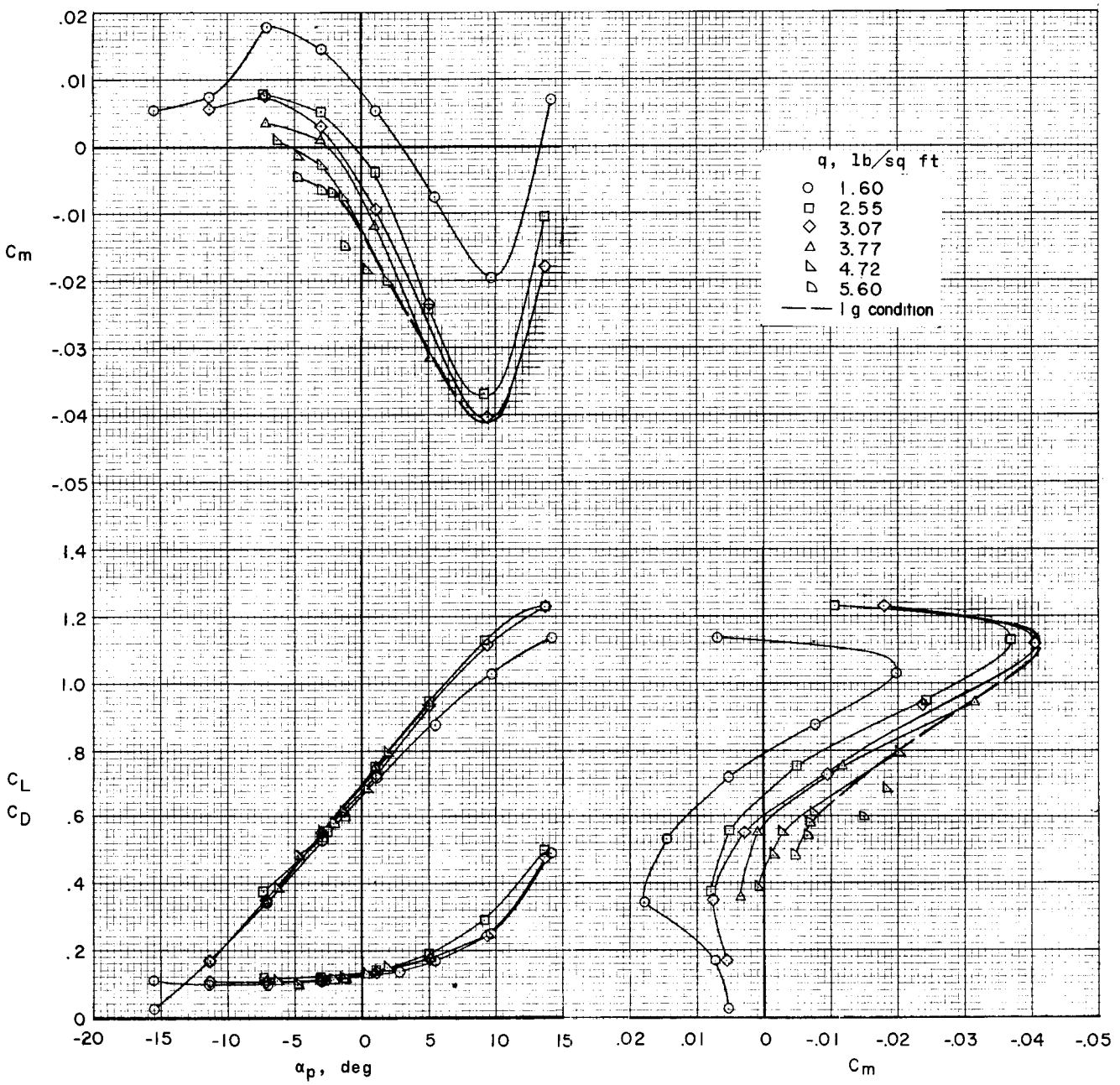

Figure 9.- Effect of dynamic pressure on static longitudinal characteristics of airplane. $i_w = 25^\circ$; $T_c = 0$.

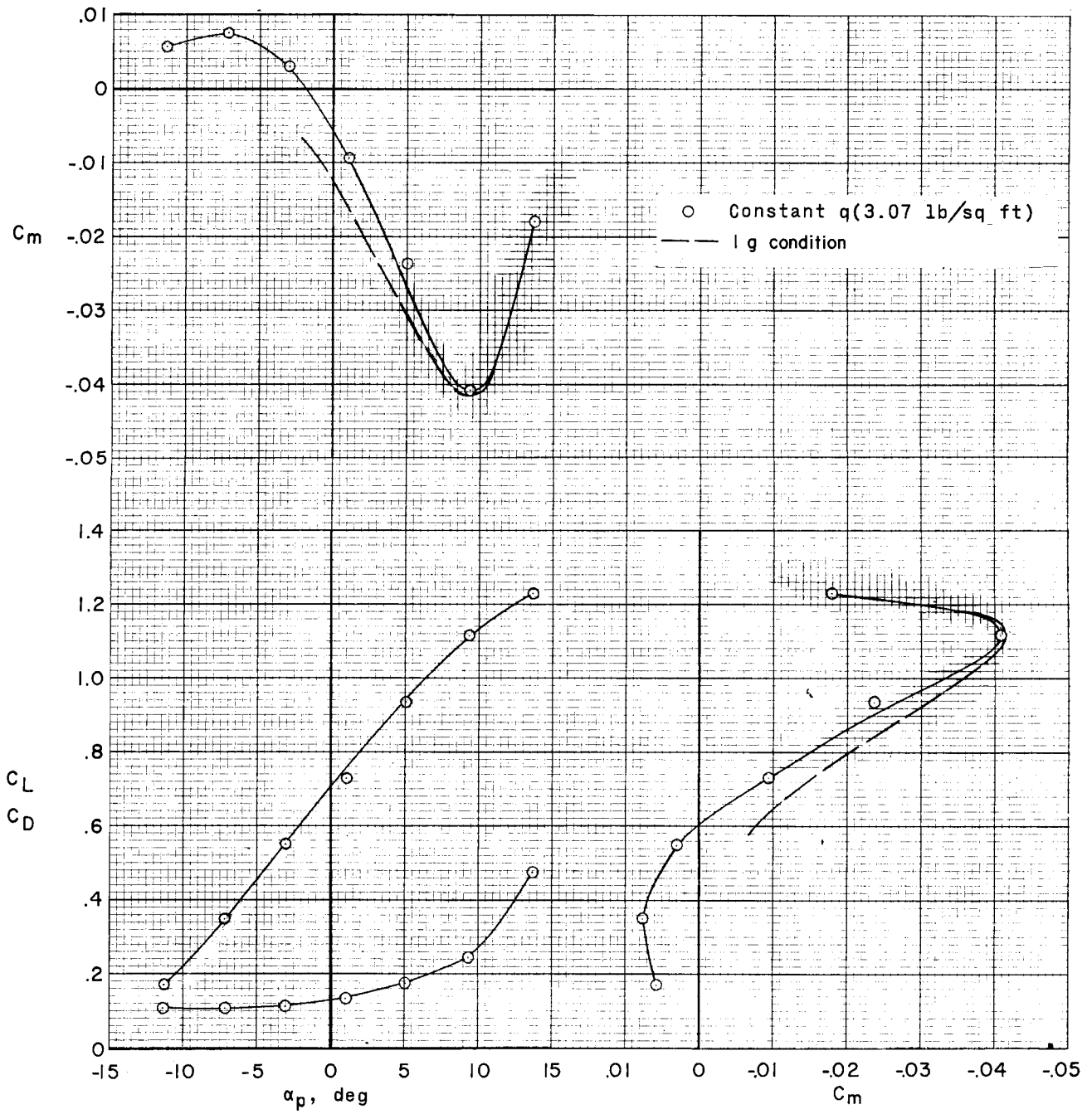

Figure 10.- Comparison of static longitudinal characteristics of airplane for constant loading and constant dynamic pressure. $i_w = 25°$; $T_c = 0$.

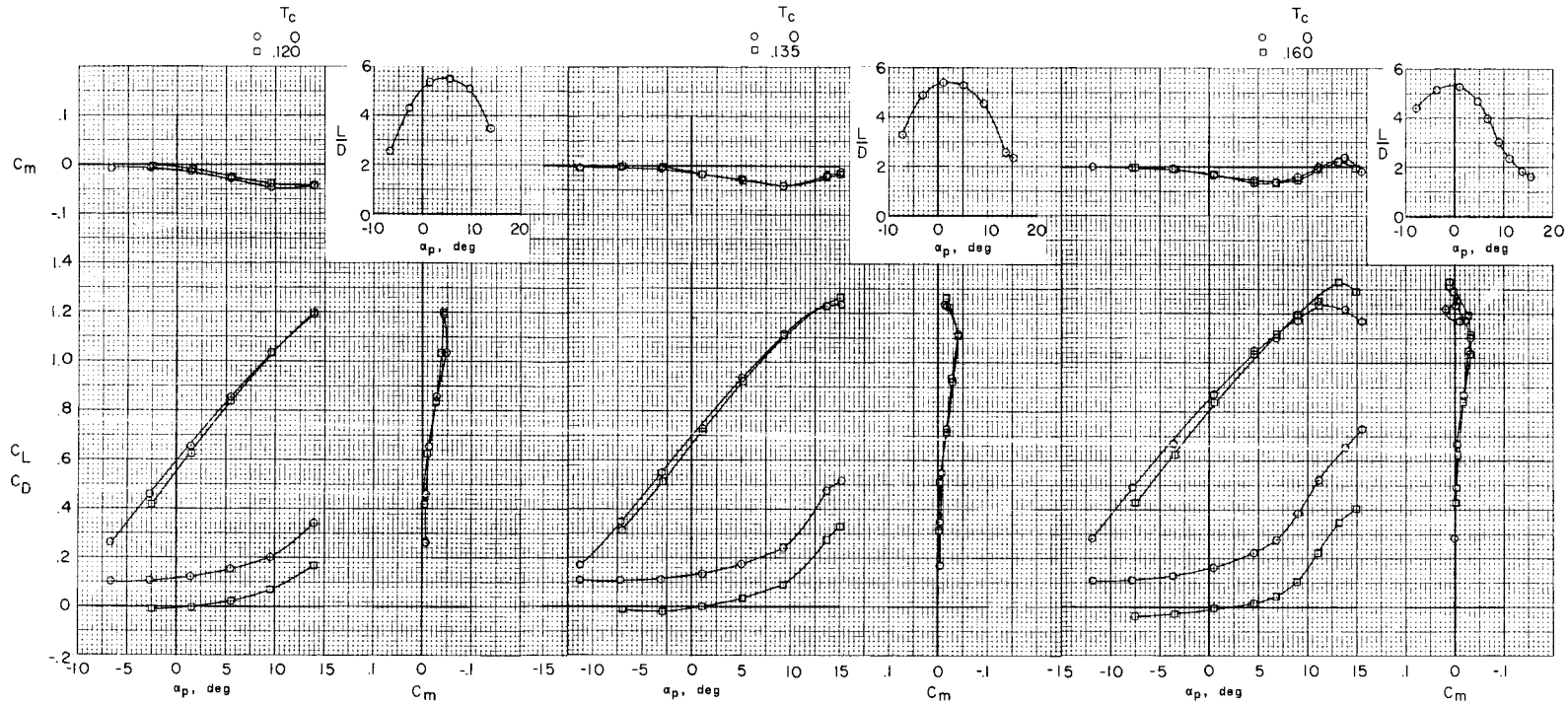

(a) $i_w = 22.5°$. (b) $i_w = 25.0°$. (c) $i_w = 28.5°$.

Figure 11.- Static longitudinal characteristics of airplane corrected for 1g condition.

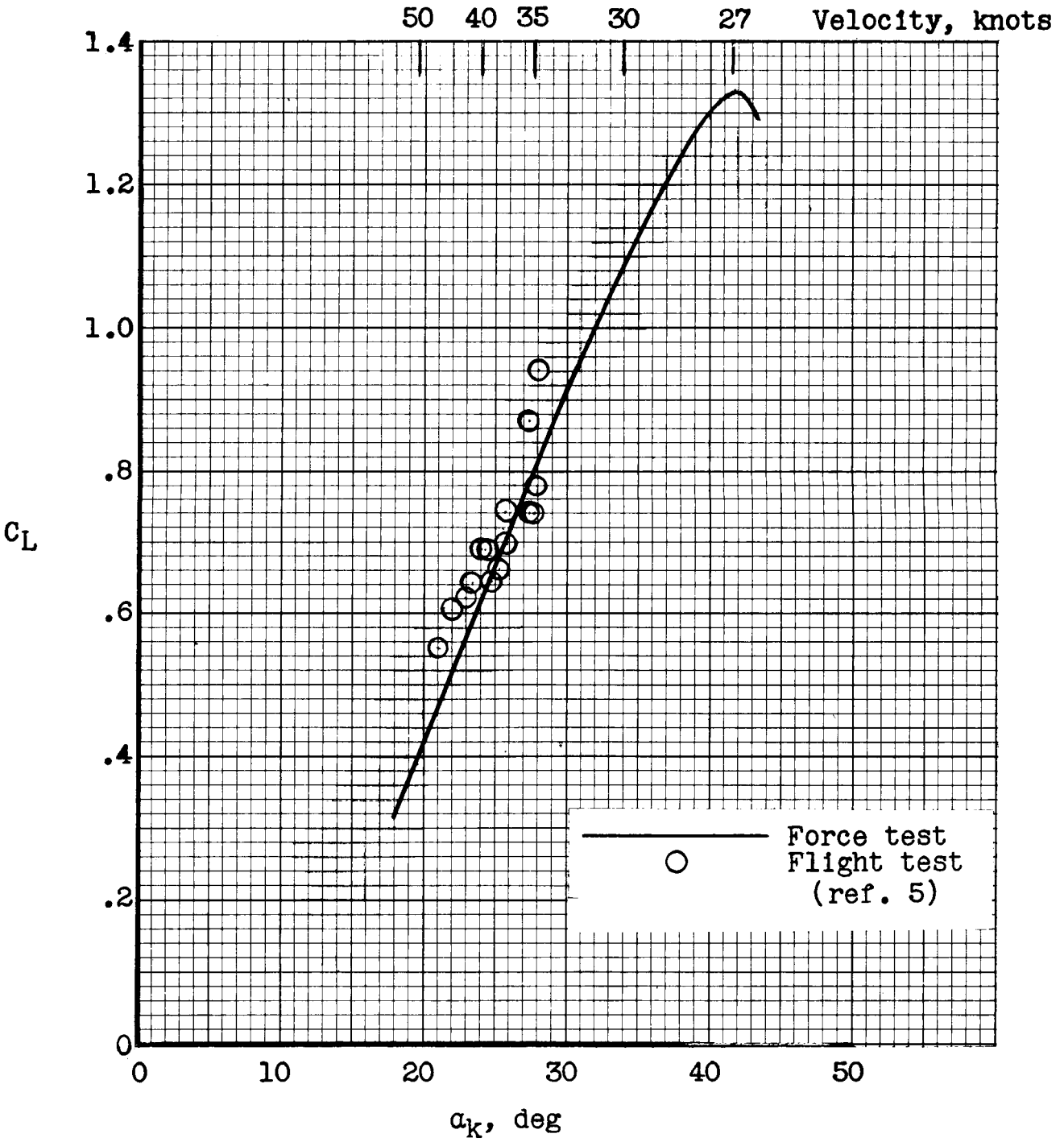

Figure 12.- Comparison of lift characteristics as measured in wind-tunnel tests and flight tests of airplane. Airspeeds were estimated for 1,840 pounds.

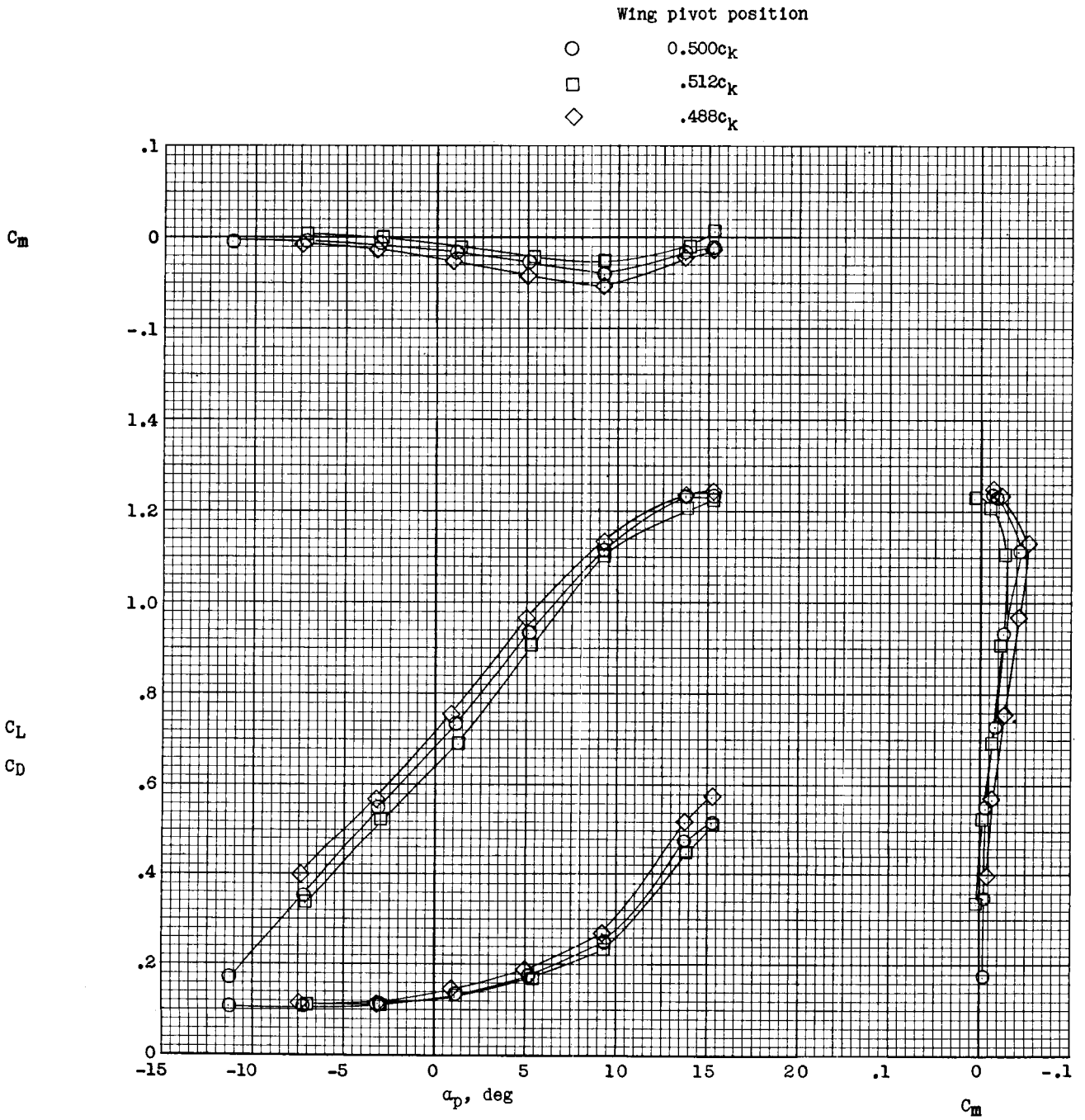

Figure 13.- Effect of wing pivot position on static longitudinal characteristics of airplane for 1 g condition. $T_c = 0$.

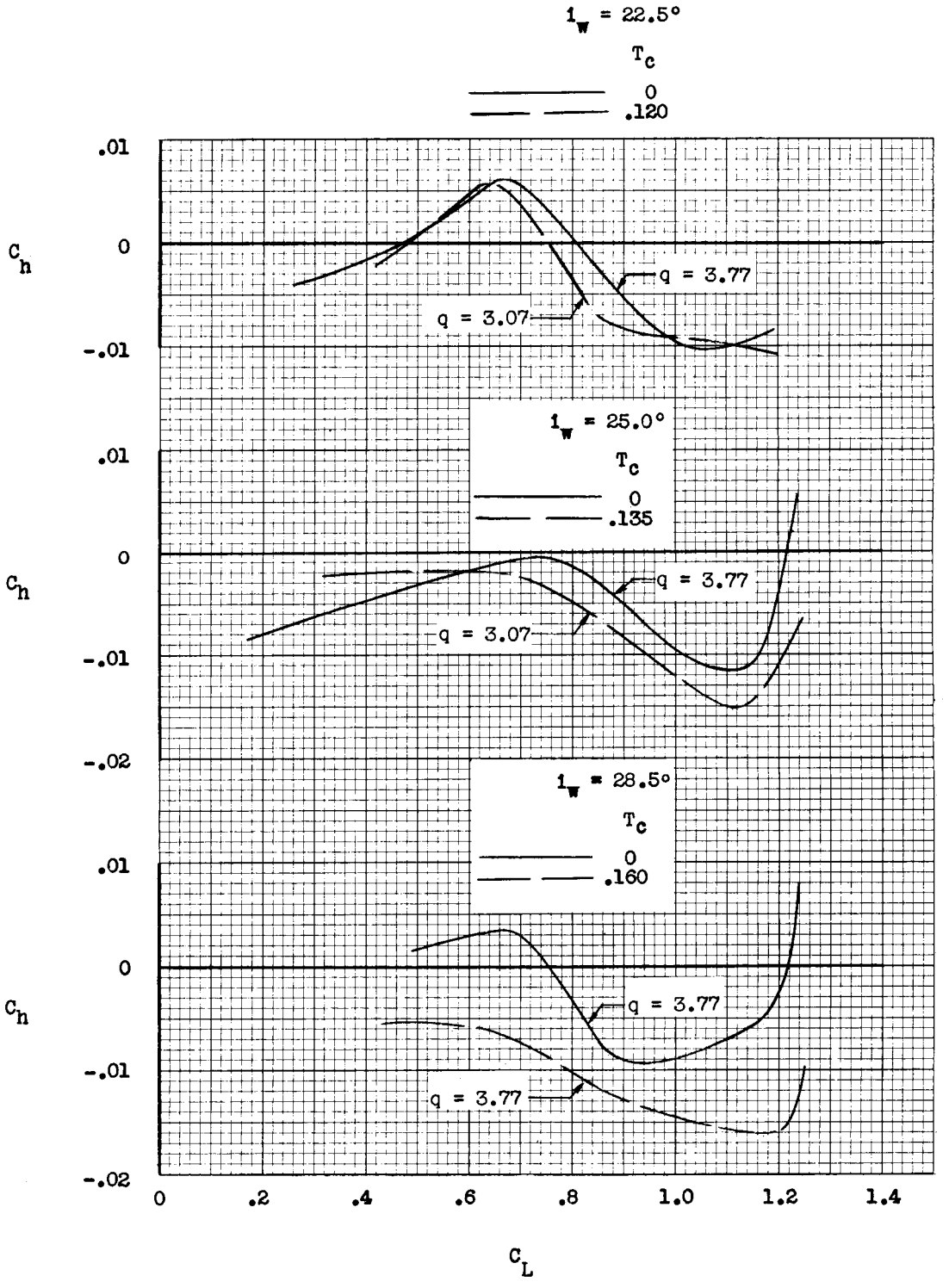

Figure 14.- Hinge-moment characteristics of wing in pitch measured about pivot ($0.50c_k$) at constant dynamic pressure.

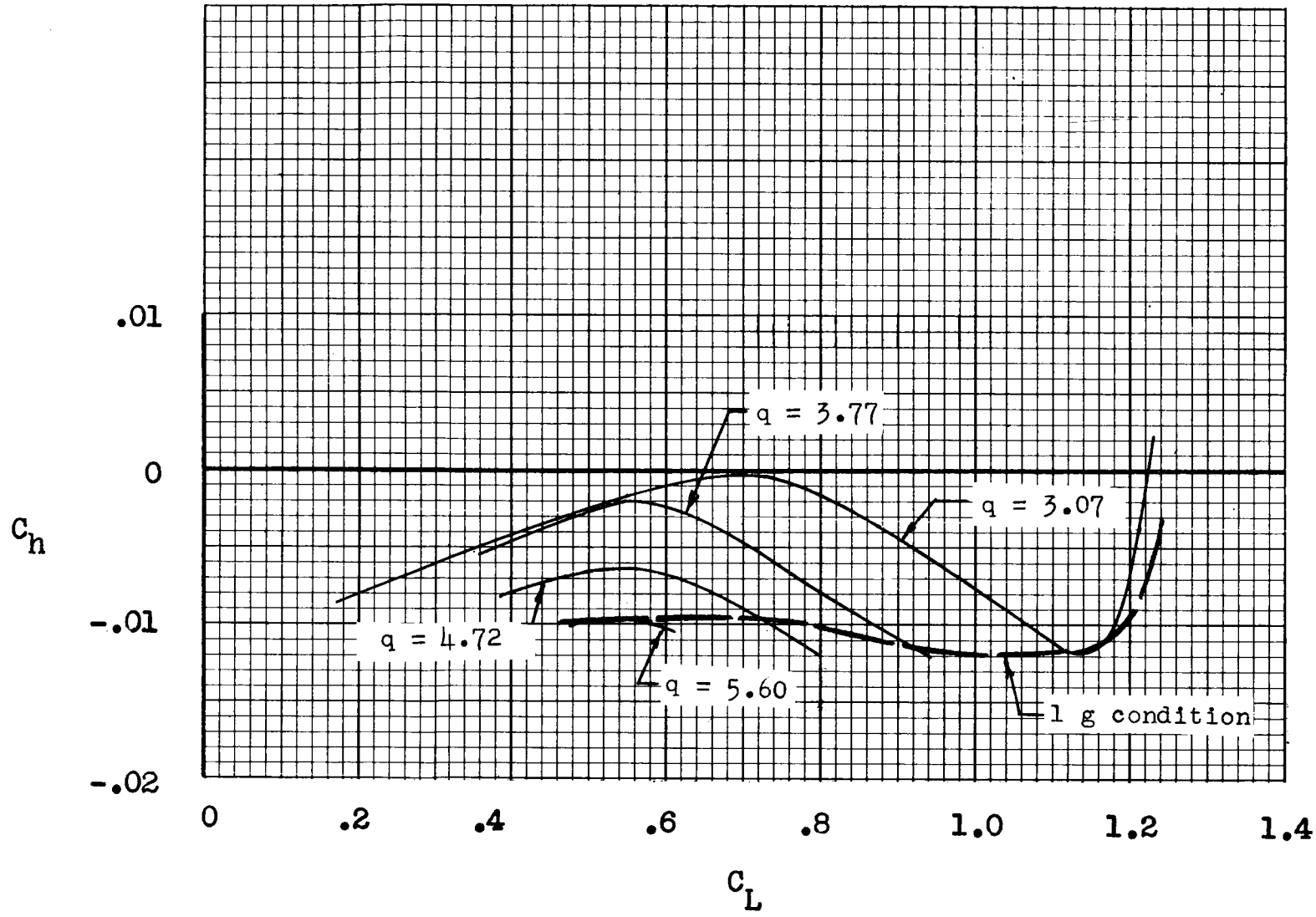

Figure 15.- Effect of dynamic pressure on hinge-moment characteristics of wing in pitch. $T_c = 0$; $i_w = 25^\circ$.

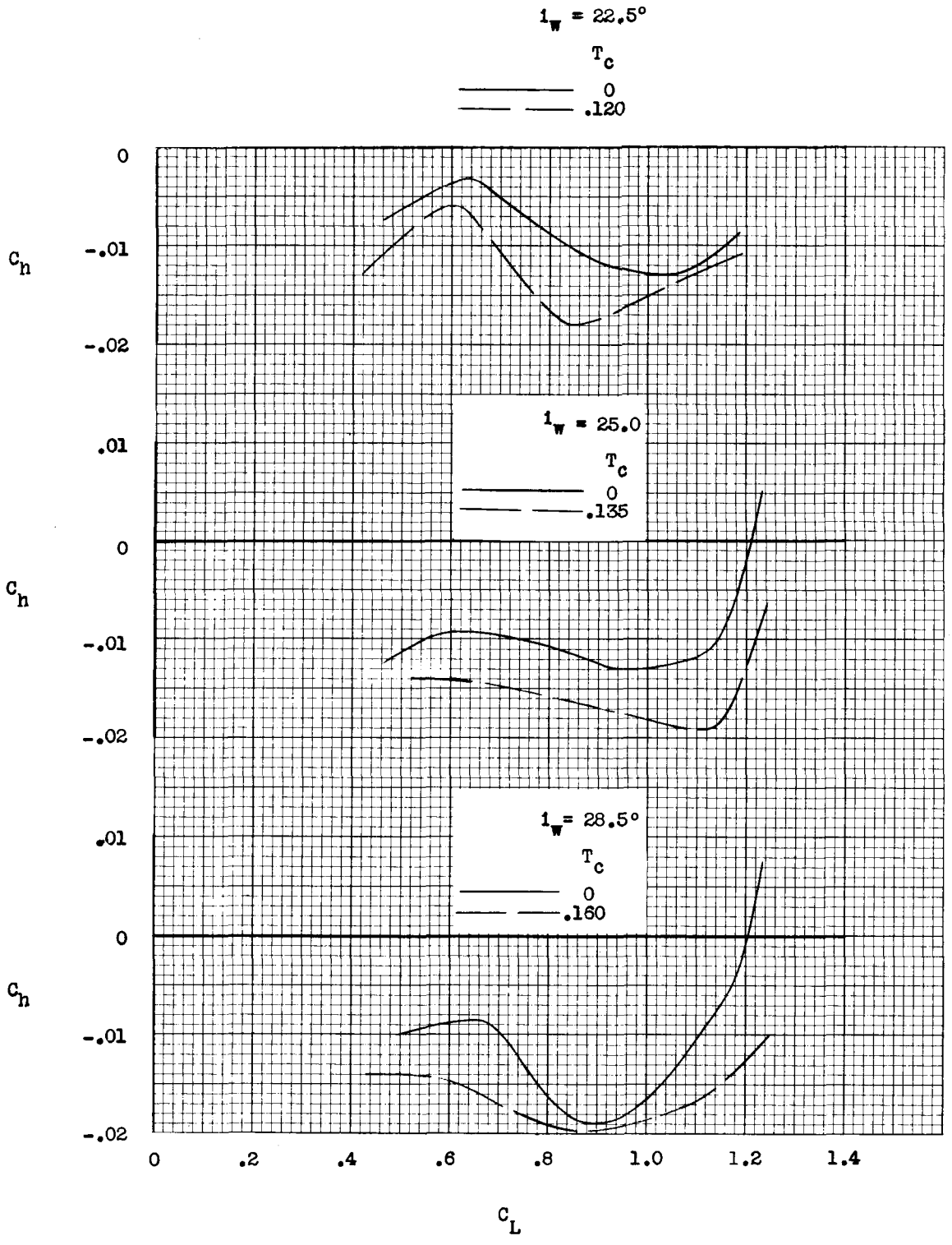

Figure 16.- Hinge-moment characteristics of wing in pitch corrected for 1g condition.

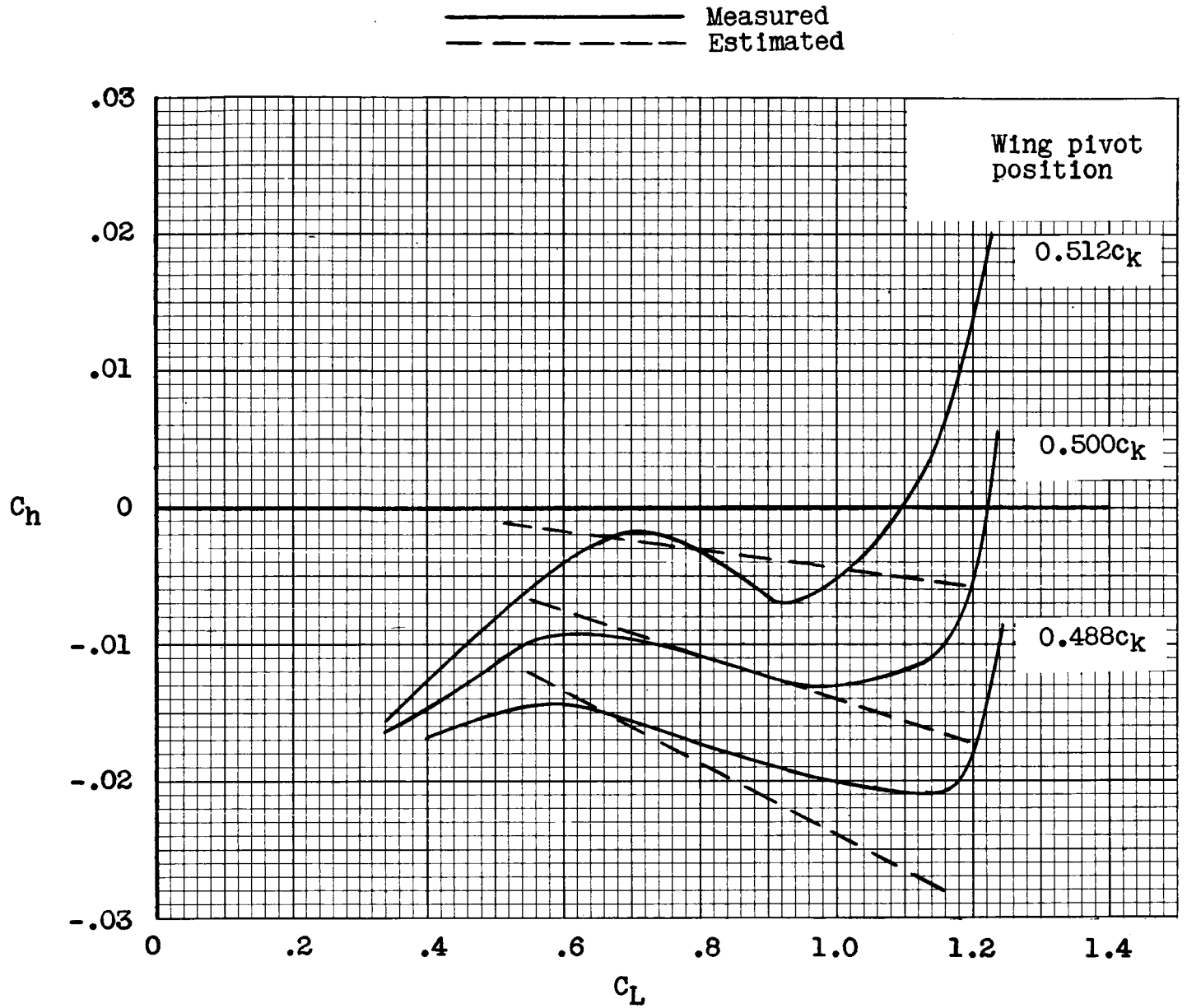

Figure 17.- Effect of wing pivot position on hinge-moment characteristics for 1 g condition. $i_w = 25^\circ$; power off.

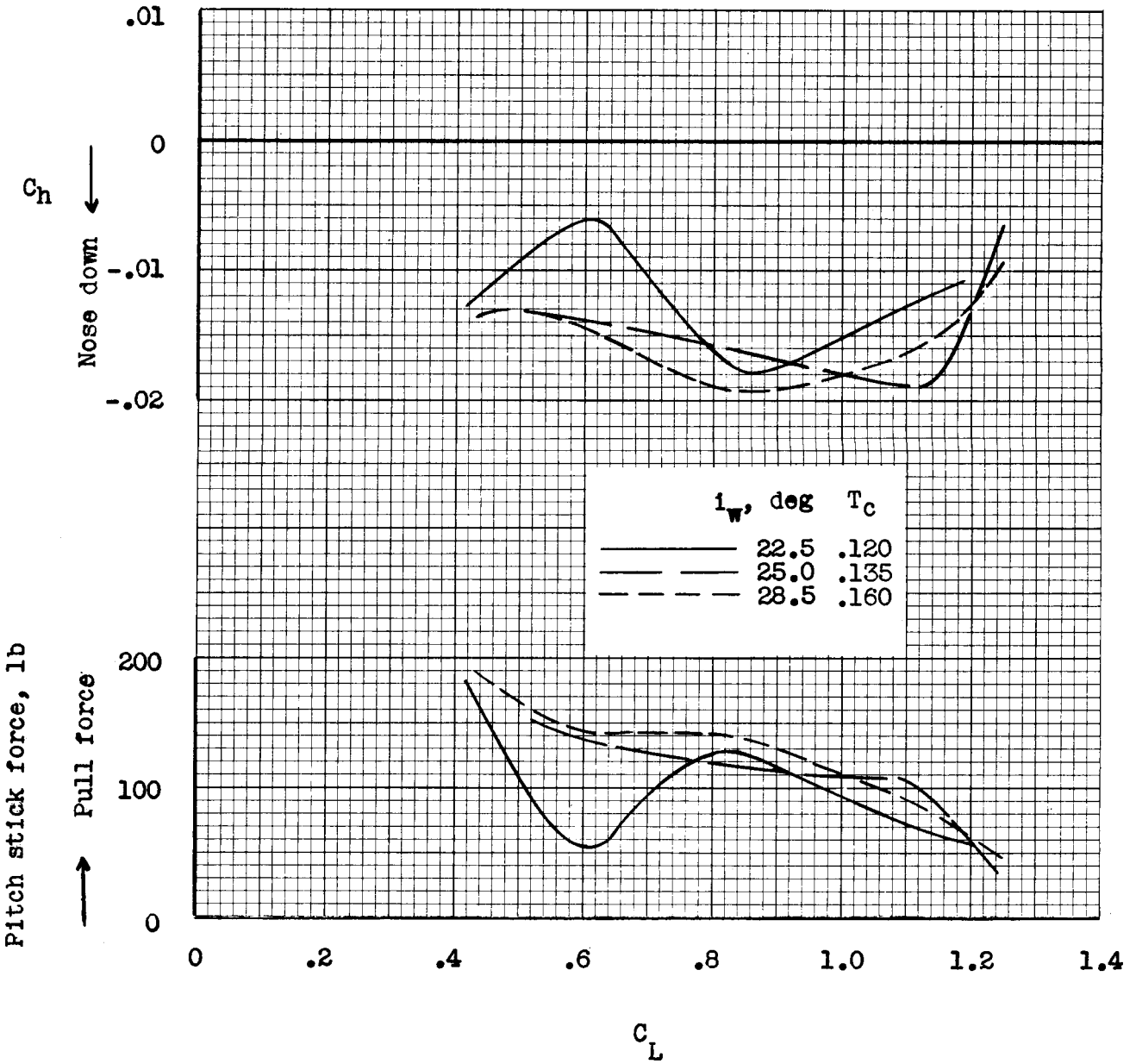

Figure 18.- Hinge-moment characteristics of wing in pitch (data from fig. 16) and corresponding pitch stick forces for three different wing incidences. Power on.

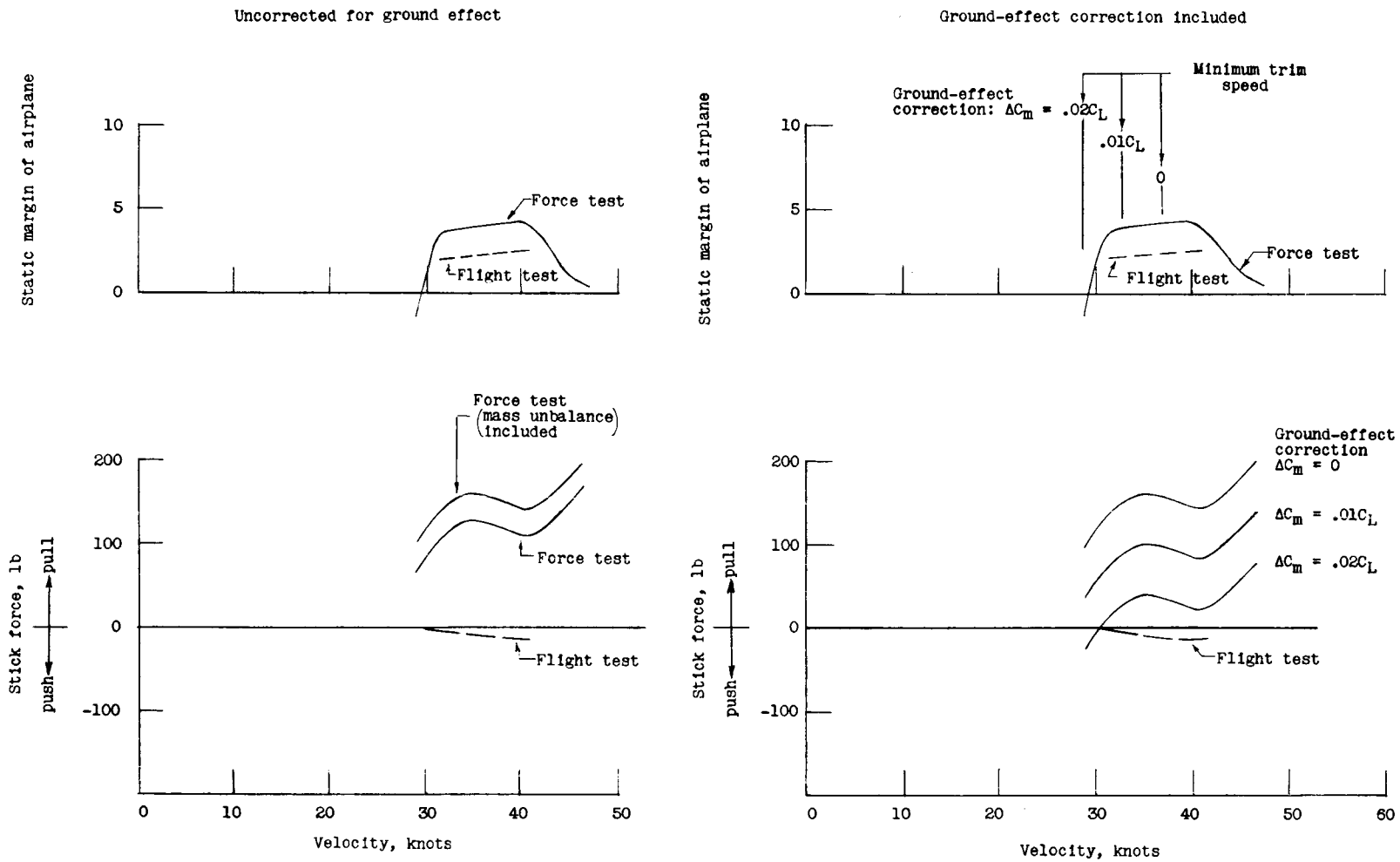

Figure 19.- Comparison of static margin and pitch stick forces as measured in wind-tunnel tests and flight tests (ref. 5) of airplane. Power on.

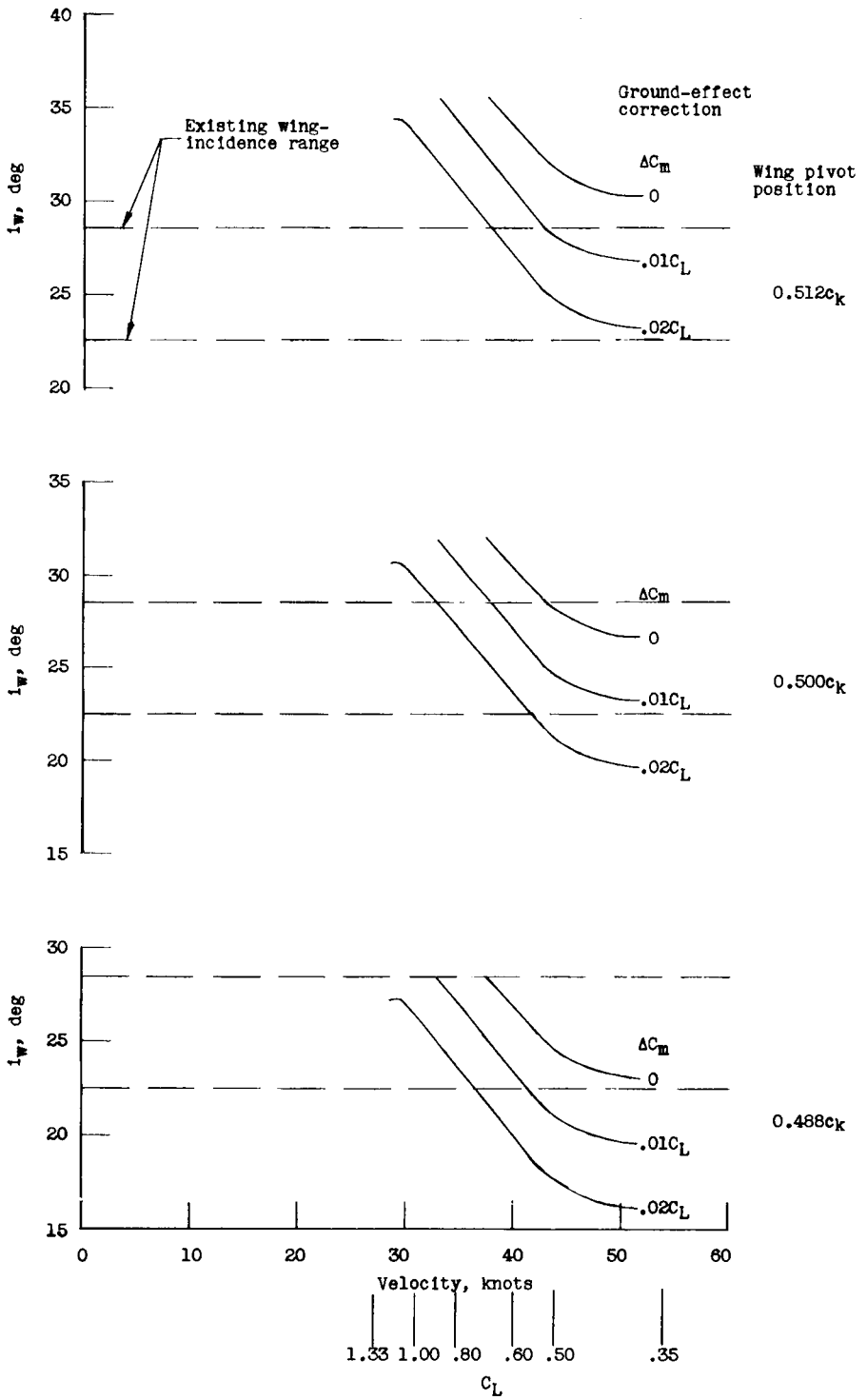

Figure 20.- Estimated angle of incidence required for pitch trim with several different values of ground effect included. Power on.

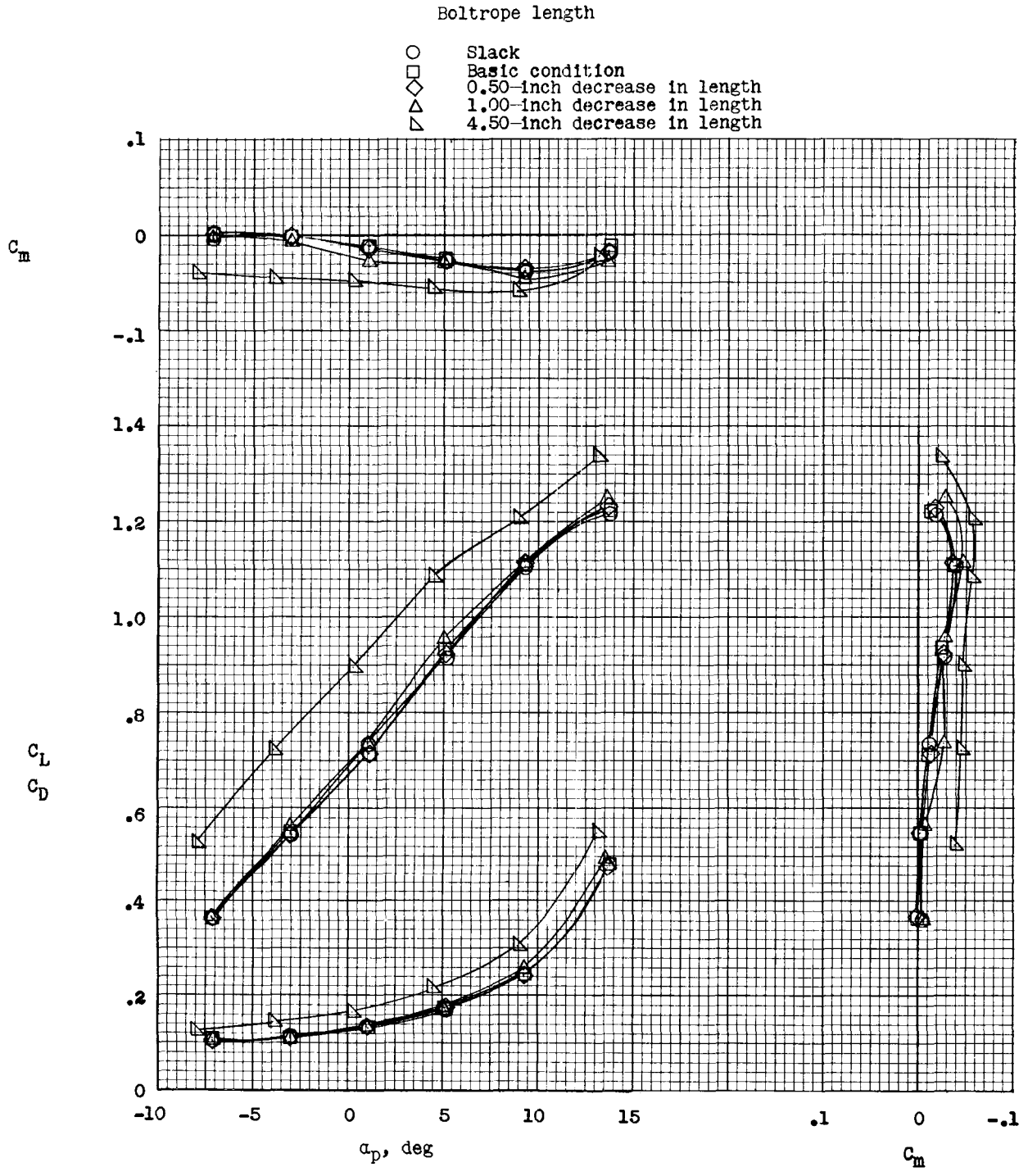

(a) Effect of boltrope length.

Figure 21.- Effect of wing trailing-edge modifications on static longitudinal characteristics of airplane for 1 g condition. $T_c = 0$.

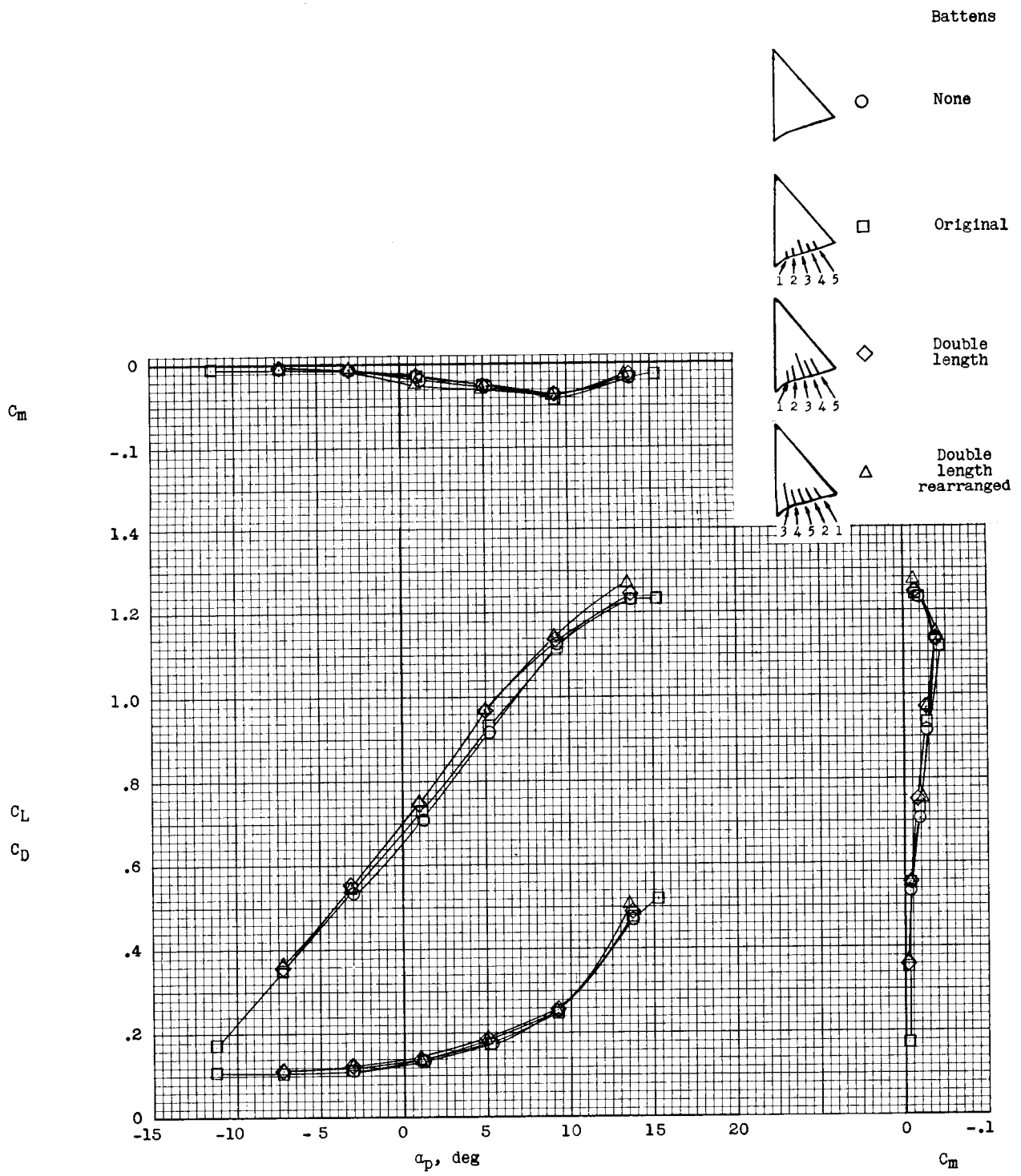

(b) Effect of batten modification.

Figure 21.- Concluded.

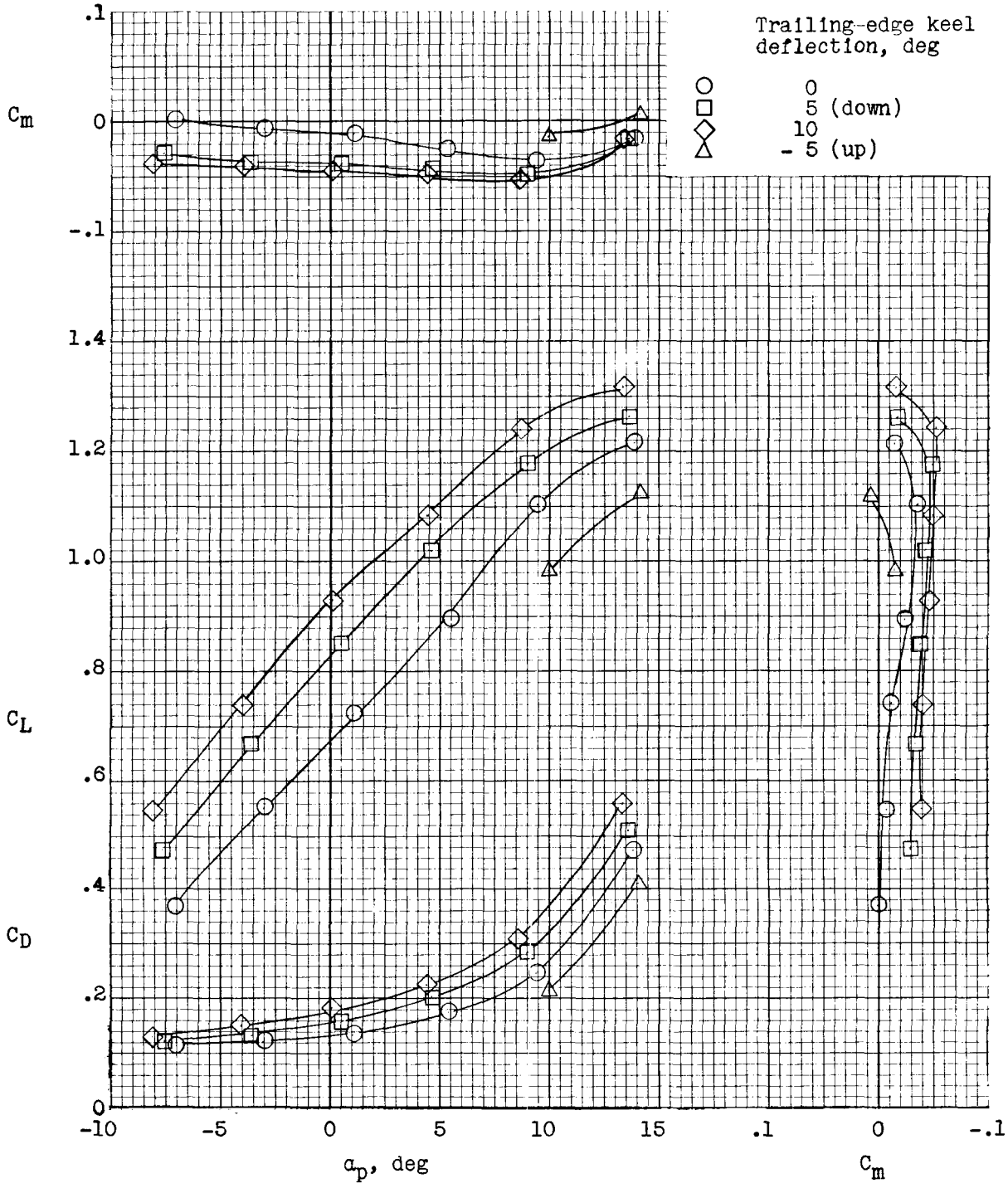

(a) Pitch effectiveness.

Figure 22.- Static longitudinal characteristics of airplane with keel trailing edge deflected for pitch control for 1g condition. $T_c = 0$; $i_w = 25^\circ$.

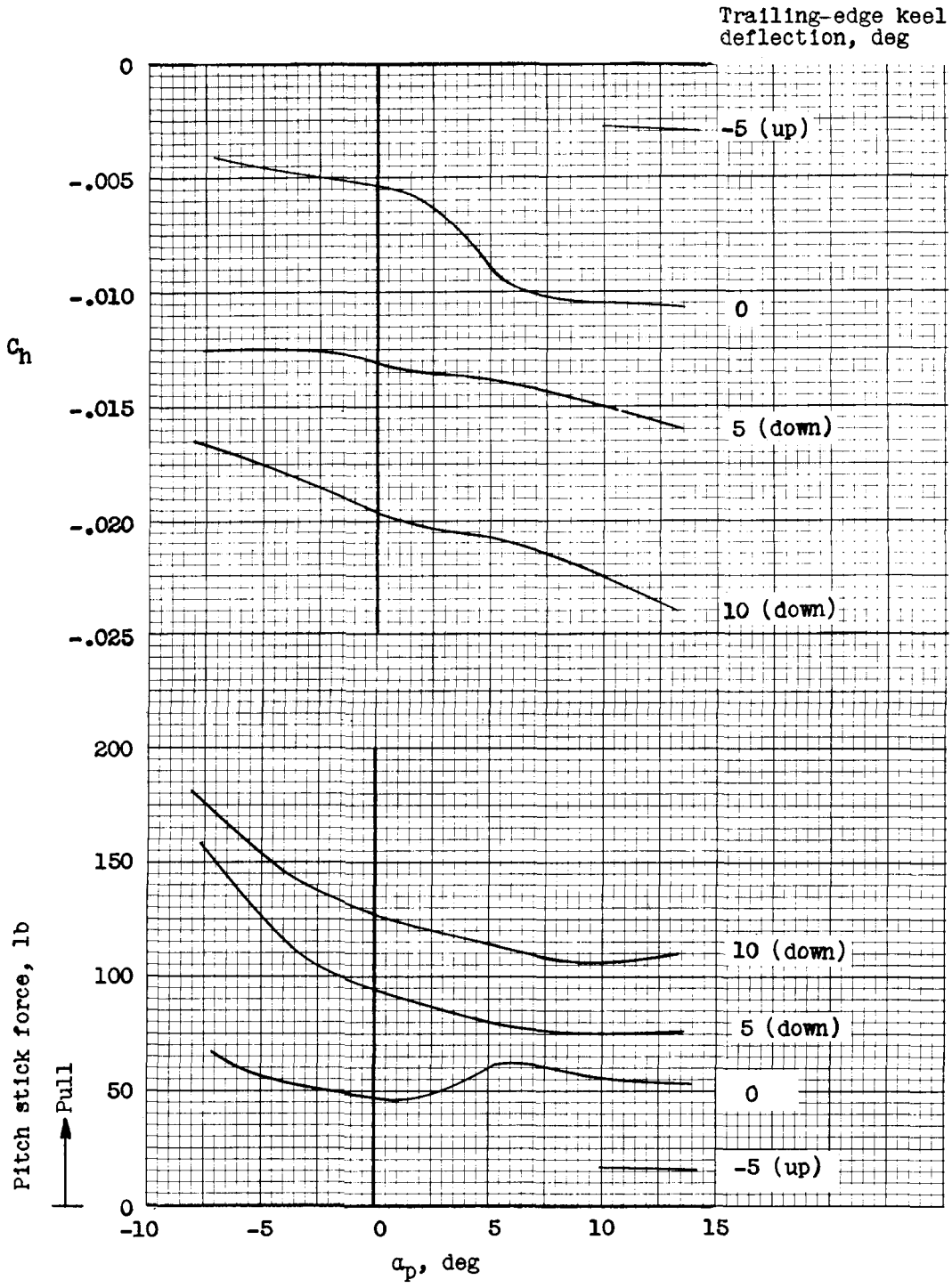

(b) Longitudinal hinge-moment and stick-force characteristics.

Figure 22.- Concluded.

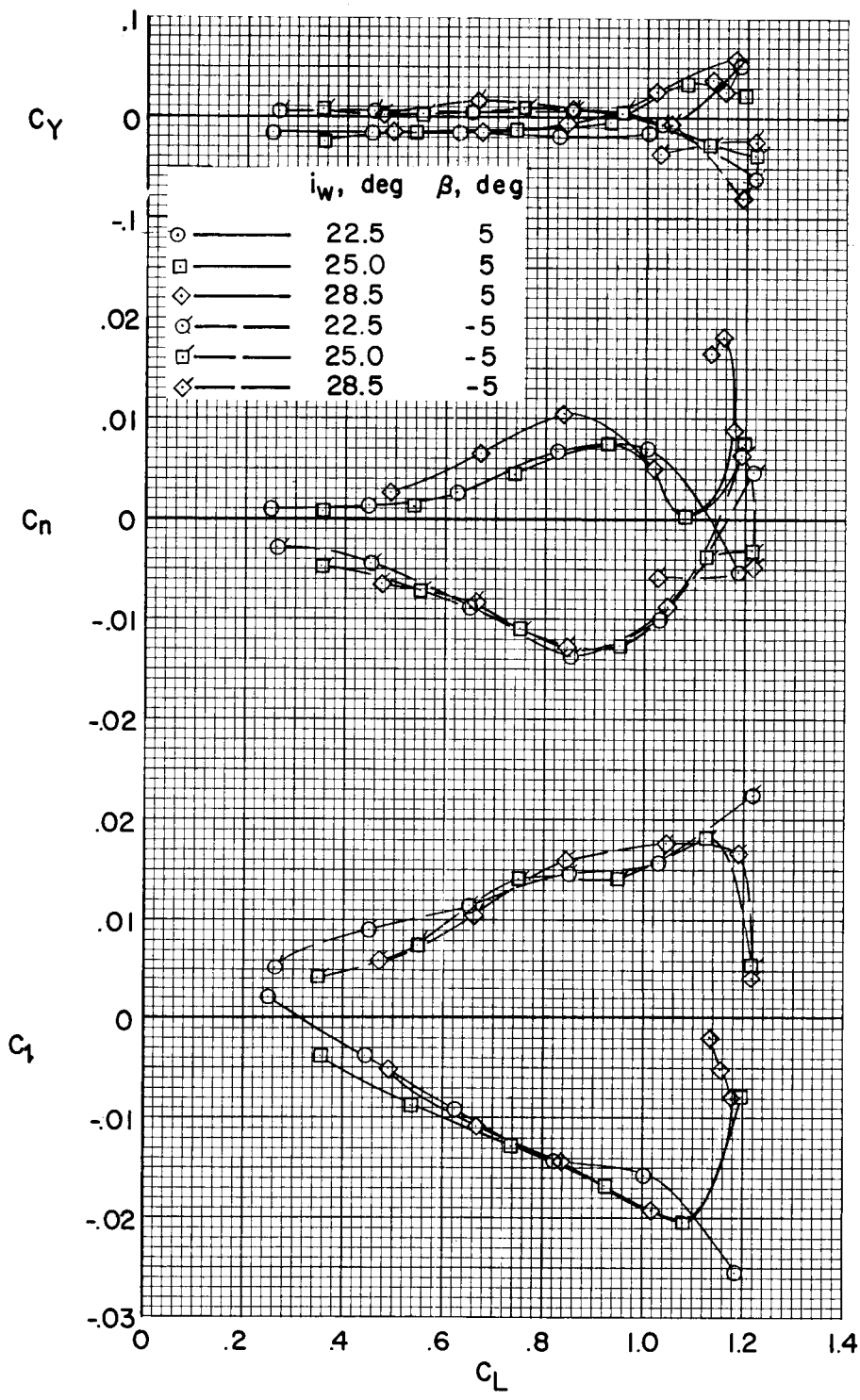

Figure 23.- Effect of wing incidence on variation of lateral coefficients with lift coefficient due to sideslip angles of 5° and -5°. T_c = 0; rudder on; δ_r = 0°; q = 3.07 to 3.77 lb/sq ft.

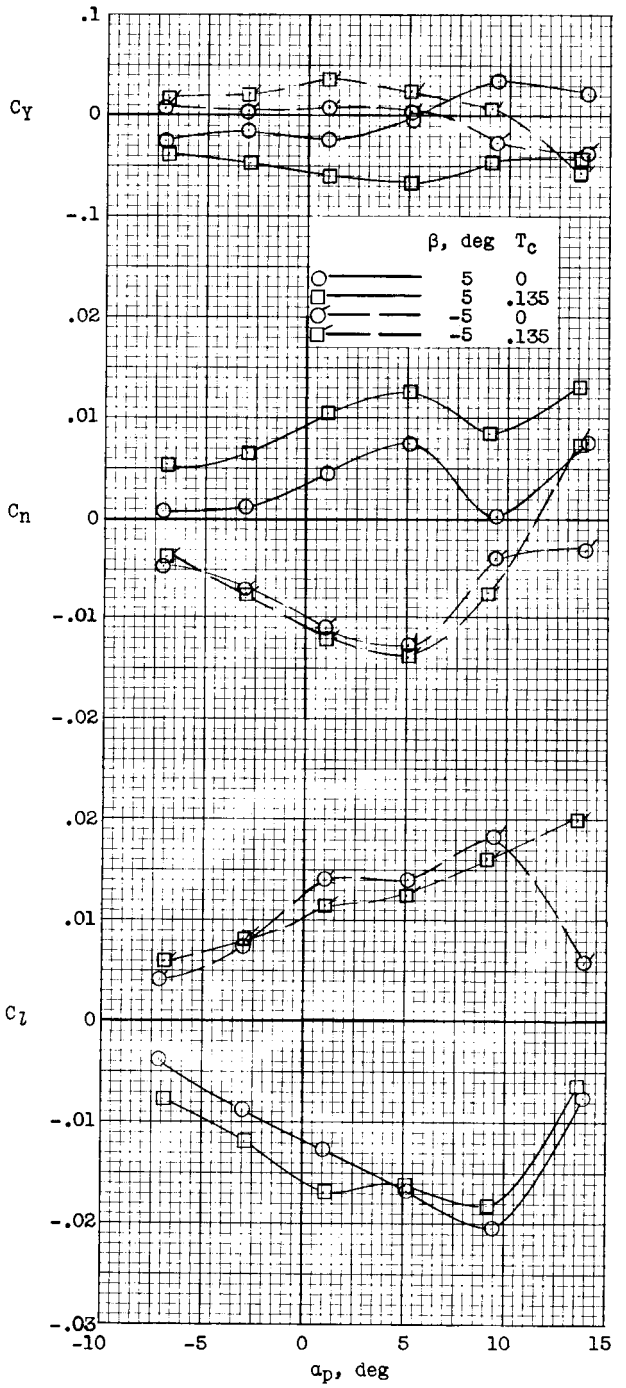

(a) Rudder on; $\delta_r = 0^\circ$.

Figure 24.- Effect of power on variation of lateral coefficients with platform angle of attack due to sideslip angles of 5° and -5°. $i_w = 25^\circ$; q = 3.07 lb/sq ft.

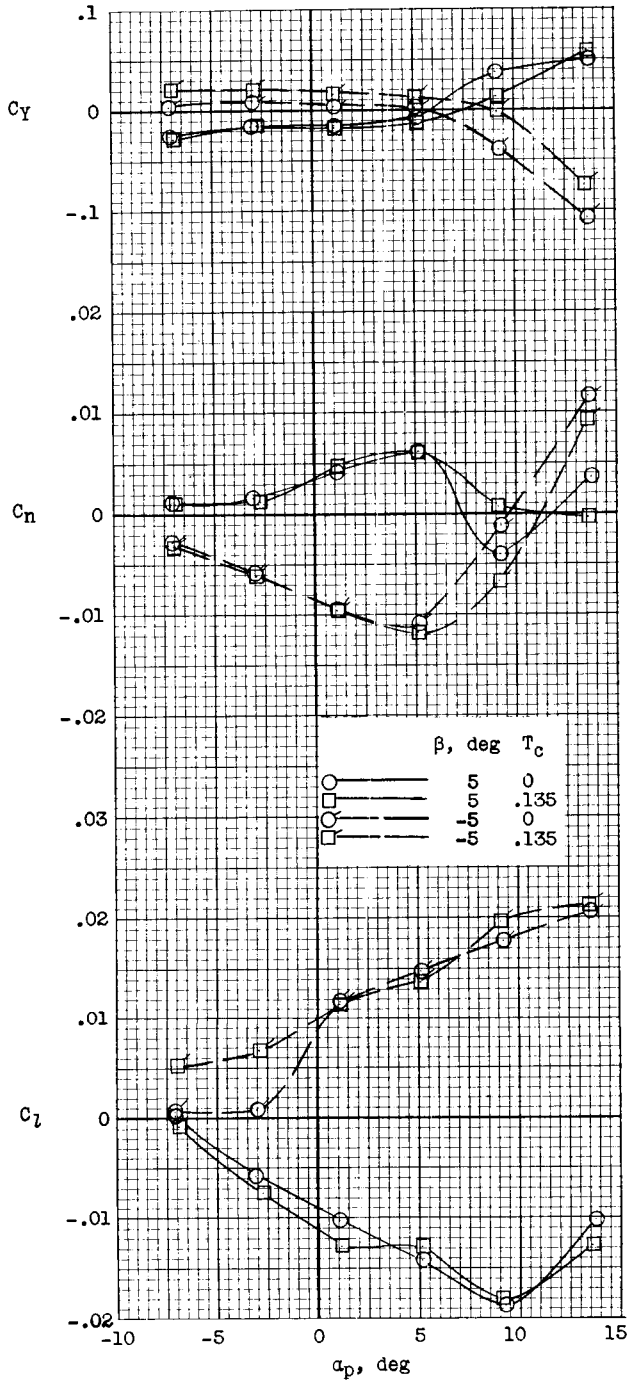

(b) Rudder off.

Figure 24.- Concluded.

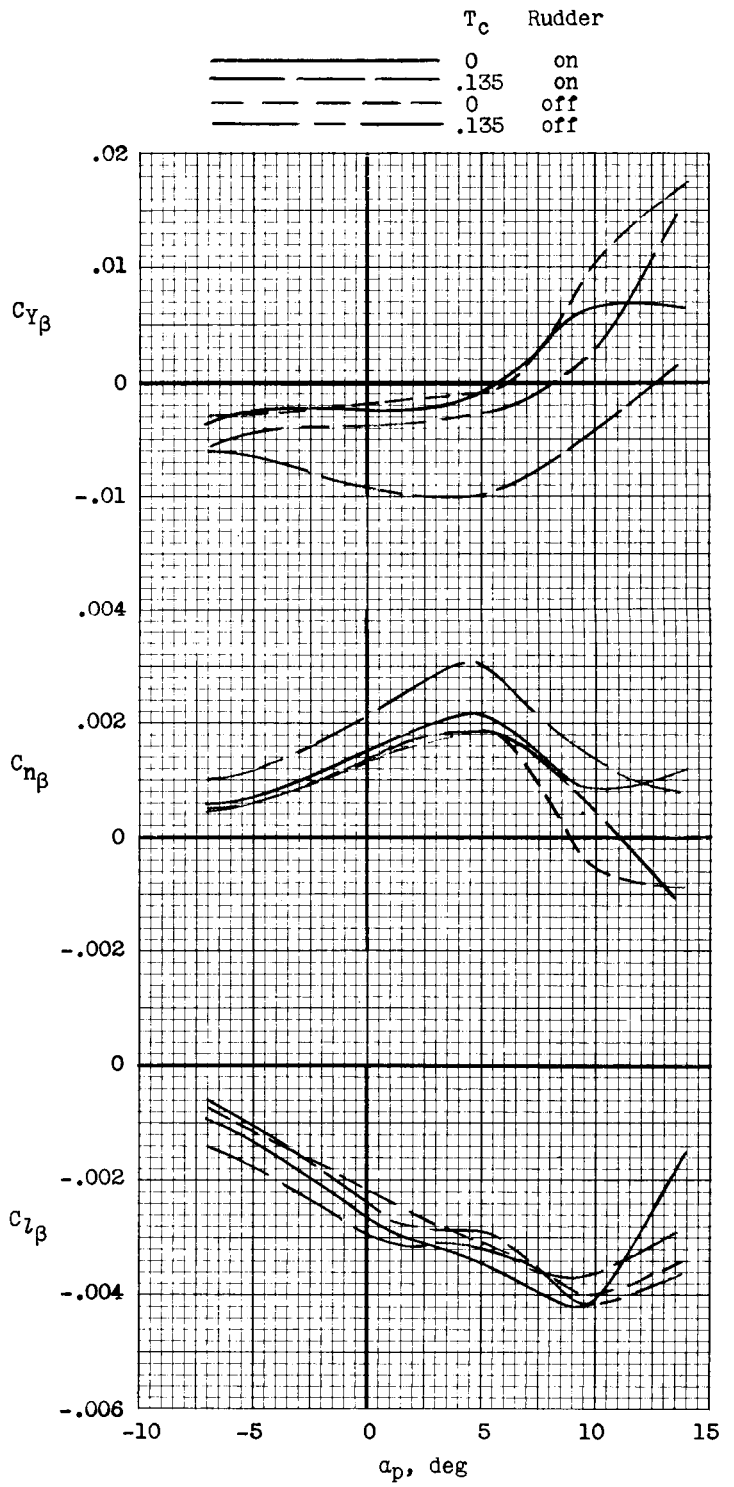

Figure 25.- Effect of power and rudder on static-lateral-stability parameters of airplane. $i_w = 25^\circ$; q = 3.07 to 3.77 lb/sq ft.

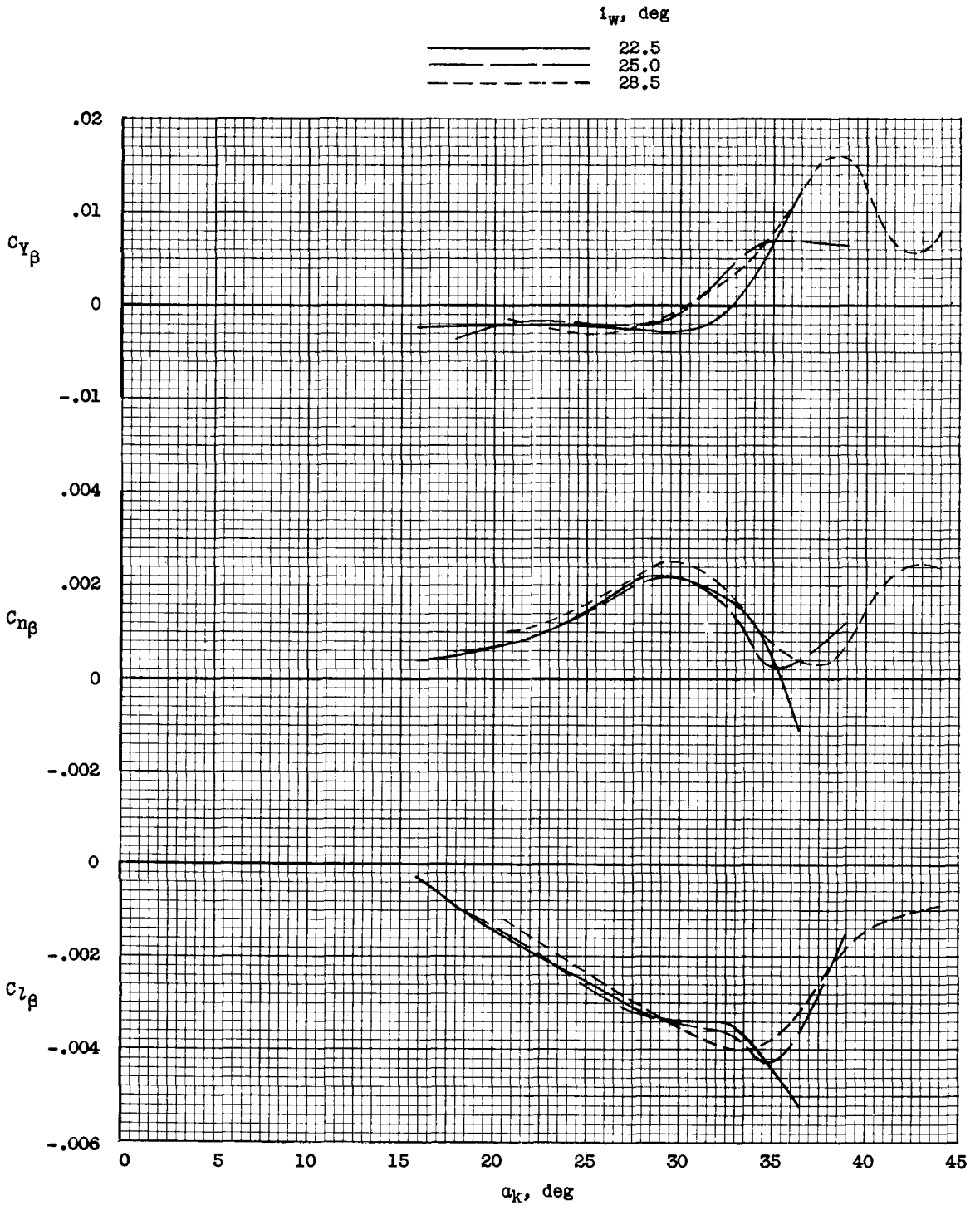

Figure 26.- Effect of wing incidence on static-lateral-stability parameters of airplane. T_c = 0; rudder on; q = 3.07 lb/sq ft.

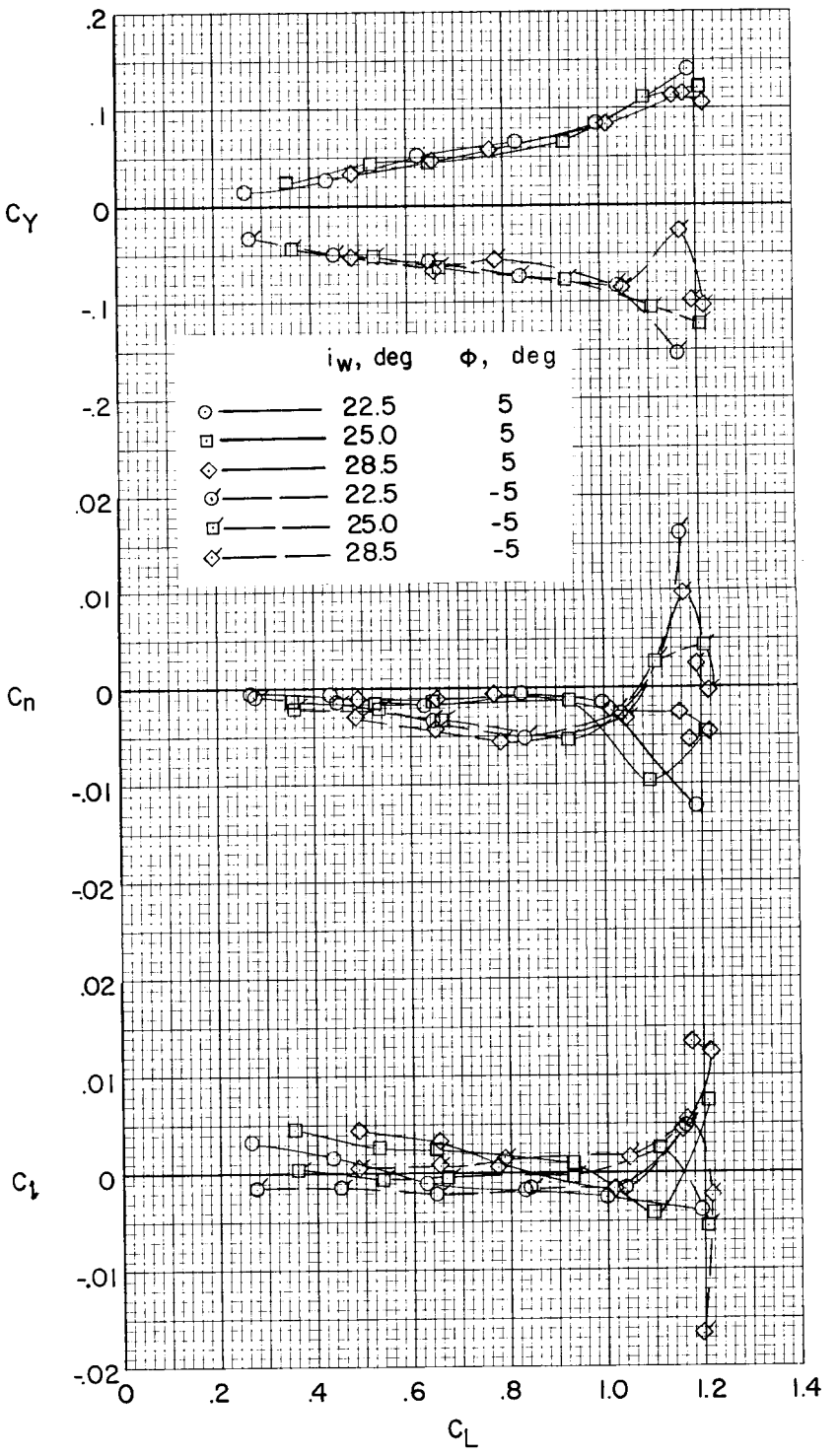

Figure 27.- Effect of wing incidence on variation of lateral coefficients with lift coefficient due to wing-bank angles of 5° and -5°. T_c = 0; q = 3.07 lb/sq ft.

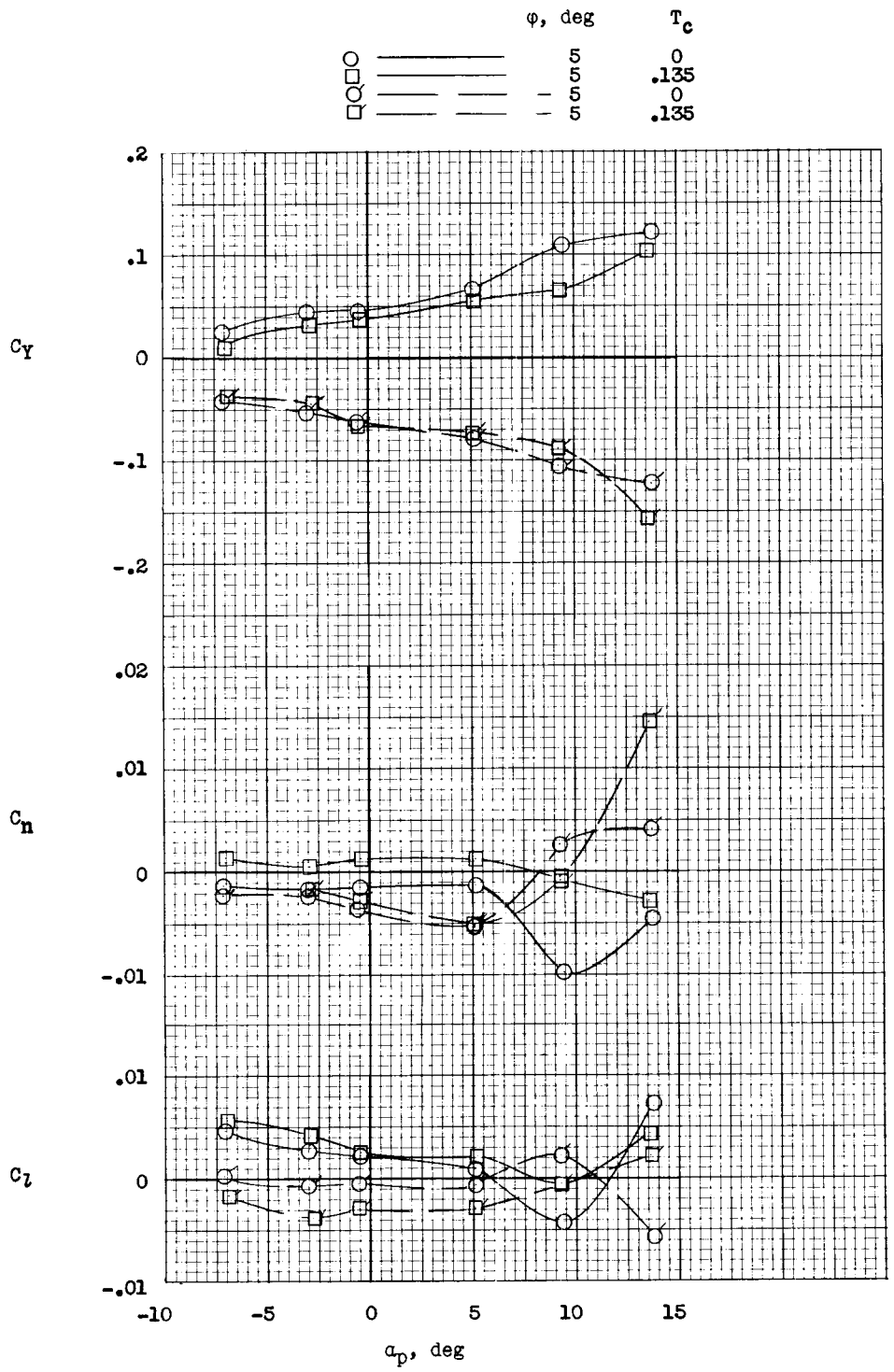

(a) $i_w = 25^\circ$.

Figure 28.- Effect of power on lateral coefficients due to wing-bank angles of 5° and -5°. q = 3.07 lb/sq ft.

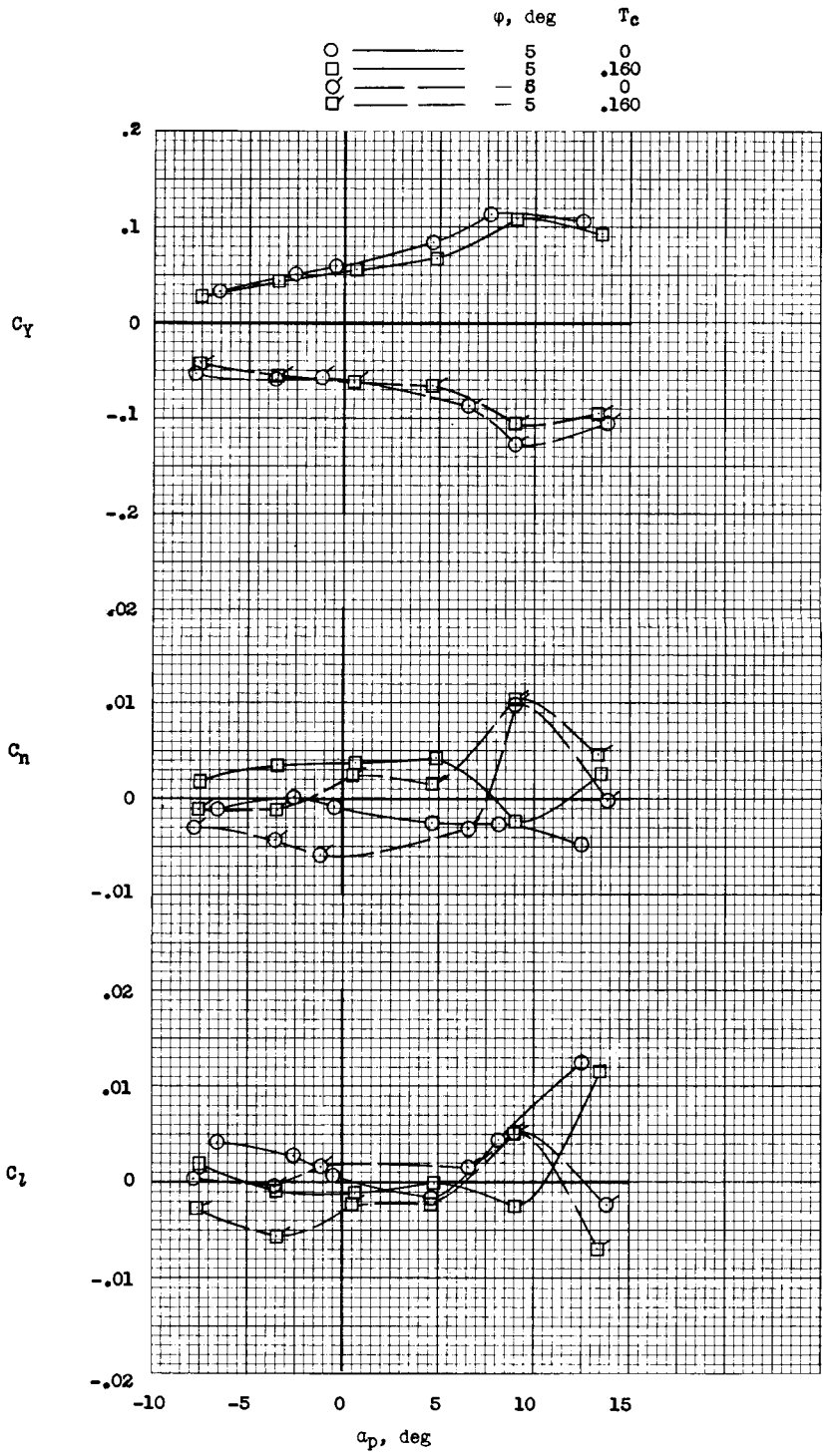

(b) $i_w = 28.5^o$.

Figure 28.- Concluded.

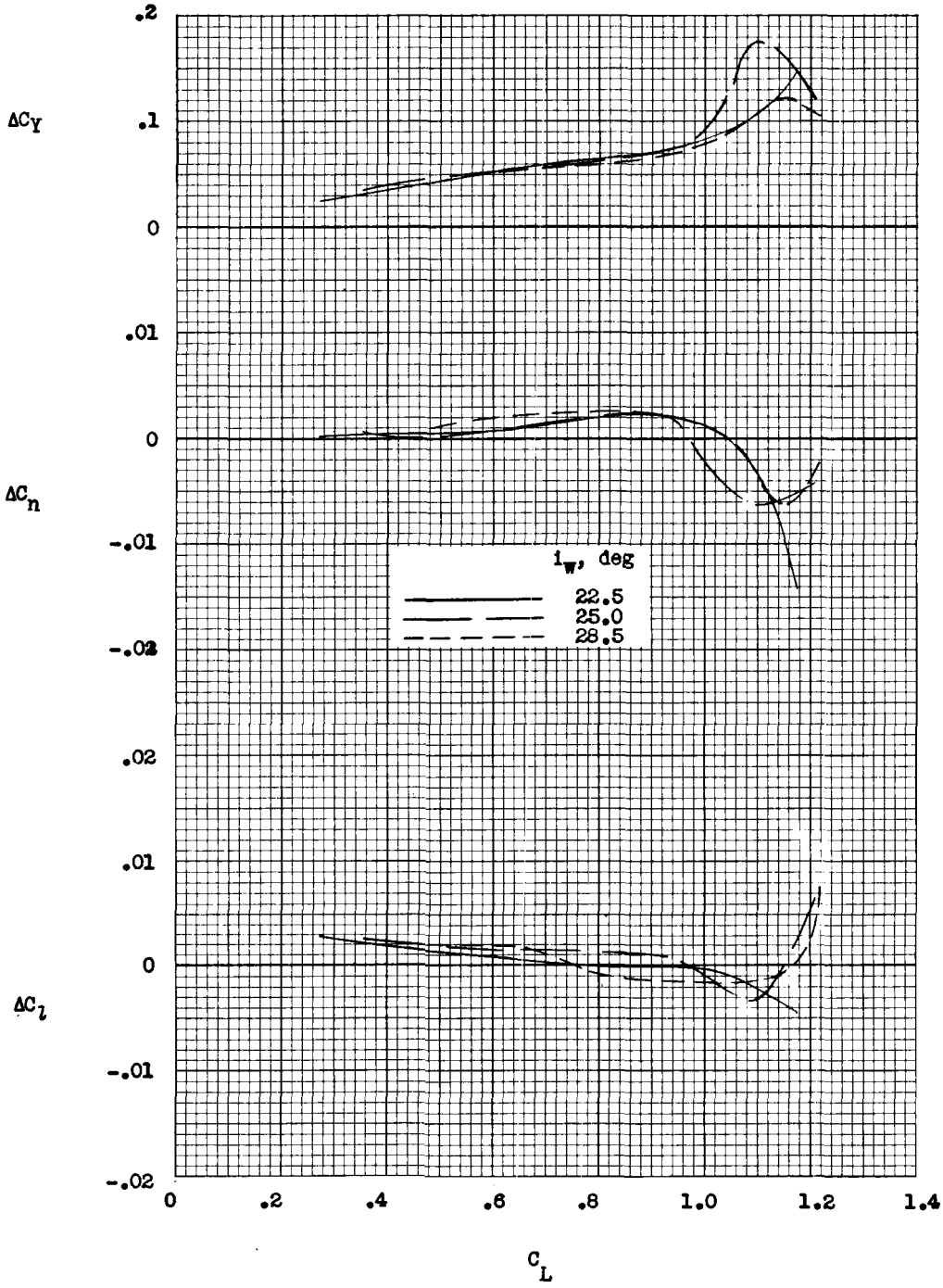

(a) Effect of wing incidence; $T_c = 0$.

Figure 29.- Incremental lateral force and moments produced by a wing-bank angle of 5°. q = 3.07 lb/sq ft.

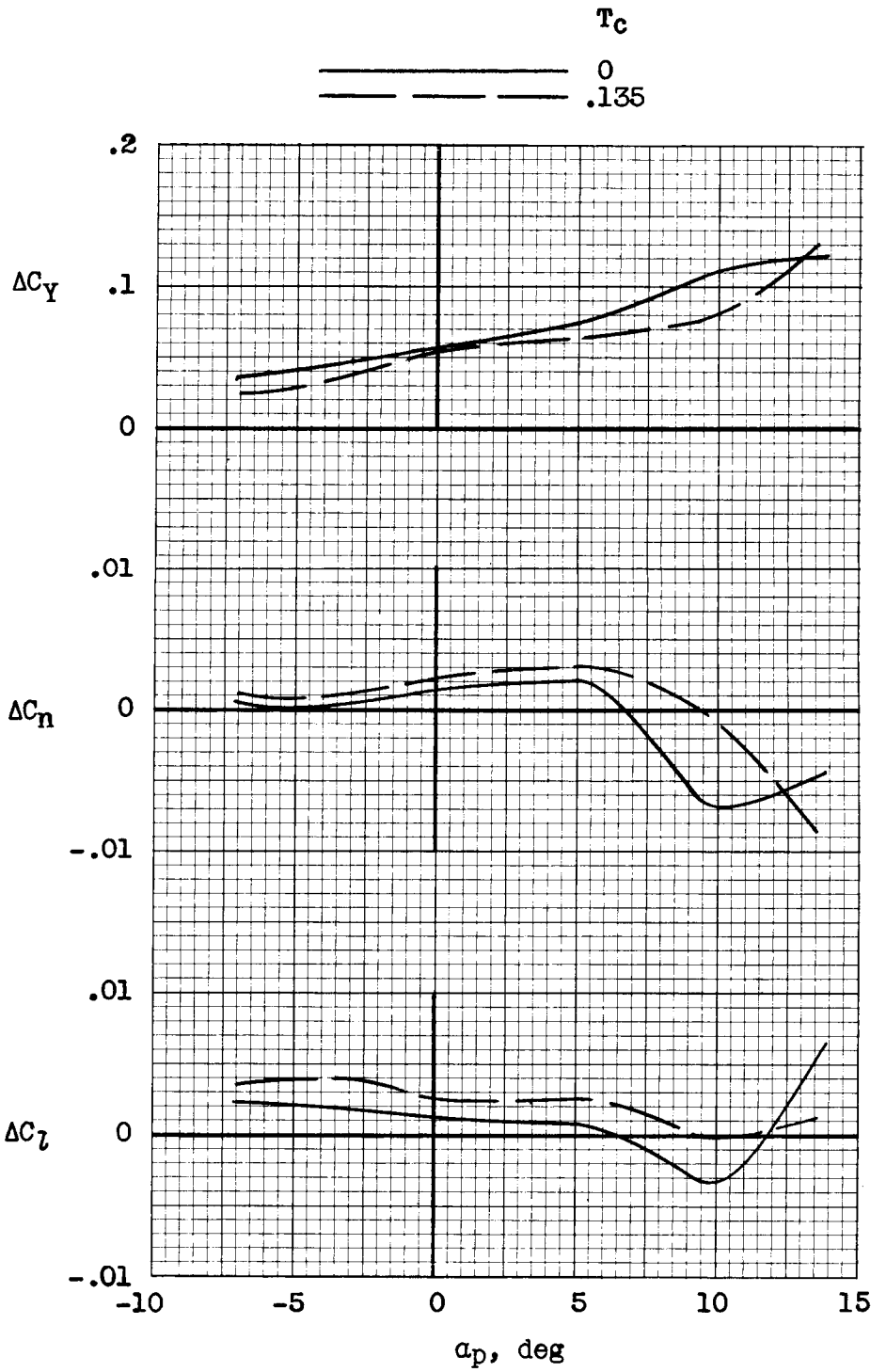

(b) Effect of power; $i_w = 25^\circ$.

Figure 29.- Concluded.

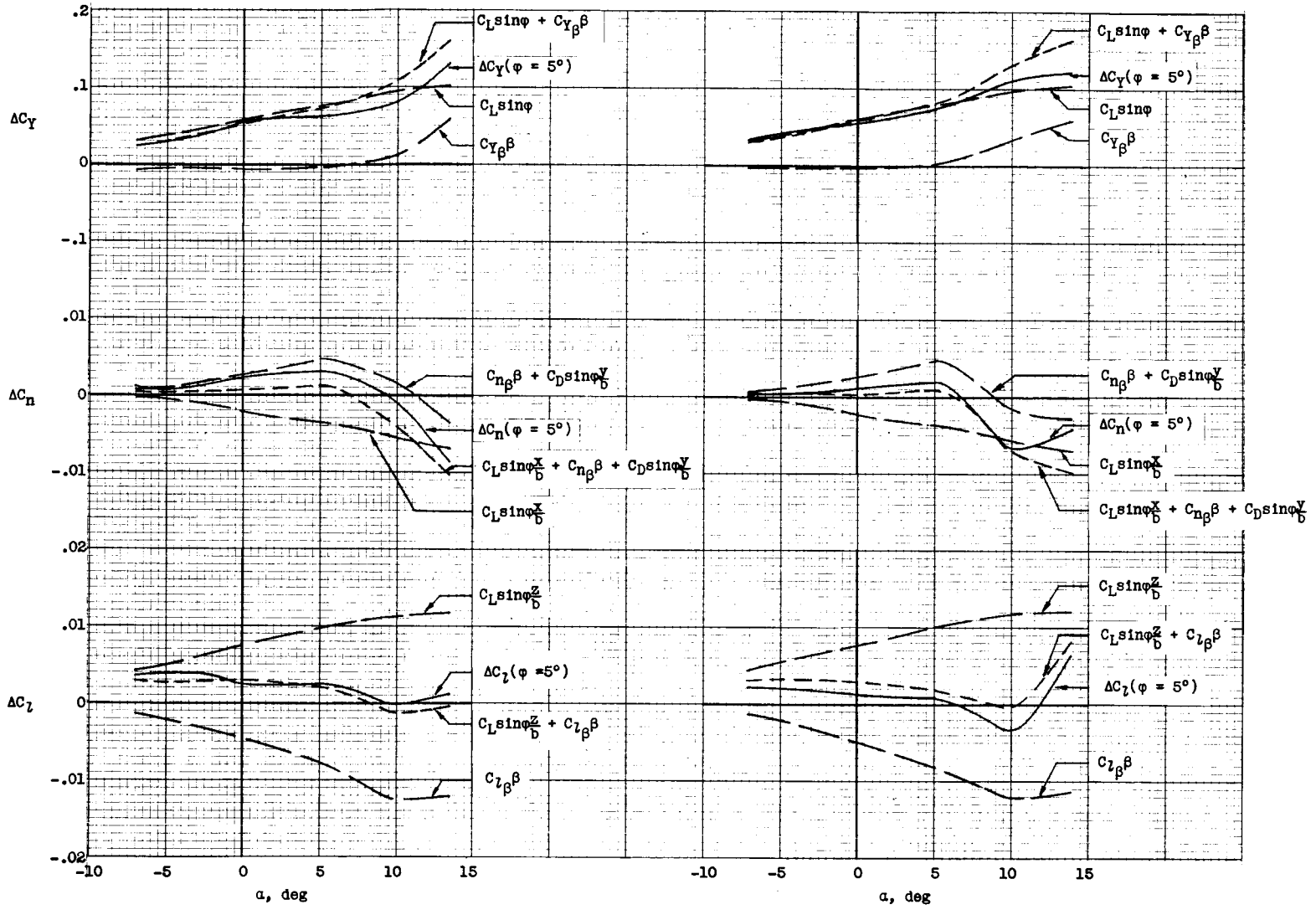

(a) Power on (T_c = 0.135).

(b) Power off.

Figure 30.- Comparison of measured incremental lateral-control coefficients with corresponding coefficients derived from tilted lift vector of wing, displaced drag vector of wing, and contribution due to wing sideslip. (The symbol y is lateral distance from drag vector of wing to center of gravity when wing is banked.) i_w = 25°; $\beta_{platform}$ = 0°.

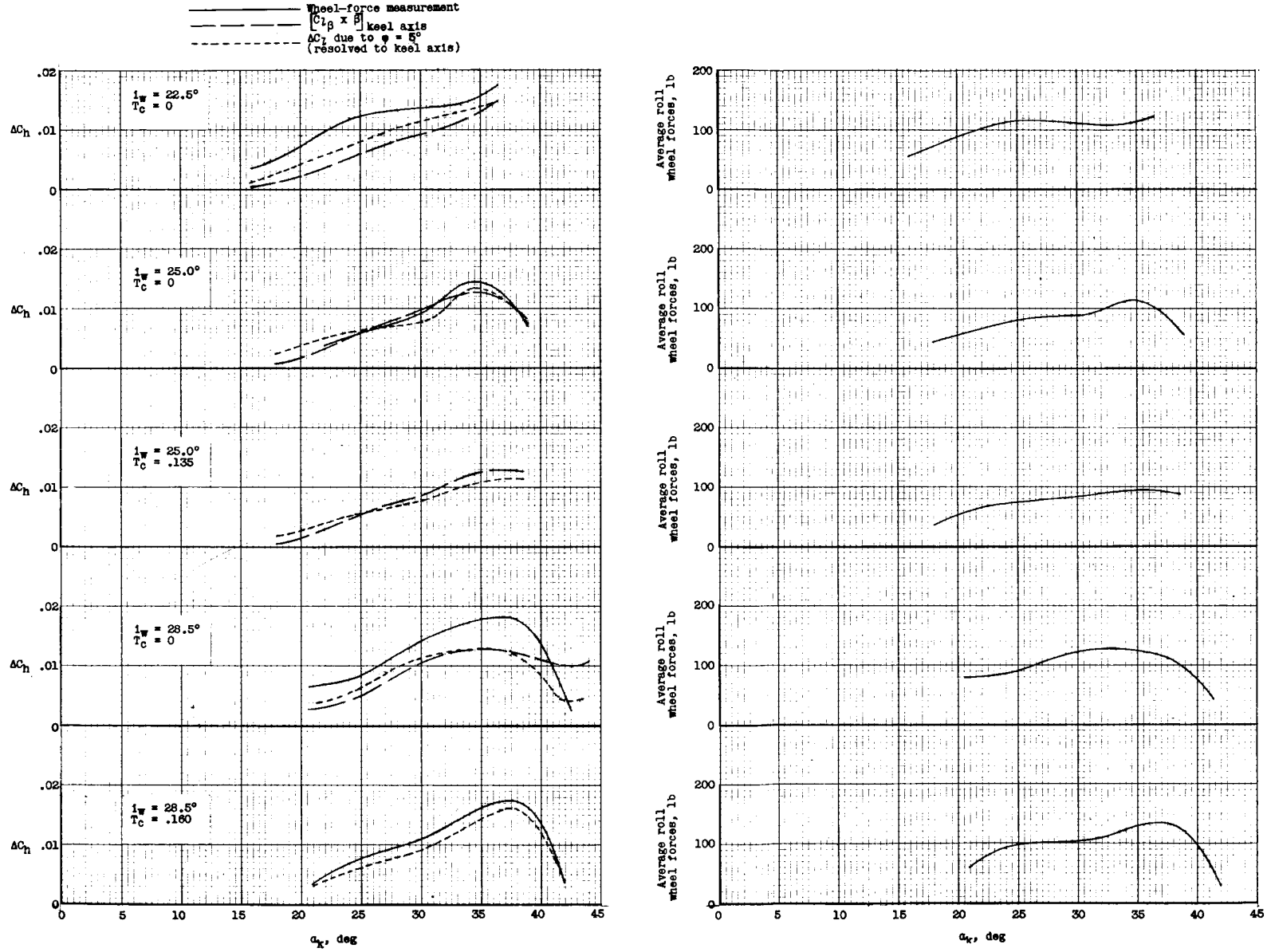

Figure 31.- Incremental hinge-moment coefficient due to banking wing 5° as determined by three methods and roll-control stick forces based on average of all hinge-moment coefficients. q = 3.07 lb/sq ft.

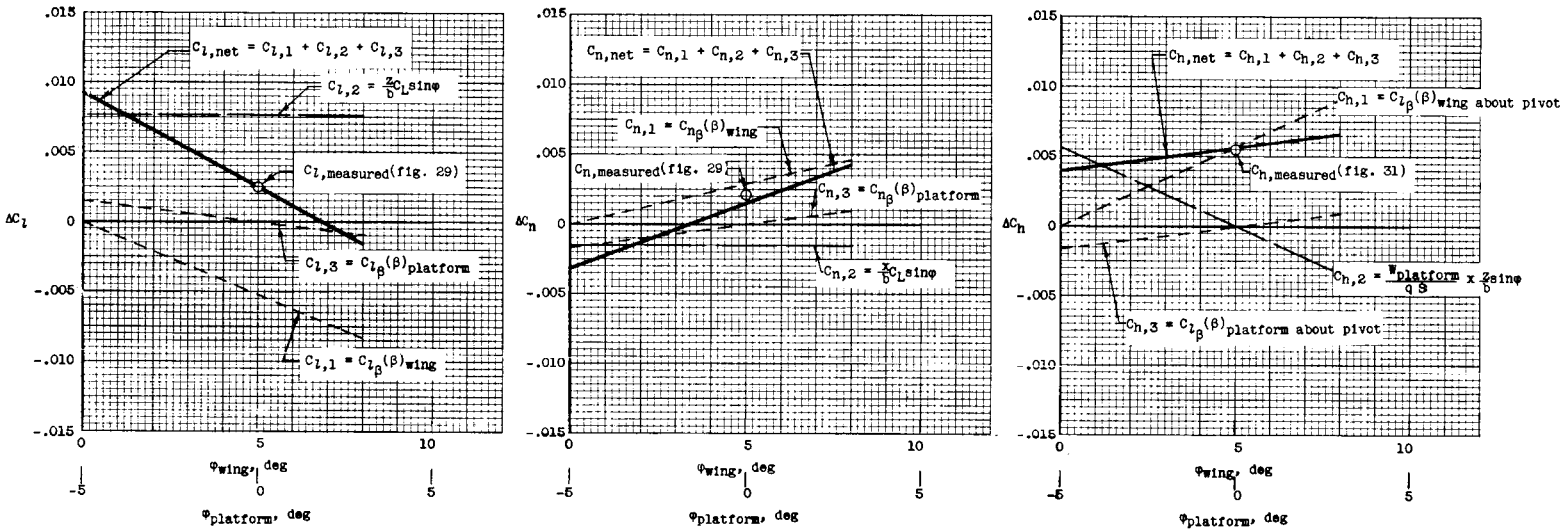

Figure 32.- Estimated incremental rolling-moment, yawing-moment, and hinge-moment coefficients as obtained by various proportions of wing and platform bank angle (relative bank angle between wing and platform held constant at 5°). $i_w = 25°$; $\alpha_p = 0°$.

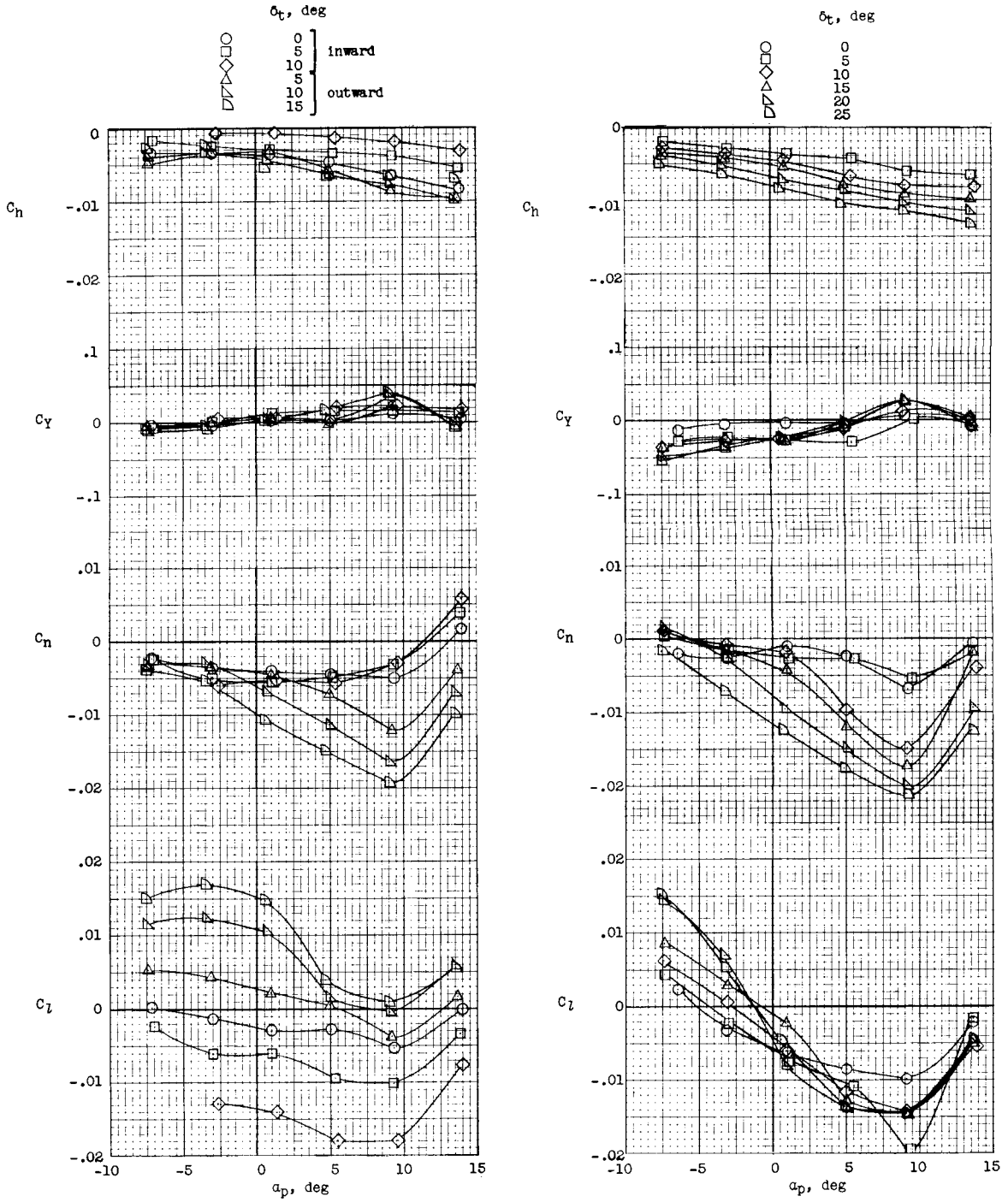

(a) Wing-tip control A.

(b) Wing-tip control B.

Figure 33.- Comparison of lateral control characteristics of two alternate roll-control devices on left wing tip only. q = 3.07 lb/sq ft.

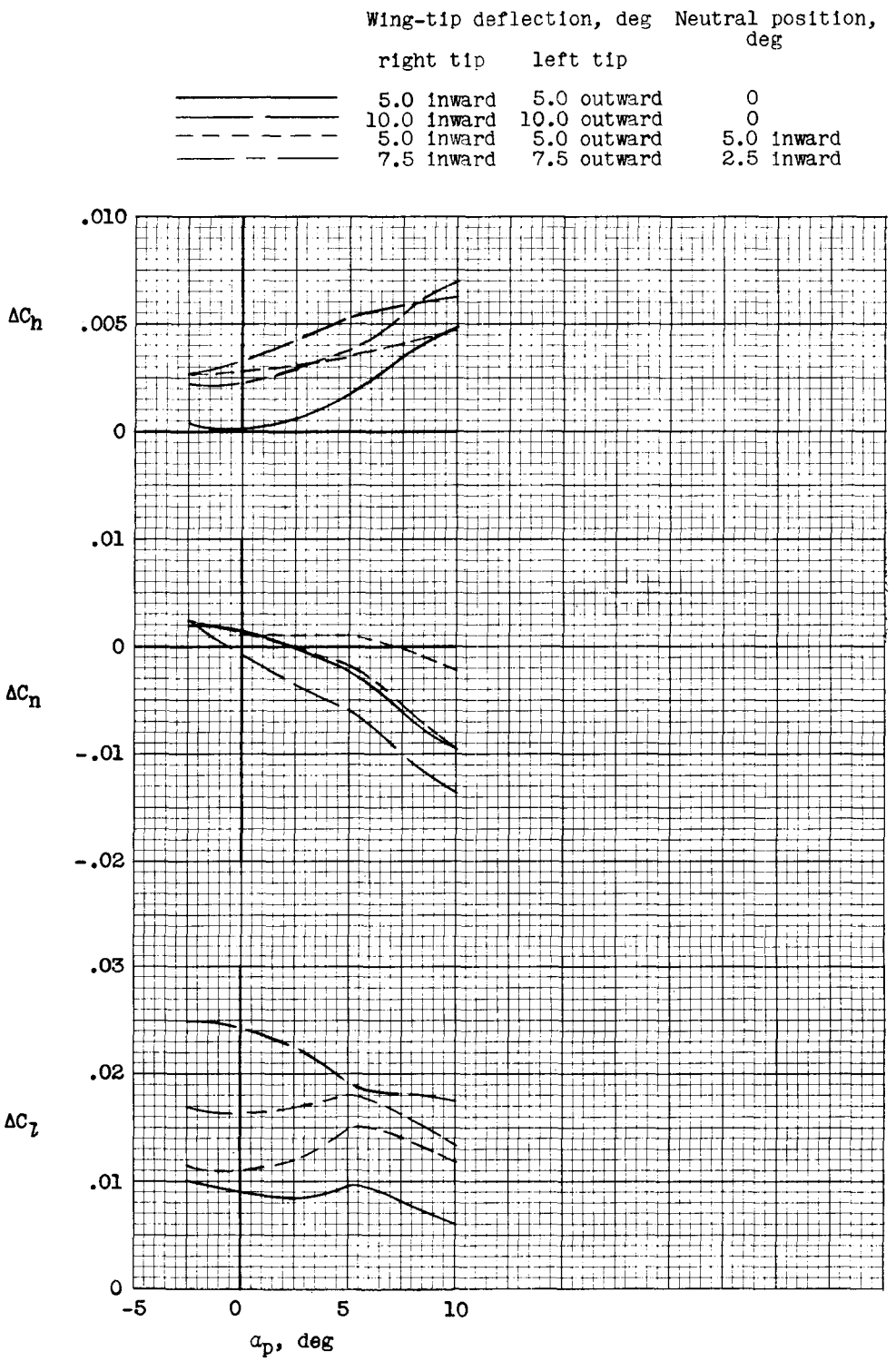

Figure 34.- Incremental lateral-control moments obtained with differential deflection of hinged wing tips for several different neutral settings.

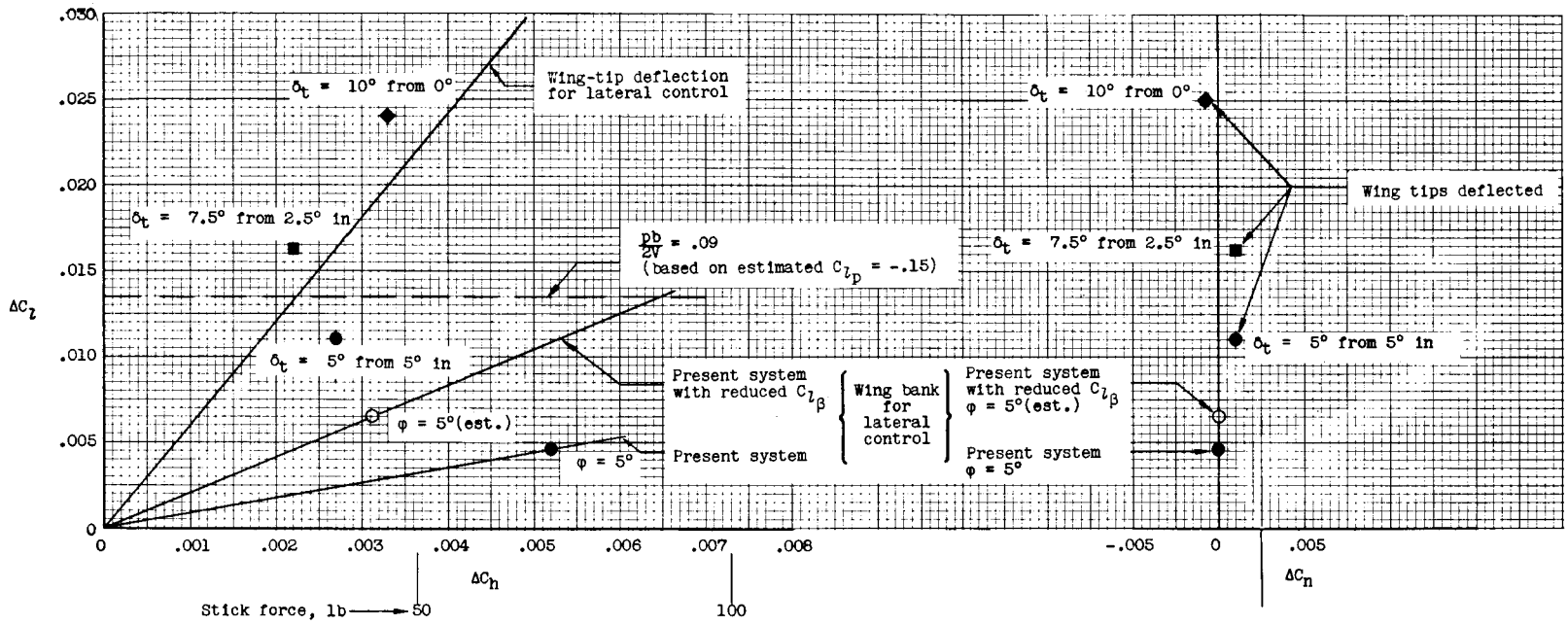

(a) Rolling-moment and hinge-moment relationship.

(b) Rolling-moment and yawing-moment relationship.

Figure 35.- Summary of existing lateral control characteristics of airplane and comparison with characteristics of a system using wing-tip deflection for lateral control. $i_w = 25^o$; $\alpha_p = 0^o$; gross weight = 1,840 pounds.

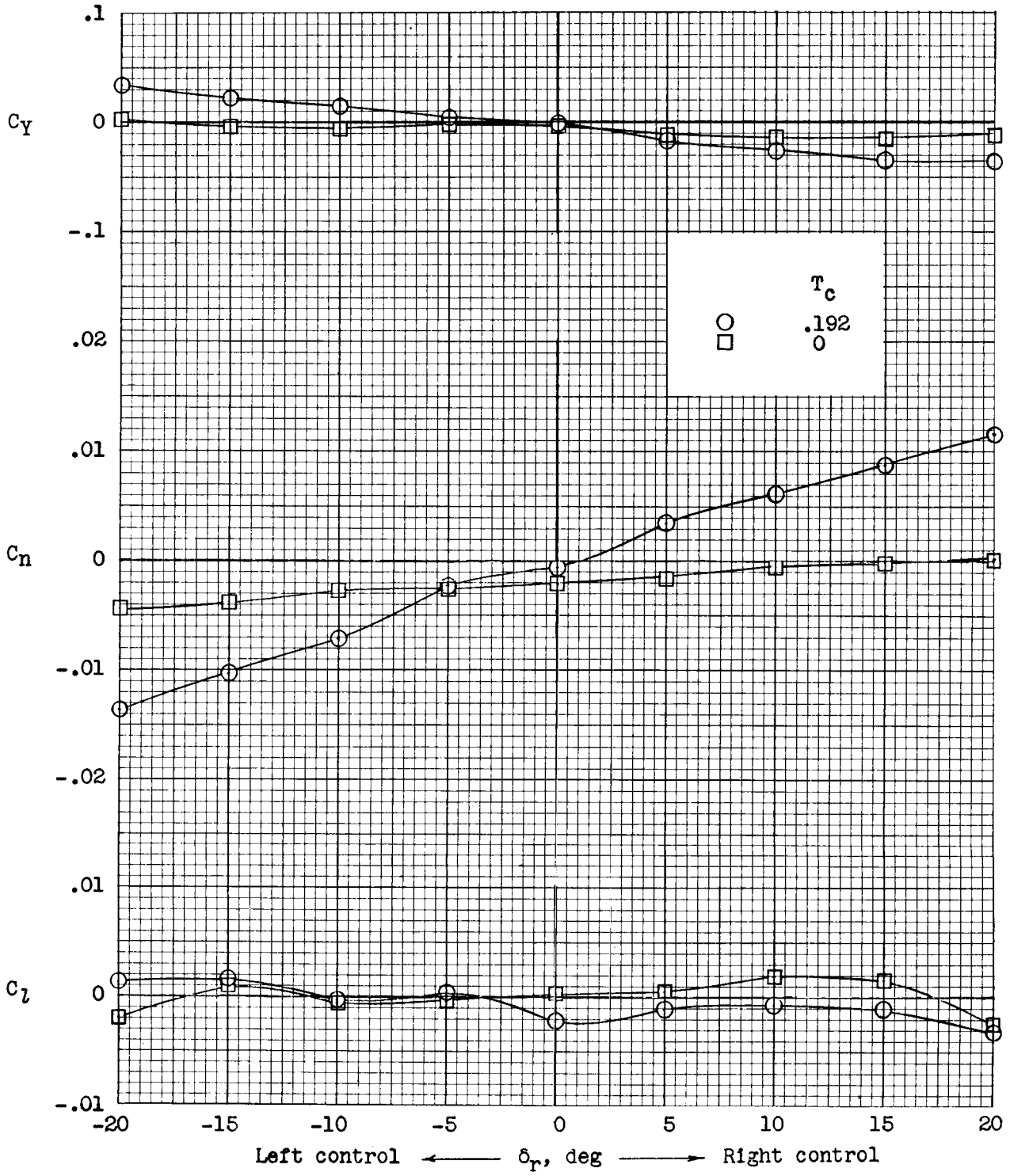

Figure 36.- Effect of power on rudder control. $\alpha_p = 0^\circ$; $i_w = 25^\circ$; q = 3.07 lb/sq ft.

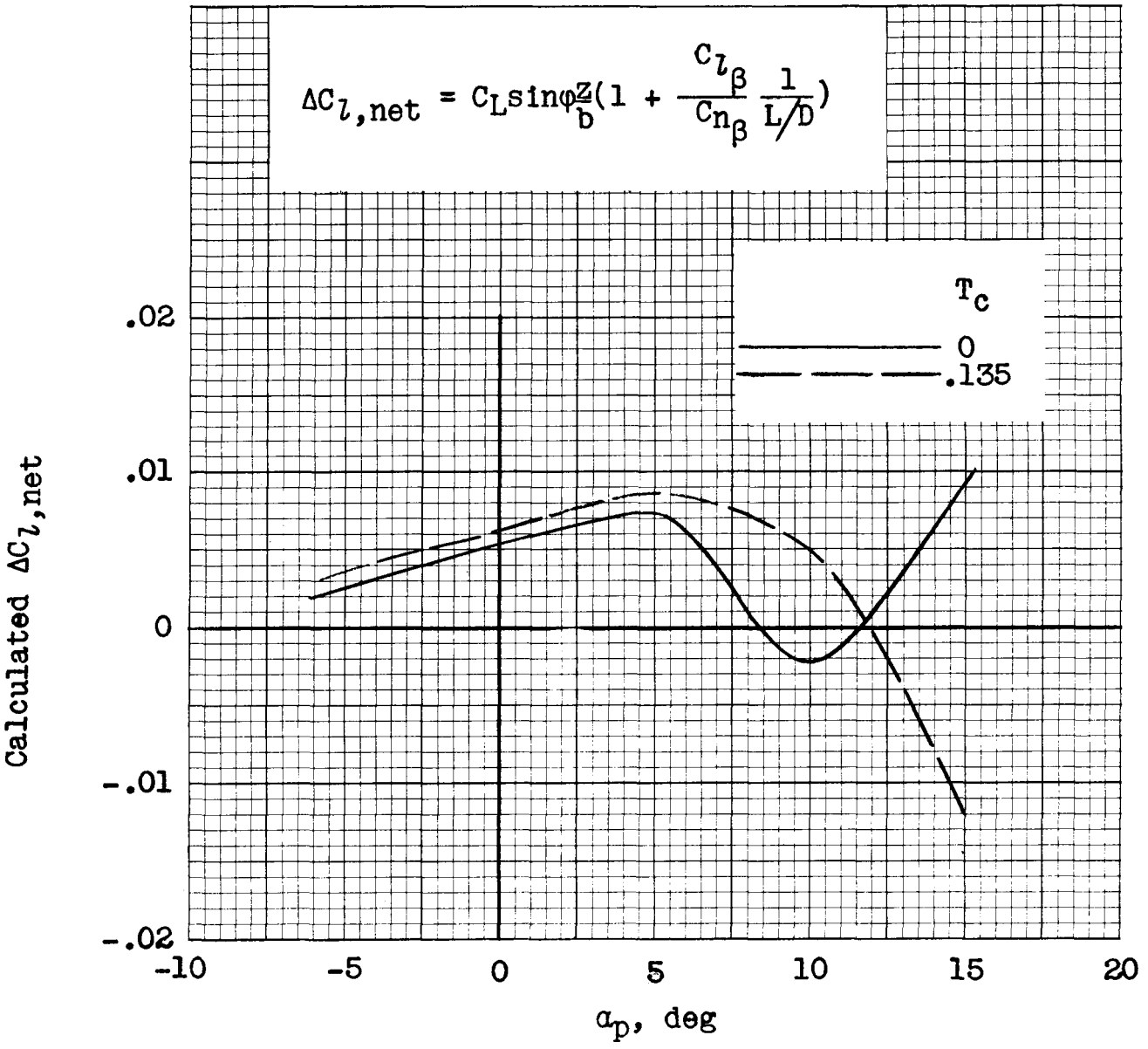

Figure 37.- Calculated incremental net rolling-moment coefficient produced by 5° of wing bank. $i_w = 25°$.